UNIVERSIDAD CARLOS III DE MADRID
Escuela Politécnica Superior
Departamento de Ingeniería Térmica y de Fluidos

"MOTION OF OBJECTS IMMERSED IN A BUBBLING FLUIDIZED BED"

Thesis for the degree of Doctor of Philosophy

Autor:
Antonio Soria Verdugo
Ingeniero Industrial

Director de Tesis:
Ulpiano Ruiz-Rivas Hernando
Ingeniero Industrial
Doctor en Ingeniería Industrial

Leganés (Madrid), a 17 de Diciembre de 2010

Tesis Doctoral

"MOTION OF OBJECTS IMMERSED IN A BUBBLING FLUIDIZED BED"

Autor: Antonio Soria Verdugo
Director de Tesis: Ulpiano Ruiz-Rivas Hernando

El tribunal, nombrado por el Magfco. y Excmo. Sr. Rector de la Universidad Carlos III de Madrid,

Presidente D. Bo Leckner, Chalmers University of Technology.

Vocal D. Jesús Arauzo Pérez, Universidad de Zaragoza.

Vocal D. Jesús Guardiola Soler, Universidad de Alcalá.

Vocal D. José Antonio Almendros Ibáñez, Universidad de Castilla La Mancha.

Secretario D. Domingo Santana Santana, Universidad Carlos III de Madrid.

Suplente Dña. Mercedes de Vega Blázquez, Universidad Carlos III de Madrid.

Suplente D. Luis Alberto Bahillo Ruiz, Centro de Investigaciones Energéticas, Medioambientales y Tecnológicas.

acuerda la calificación de: _____

El presidente El secretario

Los vocales

En Leganés (Madrid), a 17 de Diciembre de 2010

Always start by trying the simplest model and then only add complexity to the extent needed.
Levenspiel O.

The experimentalist who does not know what he is looking for, will never understand what he finds.
Bernard C.

Contents

Contents ii

List of Figures v

List of Tables vii

Agradecimientos xi

Resumen xiii

Abstract xvii

1 Introduction 1

1.1 Liquid-like behavior of fluidized beds 2

1.2 Effect of bed particles on fluidization 2

1.3 Motion of objects inside a fluidized bed. 3

1.4 Scope of the thesis 4

2 Experimental Setup 7

2.1 Introduction 7

2.2 2-D bubbling fluidized bed 8

2.2.1 2-D facility 8

2.2.2 Measurement system 9

2.2.3 Bed dynamics 11

2.3 3-D bubbling fluidized bed 13

2.3.1 3-D facility 13

2.3.2 Measurement system 19

2.3.3 Bed dynamics 20

2.4 Notation 22

Bibliography 24

3 Motion of a neutrally-buoyant object in a 2-D Bubbling Fluidized Bed **27**
3.1 Abstract . . . 27
3.2 Introduction . . . 28
3.3 Experimental Setup . . . 30
3.4 Results . . . 32
3.4.1 Dense phase and bubbles . . . 32
3.4.2 Object motion pattern . . . 34
3.4.3 Circulation time . . . 36
3.5 Discussion . . . 41
3.6 Conclusions . . . 45
3.7 Notation . . . 46
Bibliography . . . 48

4 Buoyancy effects on objects moving in a 2-D Bubbling Fluidized Bed **51**
4.1 Abstract . . . 51
4.2 Introduction . . . 52
4.3 Experimental Setup . . . 54
4.4 Results . . . 55
4.5 Conclusions . . . 65
4.6 Notation . . . 66
Bibliography . . . 67

5 Motion of objects in a 3-D Bubbling Fluidized Bed with a rotating distributor **71**
5.1 Abstract . . . 71
5.2 Introduction . . . 72
5.3 Experimental Setup . . . 74
5.4 Results . . . 76
5.4.1 Object loss . . . 76
5.4.2 Circulation time distribution . . . 80
5.5 Conclusions . . . 84
5.6 Notation . . . 86
Bibliography . . . 87

6 Conclusions **91**

Bibliography **95**

List of Figures

1.1 Geldart's classification of particles for fluidization with air at atmospheric pressure (adapted from Geldart (1973)). 2

2.1 Schematic diagram of the 2-D facility. 8
2.2 Photograph of the 2-D bed material captured by an electronic microscope. 9
2.3 2-D bed distributor scheme. 9
2.4 Schematic diagram of the measurement system for the 2-D facility. . . . 10
2.5 Standard deviation of the pressure signal measured at 0.3 m over the distributor (2-D facility). 11
2.6 Power spectra obtained for $U/U_{mf} = 2.5$. 12
2.7 Pressure drop through the distributor (2-D facility). 13
2.8 Schematic diagram of the 3-D facility. 13
2.9 Photograph of the 3-D bed material captured by an electronic microscope. 14
2.10 Particle size distribution of the 3-D bed material. 14
2.11 3-D bed distributor scheme. 15
2.12 Triangular mesh of holes of the perforated plate. 16
2.13 Discharge coefficient of the perforated plate (adapted from Karri and Werther (2003)). 17
2.14 Variation of the distributor pressure drop with the number of holes. . . 18
2.15 Jet length predicted by Equation 2.11. 19
2.16 Schematic diagram of the measurement system for the 3-D facility. . . . 20
2.17 Standard deviation of the pressure signal measured at $0.3\,m$ over the distributor (3-D facility). 20
2.18 Power spectra, operating with the rotating and static distributor. ($U/U_{mf} = 1.44$, $h_b/D = 0.5$). 21
2.19 Comparison between the analytical estimate of the pressure drop and the experimental data. 22
2.20 Effect of the distributor rotation on the pressure drop. 22

3.1 Scheme of the experimental facilityEEEE. 31
3.2 (a) Relative frequency of dense phase and (b) time-averaged dense phase velocity. 33
3.3 Relative frequency of objects at a certain position in the bed. Nominal case ($U/U_{mf} = 2.5$). 35
3.4 Relative frequency of a rising or a sinking object as a function of the x-coordinate of the bed (width). Nominal case ($U/U_{mf} = 2.5$). 35
3.5 (a) Relative frequency to find the object at a determined position as a function of the y-coordinate (height from the distributor) for the nominal case ($U/U_{mf} = 2.5$), and (b) effect of the dimensionless gas velocity on the distribution of the object through the bed. 36
3.6 (a) Object path in the bed and (b) Object velocity during the path. Nominal case ($U/U_{mf} = 2.5$). 38
3.7 Mean sinking velocity in the whole bed, sampling the velocity signal at different frequencies. 39
3.8 Mean sinking and rising velocities of an object compared with models for the dense phase and bubbles velocities. 40
3.9 Circulation time of an object for the nominal case ($U/U_{mf} = 2.5$), (a) as a function of the cycle maximum attained depth, and (b) as a function of the number of jumps employed to reach the surface of the bed. . . . 41
3.10 Relative frequency to (a) reach a determined maximum depth, and (b) find cycles with a determined number of jumps. Nominal case ($U/U_{mf} = 2.5$) 41
3.11 Probability density function of the total circulation time of an object. . 43
3.12 Box plots of (a) the experimental circulation time and (b) the estimated circulation time. 44
3.13 Experimental and estimate box plots for the circulation time of the object moving in the 3-D bed. 45

4.1 Relative frequency (a) to find cycles with a determined number of jumps, and (b) to find cycles that reach a determined maximum depth. 56
4.2 R^2 coefficient of the exponential fitting of the number of jumps for objects of different densities (a) and sizes (b). 57
4.3 Relative frequency to find cycles with a determined number of jumps for all the tests. 57
4.4 Determination coefficient of the parabolic fitting of the maximum attained depth for objects of different densities (a) and sizes (b). 59

4.5 Relative frequency to reach a determined depth. Flotsam object F2, operating at $U/U_{mf} = 1.5$. 59
4.6 Probability to find the object in the upper half of the bed for (a) different object densities and (b) sizes. 61
4.7 Mean rising velocity of objects with different densities (a) and sizes (b). 62
4.8 Mean sinking velocity of objects with different densities (a) and sizes (b). 63
4.9 Relative frequency to (a) find cycles with a determined number of jumps, and (b) reach a determined maximum depth, for the neutrally-buoyant object moving in a bed with a bed aspect ratio $h_b/W = 0.75$ operating at $U/U_{mf} = 3$. 64
4.10 Relative frequency to (a) find cycles with a determined number of jumps, and (b) reach a determined maximum depth, for the neutrally-buoyant object moving in a bed with dense material of a diameter $400 - 600\,\mu m$ operating at $U/U_{mf} = 3$. 64

5.1 Scheme of the experimental facility. 74
5.2 Power spectra for the rotating and static distributor configurations. Nominal case ($U/U_{mf} = 1.44$, $h_b/D = 0.5$). 75
5.3 Object loss probability with the static distributor. Variation with: (a) bed aspect ratio, (b) dimensionless gas velocity, (c) bed-object density ratio, and (d) object aspect ratio. 78
5.4 Histograms of the circulation time for the object to return to the bed surface: (a) rotating distributor, (b) static distributor. Nominal case ($U/U_{mf} = 1.44$, $h_b/D = 0.5$). 81
5.5 Median of the object circulation time distributions, variation with (a) bed aspect ratio, (b) dimensionless gas velocity, (c) bed-object density ratio, and (d) object aspect ratio. 82
5.6 Box plots of the circulation time distributions in Figure 5.4. Nominal case ($U/U_{mf} = 1.44$, $h_b/D = 0.5$). 84
5.7 Box plots of the circulation time distributions for varying conditions, (rd) Rotating Distributor, (sd) Static Distributor. 85

List of Tables

4.1 Characteristics of the objects used in the experiments. 55

5.1 Density, ρ_o, and length, L_O, of the cylindrical objects used in the experiments. Diameter, D_O, was always $6.4\,mm$. 74

5.2 Experimental parameters. Nominal case is in bold format. 76

List of publications

Part of the work contained in this thesis has also been presented in the following papers:

- A. Soria-Verdugo, L. M. García-Gutiérrez, S. Sanchez-Delgado, U. Ruiz-Rivas, 2010. Circulation of an object immersed in a bubbling fluidized bed. *Chemical Engineering Science* 66, 78-87.

- A. Soria-Verdugo, L. M. García-Gutiérrez, N. Garcia-Hernando, U. Ruiz-Rivas. Buoyancy effects on the motion of an object in a bubbling fluidized bed. *Submitted for publication.*

- A. Soria-Verdugo, N. Garcia-Hernando, J.A. Almendros-Ibáñez, U. Ruiz-Rivas. Motion of objects in a 3-D bubbling fluidized bed with a rotating distributor. *Submitted for publication.*

- A. Soria-Verdugo, L. M. García-Gutiérrez, S. Sanchez-Delgado, U. Ruiz-Rivas. Motion of a large object in a 2-D bubbling fluidized bed. *Fluidization XIII conference*, Gyeong-ju (Korea), May 16-21, 2010.

- A. Soria-Verdugo, N. García-Hernando, U. Ruiz-Rivas. Transport phenomena in a bubbling fluidized bed with a rotating distributor. *Interdisciplinary Transport Phenomena VI: Fluid, Thermal, Biological, Materials, and Space Sciences*, pp. 9.24-9.36. Volterra (Italy), October 4-9 2009.

The following papers have also been published while working on the thesis but are not included since their content is outside the scope of the present work.

- A. Soria-Verdugo, J.A. Almendros-Ibáñez, U. Ruiz-Rivas, D. Santana, 2009. Exergy Optimization in a Steady Moving Bed Heat Exchanger. *Annals of the New York Academy of Sciences* 1161, 584-600.

- J.A. Almendros-Ibáñez, A. Soria-Verdugo, U. Ruiz-Rivas, D. Santana. Thermal analysis and optimization of a heat regenerator composed of two coupled moving bed heat exchangers. *4th International Symposium on Advances in Computational Heat Transfer (CHT-08)*, Marrakech (Morroco), May 11-16, 2008.

- S. Sánchez-Delgado, J.A. Almendros-Ibáñez, A. Soria-Verdugo, D. Santana, U. Ruiz-Rivas. Coherent structures and bubble-particle velocity in 2-D fluidized beds. *CFB-9 Circulating Fluidized Bed Technology IX*, 1007-1012, May 13-18, 2008. ISBN 978-3-930400-57-7.

- J.A. Almendros-Ibáñez, A. Soria-Verdugo, S. Sánchez-Delgado, C. Sobrino, U. Ruiz-Rivas, A. Macías-Machín, D. Santana. Exergy Optimization of a Moving Bed Heat Exchanger. *2nd International Congress of Energy and Environment Engineering and Management (IICIIEM2007)*, Badajoz (Spain), June 6-9, 2007.

Agradecimientos

Muchas son las personas a las que debo agradecer llegado este momento. En primer lugar a mi familia: a mi abuela por ser un ejemplo de humildad y bondad, a mis herman@s y cuñad@s por ser un espejo en el que mirarme, a mis sobrin@s por dibujarnos a todos una sonrisa y a mis padres por hacerme consciente desde pequeño de la importancia de la formación y por sacrificarse tantos años para que tanto mis hermanos como yo mismo tuvieramos acceso a ella. También a mi familia política, por dejar de ser política y convertirse en familia sin más.

Gracias a Ulpiano, mi director de tesis, por ejecer de director cuando trabajamos y de amigo el resto del tiempo. Al resto de doctores del grupo ISE: Domingo, Mercedes, Néstor, Antonio Acosta, Javi Villa, Celia, Sergio, Carol y Jose Almendros por su ayuda y comentarios durante estos años. Al grupo de Mecánica de Fluidos por su generosidad a la hora de compartir su material de laboratorio con nosotros.

A los de la zona amarilla: Luismi, Alberto, Fernando, Javi Sánchez, Jorge, Will, Pablo, Ana, Iván y Dani, por las risas de las que hemos disfrutado durante las comidas y cafés. Quería agradecer también a Gabriel por ser el primero en animarme a que me lanzara a la investigación y el primero en confiar en mis capacidades.

Por último, un agradecimiento especial merece Nuria, por su cariño y paciencia durante la realización de esta tesis, ya que sin su apoyo la consecución de la tesis no habría sido posible.

Resumen

Los lechos fluidos se emplean en la industria por sus excelentes propiedades para el transporte de calor y masa y por su capacidad para albergar y promover en su interior reacciones químicas. En el interior de un lecho fluido pueden desarrollarse procesos como el secado de un material granulado, intercambios de calor con una superficie o un tubo, la conversión térmica de combustibles sólidos o el recubrimiento de partículas. Muchas de estas aplicaciones requieren del movimiento de objetos en el interior del lecho. Partículas de combustible, catalizadores y aglomerados son ejemplos típicos de partículas que se pueden encontrar en los lechos fluidos. La caracterización del movimiento de dichos objetos es necesaria para un adecuado funcionamiento y para evitar problemas como por ejemplo la existencia de puntos calientes o fríos en un reactor o la aparición de zonas defluidizadas debido a la aparición de aglomerados.

El presente trabajo recoge un estudio experimental, empleando técnicas de análisis digital de imagen, del movimiento de objetos grandes (mayores que el material del lecho) inmersos en un lecho fluido burbujeante. Los experimentos se llevaron a cabo en dos instalaciones, un lecho bidimensional y otro tridimensional y de escala laboratorio. Se analizaron diferentes objetos, variando su densidad y tamaño.

Las características fundamentales del movimiento de los objetos se estudiaron sobre el lecho bidimensional. Siguiendo la trayectoria del objeto, se observaron y caracterizaron los caminos preferentes y la homogeneidad en la distribución espacial. Posteriormente se estudiaron en detalle los ciclos descritos por el objeto en su camino desde y hacia la superficie del lecho. Cada ciclo se compone de procesos de descenso y procesos de ascenso, observándose en muchos casos una serie de movimientos de ascenso y descenso intercalados a lo largo de la trayectoria. A partir de esta evidencia experimental y considerando cada ciclo independiente de la historia previa, se desarrolló una modelización de los ciclos a partir de cuatro parámetros fundamentales: las velocidades medias de ascenso y descenso del objeto, la máxima profundidad alcanzada a lo largo del ciclo y el número de movimientos ascendentes independientes (número de saltos) que tienen lugar en el ciclo. Se estudiaron las velocidades de ascenso y descenso y se estableció una metodología de cálculo para los promedios, ante la existencia de cambios

bruscos de tendencia y movimientos vibratorios que dificultan la tarea de separación de los procesos. El proceso de ascenso del objeto está vinculado al paso de burbujas. Se cuantificó la probabilidad de ascender hasta la superficie mediante la acción de una sola burbuja (un sólo salto) y en función de ella la existencia e importancia relativa de caminos de subida con múltiples saltos, fruto de la acción de una serie de burbujas y separados por periodos de descenso. Finalmente se definió un sencillo modelo semi-empírico para caracterizar el movimiento cíclico del objeto, basado en los cuatro parámetros fundamentales, el número de saltos durante el ciclo, la máxima profundidad alcanzada y las velocidades medias de ascenso y descenso. Estos dos últimos parámetros se relacionaron con correlaciones habituales para la velocidad media de la fase densa y de las burbujas y los dos primeros se modelaron, tanto en cuanto a su relación con el tiempo de circulación del objeto como en sus respectivas distribuciones de probabilidad.

Este procedimiento se utilizó inicialmente para caracterizar el movimiento de un objeto cilíndrico grande y de densidad similar a la del lecho y posteriormente se varió su tamaño y densidad para estudiar el efecto de las fuerzas de flotabilidad, teniendo también en cuenta el efecto de la velocidad del gas. Los resultados muestran que el modelo semi-empírico cuenta con validez general dentro del rango de variación de los experimentos. Esto incluye variaciones de la densidad desde ligeramente superiores a la del lecho a valores inferiores a la mitad, cambio de tamaño en el entorno del orden de magnitud e incluso para cambios de altura del lecho y de la distribución de tamaños del material que forma el lecho. La distribución de probabilidades para el número de saltos sigue una proporción geométrica. En función de ello se obtiene un valor de 45 % para la probabilidad media de que una burbuja que mueva al objeto acabe depositándolo en la superficie del lecho y supone un 55 % de probabilidad de que el ciclo conlleve un nuevo salto. Este valor medio se mantiene constante para todos los experimentos. También se obtiene un perfil parabólico para la distribución de profundidades, que se explica en función de los caminos preferentes de objetos y burbujas. En todos los procesos se observa un efecto despreciable de las fuerzas de flotabilidad en el ascenso de objetos y coherente con dichas fuerzas en los caminos de bajada.

Por último, se estudió una aplicación práctica del movimiento de objetos, utilizando un lecho 3-D de escala laboratorio. En este lecho se midieron los tiempos de circulación de los objetos mediante la adquisición de imágenes de la superficie del lecho. En el estudio se compararon las distribuciones de tiempos de recirculación para un lecho estándar y para otro en el que se introduce un actuador para modificar y mejorar las características de funcionamiento del lecho. El actuador empleado consiste en la rotación a baja frecuencia del distribuidor. Los resultados muestran la mejora de la

circulación de objetos en todo el rango de medida. El aspecto fundamental consiste en que en un lecho estándar con distribuidor de placa perforada, el objeto acaba por desaparecer, quedando inmóvil en los huecos entre agujeros de la placa distribuidora. Por otro lado aumenta la incidencia de periodos de circulación muy largos a causa del paso del objeto por la zona. Estos efectos no existen (desaparición del objeto) o se minimizan (periodos largos) con el distribuidor rotatorio, lo que permite aumentar el rango de acción del lecho o recuperar objetos mediante la aplicación del actuador. Este trabajo incluye asimismo el estudio de la evolución de las distribuciones de probabilidad de los tiempos de circulación en función del tamaño del lecho, de la velocidad del gas y de la densidad y tamaño del objeto.

Abstract

Fluidized beds are employed in industry because of their excellent properties involving heat and mass transfer, and their capability to establish and promote chemical reactions inside them. A variety of processes can occur inside a fluidized bed, including drying, heat exchange, thermal conversion of solid fuels, and coating of particles. Most of the applications of fluidized beds involve the motion of objects inside the bed. Fuel particles, catalysts, and agglomerates are examples of typical objects found inside a fluidized bed. It is necessary to characterize the motion of these objects within the bed to establish the region of proper performance and to prevent operational problems such as the existence of hot or cold spots in a reactor or the appearance of de-fluidized zones due to the existence of agglomerates.

In this PhD thesis, the motion of large objects immersed in a bubbling fluidized bed was experimentally studied using digital image analysis. The experiments were performed in two facilities designed for such purpose, a 2-D bed and a lab-scale 3-D bed. Different objects were tested, varying density and size.

The main characteristics of the object motion were studied in the 2-D bed. By direct visualizations of the object trajectory, the preferential paths and the homogeneity of its spatial distribution were characterized. Then, the cycles described by the object in his way from and towards the surface of the bed were studied in detail. Every cycle consists of processes of descent and processes of ascent. In most cases, a series of movements of ascent and decrease interleaved along the path are observed. From this experimental evidence and considering every cycle independent from the previous history, four fundamental parameters can be used to characterize the cycles: the average rising and sinking velocities of the object, the maximum depth attained along the cycle and the number of independent rising movements (number of jumps) that take place in each cycle. Concerning the rising and sinking velocities, a methodology was established for the averaging calculations, as the existence of sudden changes of trend and vibratory movements complicate the separation of the processes. The object sinking motion is linked to the dense phase sinking motion and the object rising motion is linked to the evolution of bubbles. The probability of reaching the surface by the action of a

single bubble or jump was quantified, along with the existence and relative incidence of cycles with multiple jumps. Finally a simple semi-empirical model was defined to characterize the cyclical motion of the object, using the four fundamental parameters, the number of jumps during the cycle, the maximum attained depth and the average rising and sinking velocities. These latter two parameters were associated to well-known correlations for the average sinking velocity of the dense phase and the average bubble velocity, while the former ones were characterized in relation with the circulation time of the object and also in his respective distributions of probability.

The procedure is tested for a neutrally-buoyant object and the results are presented. Then, the procedure is applied to objects with different sizes and densities to study the incidence of buoyant forces. The effect of the gas velocity is also studied. The results show that the semi-empirical model possesses general validity within the range of our experiments. This includes variations of the object density from lightly higher to that of the bed to values lower than half of it, changes of object size around one order of magnitude and even changes of the height of the bed and of the distribution of sizes of the material that conforms the bed. The distribution of probabilities for the number of jumps follows a geometric decay. As a consequence, a value of 45 % is obtained for the average probability by which an object that starts rising by the action of a bubble finishes in the surface of the bed without detaching from it or its trail. This also implies that there is a 55 % probability that the cycle will have a new jump. This average value is kept constant for all the experimental conditions tested. Also a parabolic profile is obtained for the distribution of depths, which can be explained considering the preferential paths of both objects and bubbles. Throughout the study, a negligible effect of buoyant forces is observed during the object rising motion, while it is relatively important and coherent with the above mentioned forces in the sinking path.

Finally, a practical application of object motion in a 3-D bed is presented. The circulation time of the objects is measured acquiring images of the surface of the bed. A comparison is made between the distributions of circulation times for a standard bed and for a bed in which an actuator is used to modify and improve the bed dynamics. The actuator consists on a low-frequency rotation of the bed distributor. The results show an improvement of the circulation of objects in the whole range measured. The fundamental aspect consists on the fact that in a standard bed with a perforated plate distributor, the object usually disappears after several cycles, and remains in the dead zones between the holes of the distribution plate. On the other hand, the incidence of long periods increases as a consequence of objects passing though the surroundings and being affected proportionally. These effects do not exist (disappearance of the

object) or are minimized (long periods) when using the rotating distributor. This result suggests the possibility of increasing the range of bed parameters that assure a proper object circulation, or that to recover objects, by means of the application of the actuator. This work also includes a study of the evolution of the probability distributions of the circulation time depending on the height of the bed, on the speed of the gas and on the density and size of the object.

Chapter 1

Introduction

Fluidization is the phenomenon by which solid particles behaves in a fluid-like manner when there is a vertical flow of fluid. The characteristics of the fluidized bed vary depending on whether the fluid is a gas or a liquid, giving gas-solid or liquid-solid fluidization. For gas-solid fluidized beds, different regimes appear inside the bed, depending on the gas velocity.

Fluidization requires a fluid flow beyond a certain minimum. When a low flow of gas passes through a bed of fine particles, the gas merely percolates through the spaces between stationary particles. This is called a fixed bed. For higher flow rates, when the local gas velocity equals the terminal velocity of the solid particles, the particles begin to be suspended in the gas, presenting a radical reduction of the friction between adjacent particles. This kind of bed is referred to as incipiently fluidized bed or bed at minimum fluidization. The increase of the gas velocity above minimum fluidization velocity usually produces instabilities in the bed and the appearance of bubbles of gas, which is called a bubbling fluidized bed. Next, a turbulent motion of solids and voids is observed when increasing the gas velocity even more, resulting in a turbulent fluidized bed. Higher gas velocities produce the pneumatic transport of the solids that conform the bed. This regime is used in circulating fluidized beds.

Fluidized beds are employed in industry because of their excellent properties involving heat and mass transfer, and their capability to establish and promote chemical reactions inside them. In parallel to the wide range of applications, there is a wide range of scales concerning fluidized beds, from small dryers to huge fluidized bed reactors.

The focus of this PhD thesis is the study of the motion of objects immersed in a bubbling fluidized bed (BFB hereafter).

1.1 Liquid-like behavior of fluidized beds

A fluidized bed exhibits a liquid-like behavior, provided that the gas velocity exceeds the minimum fluidization velocity. This liquid-like behavior can be observed carrying out some easy experiments:

- When the fluidized bed vessel is tilted, the surface of the bed will remain horizontal.
- If there is a hole at the bed wall, a jet of particles comes out of the bed, with a velocity similar to $\sqrt{2 \cdot g \cdot h_b}$, where h_b is the height of the bed.
- The surfaces of two beds that are connected are at the same height; otherwise a flow of particles would pass from the deeper bed to the shallower one.
- The differential pressure between two points of the bed can be calculated as the weight of the bed per unit area between the two points (hydrodynamic pressure).
- An object with a lower density than the bed (generally named flotsam object) would suffer an ascending buoyant force, while an object with a higher density than the bed (jetsam object) would suffer a descending force.

1.2 Effect of bed particles on fluidization

The properties of a gas-solid fluidized bed may differ due to differences on the characteristics of the particles that conform the bed. Geldart (1973) classified solids into four different groups with similar properties, depending on the difference in density between solid and gas, and the solids diameter. Geldart's groups are reported in Figure 1.1.

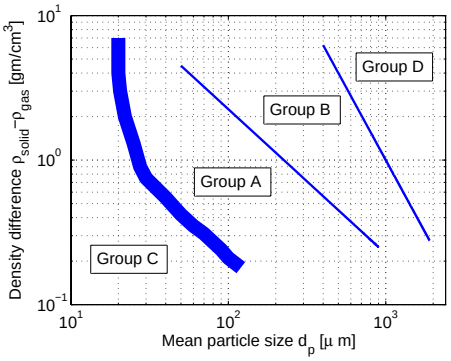

Figure 1.1: Geldart's classification of particles for fluidization with air at atmospheric pressure (adapted from Geldart (1973)).

Type A particles (aeratable particles) can be easily fluidized. The bed shows a large expansion prior to the appearance of bubbles. Bubbles rise faster than the gas

percolating through the emulsion and there is a maximum size for bubbles, which is relatively small, around 10 cm.

When fluidizing type B particles (sand-like particles), bubbles appear in the bed as soon as the minimum fluidization velocity is exceeded. Bubbles are produced near the distributor and grow and coalesce during their rising path through the bed, becoming large and producing a vigorous fluidization.

The fluidization of type C particles (cohesive particles) is extremely difficult since inter-particle forces are larger than the forces produced by the gas motion. Channels are formed from the distributor of the bed to the bed surface, with no fluidization of solids.

Type D particles (spoutable particles) are difficult to fluidize due to its erratic behavior. Large exploding bubbles or severe channels are formed, and the presence of spouts is typical of beds using these particles.

Molerus (1982) explained the four groups based on the forces that appear inside the fluidized bed. These forces include cohesive inter-particle forces, gravity forces and drag forces. Cohesive inter-particle forces are the relevant forces when fluidizing type C particles, whereas for type D particles gravity is the dominant force. Gravity and drag forces are of the same order when operating with type B particles, whereas the three forces are similar for type A particles.

1.3 Motion of objects inside a fluidized bed.

A large variety of fluidized bed applications involve the motion of objects within the bed. Fuel particles, catalysts, and agglomerates are typical examples of such objects. Others are involved in drying or coating processes. It is necessary to characterize the motion of these objects within a bed for a proper design, to ensure overall circulation and to prevent operational problems such as the existence of hot or cold spots and the appearance of de-fluidized zones due to the existence of agglomerates.

Several authors have analyzed the motion of objects inside fluidized beds, based on experimental studies carried out in 2-D or 3-D beds. This studies can be divided in two categories, depending on the focus of the work: i) those in which the object has similar characteristics (size and density) than the bed material and can be considered a tracer, intended to analyze the motion of the dense phase, and ii) those in which the object is larger than the bed material or/and has a different density, where the motion of the object (reactant, catalysts, passive particle or agglomerate) is the focus of the work.

A detailed revision of the literature can be found in the introductions of chapters

3 to 5. The main picture, however, is as follows:

- Objects sink in the bed following the dense phase motion and rise by the action of ascending bubbles.
- Both sinking and rising processes are subjected to modifications when buoyant forces are present.
- Bubbling beds (except when very shallow) usually establish a 2-vortex configuration. In such cases the object usually sinks at the sides of the bed and rises through the central part.
- An object usually needs a number of passing bubbles to rise to the freeboard. This is called multiple-jerk or multiple-jump behavior. Between the rising jumps, the object performs sinking processes following the local dense phase.
- Objects with densities similar to the bed density usually circulate throughout the whole bed, with a sinking velocity in good agreement with the Kunii and Levenspiel (1991) correlation for the velocity of the dense phase.
- Objects with large density differences to that of the bed show a relative motion to the dense phase due to significant buoyant forces. The relative velocity is then linear with density.
- The mean rising velocity of objects is lower than the velocity of bubbles. There are huge differences between authors concerning the mean rising velocity of a neutrally buoyant object. It is expected to range roughly between 10 % and 30 % of the mean bubble velocity along the bed. There are well established correlations for this last velocity. The huge gap between the results of different authors may lay in the lack of knowledge concerning the multiple-jump behavior and in some uncertainty in defining bed and object density. This last one may vary by means of a de-fluidized hood of dense phase particles forming on top of the object.

1.4 Scope of the thesis

This thesis presents an experimental work focused on the study of the motion of large objects within a bubbling fluidized bed. Different measurement techniques have been employed. A set of different Digital Image Analysis (DIA) techniques were used to track the object and to characterize the bubbles, Particle Image Velocimetry (PIV) was used to determine the dense phase velocity, and pressure measurements were employed to describe the bed dynamics.

Two different experimental setups have been used in this thesis, a 2-D BFB where the entire object path can be observed and a 3-D BFB where the object can only be observed when it reaches the freeboard. The general aspects of the motion of objects, the multiple-jump behavior and the mean sinking and rising velocities were studied in the 2-D bed and compared with the dense phase and bubbles motion. Also the incidence of buoyant forces and the effect of object density and size was characterized. An experimental model to characterize object circulation times is developed and extended to 3-D beds. Finally, when operating with the 3-D bed, an actuator in the form of a rotation was applied to the distributor and its effect on the object motion was analyzed. The interest for industrial applications of such an actuator was described.

This PhD thesis has been organized in six chapters. Chapters 3 to 5 present the results of this work and have been written as independent articles with its own abstract, introduction, notation, and bibliography.

Chapter 2 describes the two experimental facilities employed during the tests. The bed design, the measurement systems and the general bed dynamics are described for both facilities. In the case of the 3-D facility the design of the distributor was also explained.

Chapter 3 shows an analysis of the motion of a neutrally-buoyant object immersed in a 2-D BFB. Special attention is focused on the circulation time of the object and its distribution. It was found to depend on four main parameters: i) the mean sinking velocity of the object, ii) its mean rising velocity, iii) the maximum depth attained by the object, and iv) the number of jumps or number of bubbles needed for the object to go back to the freeboard. Empirical expressions are given in this chapter to estimate the circulation time distribution of the object. The object was also tested in the 3-D bed and the expressions obtained in the 2-D bed to estimate the circulation time were extended to the 3-D bed, and compared with the experimental data.

Chapter 4 discusses the effect of buoyant forces on the object motion. Different objects were analyzed in the 2-D BFB and a similar analysis to that presented for the neutrally-buoyant object was carried out.

Chapter 5 presents an analysis of the effect of a rotating distributor on the motion of objects within a 3-D BFB. The improvements linked to the distributor rotation are analyzed based on the capability of the bed to produce the circulation of a variety of objects and the reduction of the incidence of large circulation times.

Finally, the main conclusions of the thesis are summarized in chapter 6.

Chapter 2

Experimental Setup

Contents

2.1 Introduction 7

2.2 2-D bubbling fluidized bed 8

2.2.1 2-D facility 8

2.2.2 Measurement system 9

2.2.3 Bed dynamics 11

2.3 3-D bubbling fluidized bed 13

2.3.1 3-D facility 13

2.3.2 Measurement system 19

2.3.3 Bed dynamics 20

2.4 Notation 22

Bibliography 24

2.1 Introduction

Two different experimental facilities were employed in this PhD thesis, a 2-D and a 3-D bubbling fluidized beds. Chapters 3 and 4 show results taken from the 2-D facility, whereas in Chapter 5 the tests were carried out in the 3-D bed.

2.2 2-D bubbling fluidized bed

2.2.1 2-D facility

A 2-D facility was employed since 2-D beds permit to study bubble properties and object paths throughout the whole bed, using visualization techniques. Qualitative information about the fluidization phenomena can be also obtained (Grace and Baeyens, 1986). The facility consists on a 2-D column with a width, W, of $0.5\,m$, a height, H_{2D}, of $2\,m$, and a thickness, T, of $0.01\,m$. Figure 2.1 shows a schematic diagram of the experimental facility. The column was made of aluminum with a glass front wall to allow optical access. The rear wall of the bed was covered with a black paper to obtain a high contrast between dense phase (white) and bubbles (black).

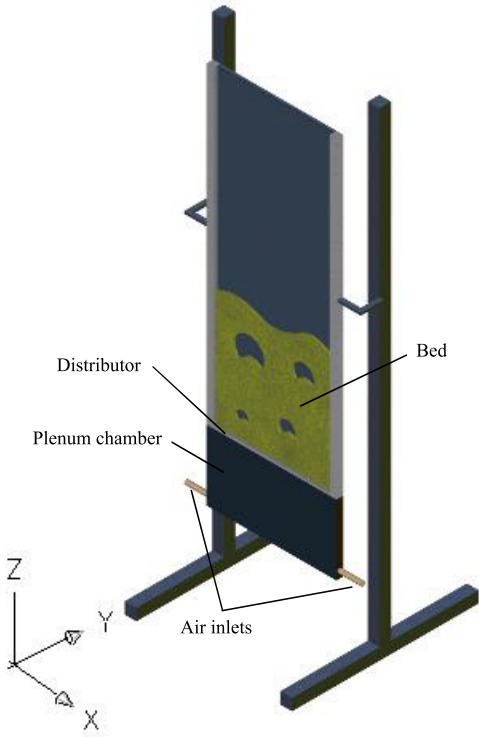

Figure 2.1: Schematic diagram of the 2-D facility.

The fixed bed height, h_b, was $0.5\,m$. This is high enough to guarantee the existence of a preferential path of bubbles, operating in a 2-vortex configuration according to Pallarès and Johnsson (2006) nomenclature. The dimensionless gas velocity U/U_{mf} was varied between 1.5 and 3, corresponding to a bubbling fluidization regime and reaching gas velocities similar to that employed in industrial applications (Koornneef et al., 2007). Higher dimensionless gas velocities produced a slugging regime in our bed, which is not the focus of this thesis.

Bed material

The bed material was glass spheres, ballotini particles, with diameters in the range $600 - 800\,\mu m$ and a density of $2,500\,kg/m^3$. This corresponds to type B according to Geldart's classification (Geldart, 1973). Figure 2.2 shows a photograph of the bed material captured by an electronic microscope. The bulk density of the fixed bed was measured to be $1,560\,kg/m^3$ according to *UNE-CEN/TS 15103 EX*, which corresponds with a void fraction of the packed bed, $\varepsilon_{packed} = 0.38$.

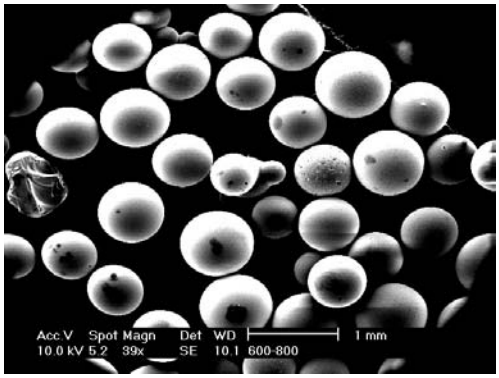

Figure 2.2: Photograph of the 2-D bed material captured by an electronic microscope.

Distributor

The air distributor was a perforated plate made of aluminum ($0.5 \times 0.01\,m^2$) with 2 lines of holes, each one consisting of 50 holes of $1\,mm$ diameter, d_0, and spaced $10\,mm$ apart, d_1. The two lines were separated by a distance, s, of $3.3\,mm$. Therefore, there was an open area of $1.5\,\%$. A schematic of the distributor is present in Figure 2.3.

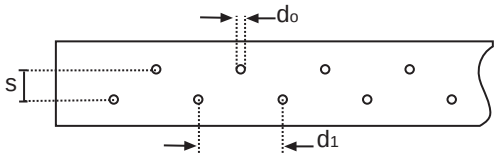

Figure 2.3: 2-D bed distributor scheme.

2.2.2 Measurement system

The measurement system is intended to characterize the motion of an object immersed in the bed. The motion of the dense phase and the bubbles was also studied for comparison. All those measurements were obtained using visualization and a set of imaging techniques, digital image analysis and particle image velocimetry. Finally, the bed performance was established by means of pressure probes.

Four spotlights of $650\,W$ were used during the characterization of the bubbles and dense phase to get a uniform illumination on the bed. The measurements of the object motion, both position and velocity, were carried out in complete darkness, since the object was coated with strontium aluminate to emit green light.

The bed performance was analyzed based on pressure measurements and visualization techniques, a schematic of the measurement system can be observed in Figure 2.4. Three piezo-electric pressure transducers (*Kistler type 5015*) were used to measure pressure fluctuations at the plenum chamber, at 0.2 and $0.3\,m$ above the distributor. Pressure fluctuations were measured through a $4\,mm$ internal diameter and $50\,mm$ long steel tube connected to the piezo-electric pressure transducer. The signal from the piezo-electric sensor was amplified by a Kistler amplifier. The response of this kind of probe and transducer is in good agreement with the model of Bergh and Tijdeman (1965), as stated by van Ommen et al. (1999). This model predicts the first resonance frequency to occur at $670\,Hz$, which is far away from typical characteristic frequencies in fluidized beds (in the $1-5\,Hz$ range). The sampling frequency was $200\,Hz$ and 12,032 samples per test were recorded. The amplifier acts as a high-pass filter with a frequency of $0.16\,Hz$, in order to obtain the pressure fluctuations relative to the local average pressure. The signal was also low-pass filtered at the Nyquist frequency by the amplifier. The pressure signals were analyzed in the time and in the frequency domains to obtain the minimum fluidization velocity and the characteristic frequency of the bed, respectively.

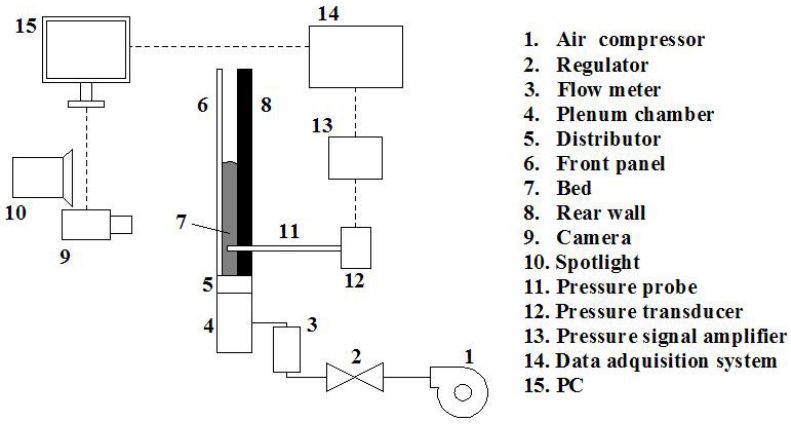

Figure 2.4: Schematic diagram of the measurement system for the 2-D facility.

Three different image acquisition systems were used during the experiments. A standard camera (*Nikon D80 10.6 Mpx*) was used to obtain the average motion patterns of the object and its velocity. The acquisition frequency was $1.6\,fps$ for position measurements (motion patterns) and $30\,fps$ for velocity measurements. The dense phase and bubble velocities were obtained using a high speed video camera (*Redlake Motion pro*

X3 4 Gb) with an acquisition frequency of 125 fps. Dense phase and bubbles were discriminated using a threshold of the grayscale map. Particle Image Velocimetry (PIV) was employed to determine the dense phase velocity, using the MatLab®, MatPIV 1.6.1 (Sveen, 2004). Digital Image Analysis (DIA) and averaging techniques were also performed using MatLab®, in order to characterize the bubbles in the bed.

2.2.3 Bed dynamics

Minimum fluidization velocity

The minimum fluidization velocity was determined by a linear regression of the standard deviation of the pressure signal, as proposed by Puncochár et al. (1985). They found that the variation of the pressure signal in a bed was due to the existence of bubbles and the standard deviation of the signal was a linear function of the gas velocity, as expressed in Equation 2.1.

$$\sigma = n + m \cdot U \tag{2.1}$$

The minimum fluidization velocity can be calculated as the velocity for which the standard deviation of the pressure signal is equal to zero (i.e. there are no bubbles), since the minimum bubbling velocity equals the minimum fluidization velocity for Geldart B particles (Geldart, 1973).

$$U_{mf} = -\frac{n}{m} \tag{2.2}$$

Figure 2.5 shows the standard deviation of the pressure signal for the pressure transducer installed at 0.3 m over the distributor as a function of the gas velocity.

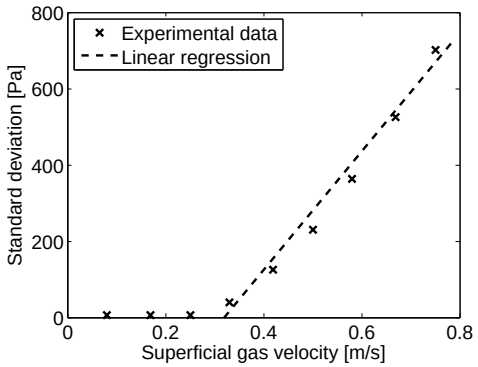

Figure 2.5: Standard deviation of the pressure signal measured at 0.3 m over the distributor (2-D facility).

The linear regression of the standard deviation is also plotted, and the minimum fluidization velocity obtained is 0.32 m/s. The experiments carried out in this thesis

with the 2-D facility were performed with gas velocities from 0.48 to 0.96 m/s, giving dimensionless velocities ranging from 1.5 to 3.

Characteristic frequency of the bed

The characteristic frequency of the fluidized bed was determined by a frequency domain analysis for a dimensionless gas velocity, U/U_{mf}, of 2.5. Figure 2.6 shows the power spectra using the Welch (1967) method, with all sub-spectra based on 4,096 samples. Considering the sampling frequency, 200 Hz, the power spectra have a frequency resolution of 0.049 Hz, which is a common and accepted value (Johnsson et al., 2000).

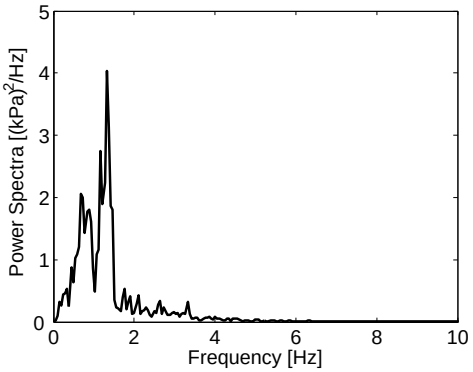

Figure 2.6: Power spectra obtained for $U/U_{mf} = 2.5$.

The characteristic frequency obtained from the power spectra was 1.51 Hz, which is in the range of typical frequencies for fluidized beds ($1 - 5\,Hz$).

Distributor pressure drop

According to Karri and Werther (2003) and Kunii and Levenspiel (1991) the pressure drop along the distributor, ΔP_{dist}, should be larger than 30 % the pressure drop along the bed, ΔP_{bed}, for a proper velocity distribution. This value guarantees the equal distribution of gas through parallel paths even if unsteady pressure fluctuations appear inside the bed. This was ensured for all experiments in this thesis.

The pressure drop along the bed is

$$\Delta P_{bed} = (1 - \varepsilon) \cdot \rho_p \cdot g \cdot h_b \tag{2.3}$$

where ΔP_{bed} is the pressure drop along the bed, ε the bed void fraction, ρ_p the dense phase particles density, g the gravity, and h_b the bed height.

Figure 2.7 shows the parabolic fitting of the experimental pressure drop through the distributor versus the dimensionless gas velocity, U/U_{mf}. The 30 % of the bed pressure

drop, determined for a bed aspect ratio of 1, is also plotted in the figure. Dimensionless gas velocities during the experiments in the 2-D facility ranged from 1.5 to 3.

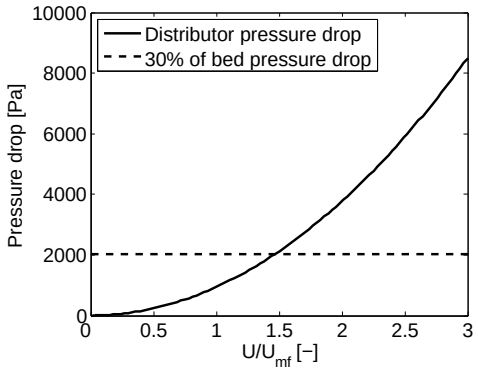

Figure 2.7: Pressure drop through the distributor (2-D facility).

2.3 3-D bubbling fluidized bed

2.3.1 3-D facility

The experimental setup consists on a lab-scale cylindrical BFB, equipped with an electrical motor in order to produce a rotation of the distributor. The cylindrical vessel of the bed is a transparent tube with an inner diameter of $0.192\,m$, D, and $1\,m$ in height, H_{3D}. The fixed bed height, h_b, was varied throughout the experiments between $0.25D$ and $0.75D$, being $0.5D$ the nominal case. Figure 2.8 shows a schematic diagram of the 3-D facility.

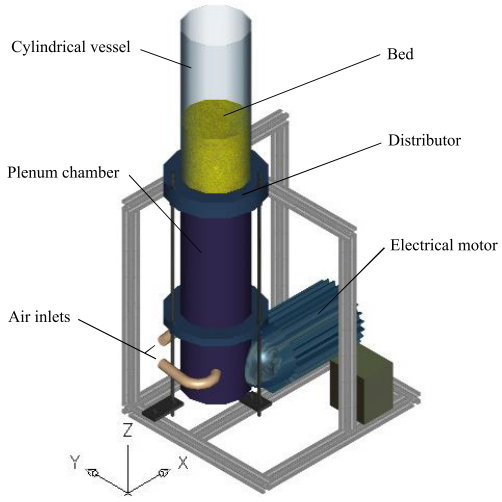

Figure 2.8: Schematic diagram of the 3-D facility.

Bed material

Silica particles, classified as Group B according to Geldart's classification (Geldart, 1973), were used as bed material. The particle density was determined by a pycnometer, giving an averaged density of $2,632.5\,kg/m^3$ and a standard deviation of $2.5\,kg/m^3$. A photograph of the particles captured by an electronic microscope is shown in Figure 2.9. The bulk density of the fixed bed was also measured according to *UNE-CEN/TS 15103 EX*, giving a value of $1,630\,kg/m^3$, which corresponds with a void fraction of the packed bed, $\varepsilon_{packed} = 0.38$.

Figure 2.9: Photograph of the 3-D bed material captured by an electronic microscope.

The particle size distribution of the bed material was measured, according to *UNE-EN 933-1*, for a dry sample of $2\,kg$ that was poured over a sieving column consisting on 8 sieves, with apertures of 1000, 850, 600, 425, 250, 180, 106, and $53\,\mu m$. The mass of sample retained in each sieve was weighted, after a time period of mechanical vibration large enough to guarantee steady conditions, and the percentage in each sieve was calculated. Figure 2.10 shows the cumulative particle size distribution, such a distribution has a mean diameter of $637\,\mu m$.

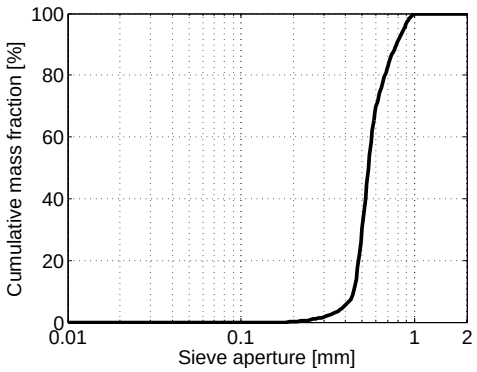

Figure 2.10: Particle size distribution of the 3-D bed material.

Distributor

Generally speaking, the fluidized bed gas distributor is intended to: i) support the bed material weight during non-operational periods, ii) avoid weepage of solids into the plenum, iii) operate for long periods providing uniform and homogeneous fluidization across the whole bed, and iv) minimize de-fluidized zones (dead zones) above the plate.

There are several kinds of distributors, such as perforated plates, porous plates, bubble caps and nozzles, spargers, conical grids, and pierced sheet grids among others. In our case, a perforated plate was selected since they are the most common distributor used in industry due to simple fabrication, capability of modification, durability, and price. Perforated plate distributors have some drawbacks such as weepage of bed material to the plenum, possible heterogeneous fluidization, existence of dead zones between holes, and requirement of sealing in the distributor-vessel link. All these drawbacks should be minimized during the design process of the distributor.

Weepage of bed material into the plenum was avoided by adding a grid, with 200 μm in aperture and 30 % open area, just under the perforated plate. The grid aperture was smaller than 99.9 % of the particles that conformed the bed, so weepage to the plenum was prevented. The sealing was carried out by a velvet joint placed between the perforated plate and the flanges, which also reduced the friction between the plate and the flanges, allowing it to rotate. Figure 2.11 shows a scheme of the arrangement.

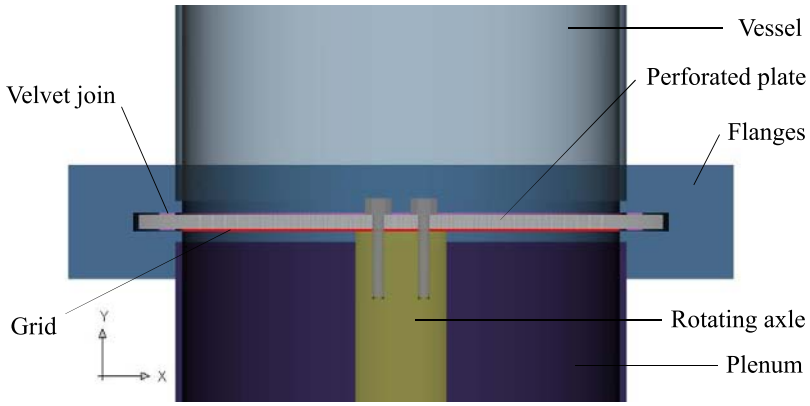

Figure 2.11: 3-D bed distributor scheme.

As far as the dead zones over the distributor are concerned, the number of holes of the perforated plate should be as greater as possible in order to reduce the pitch, L_h (distance between adjacent holes). On the other hand, taking into account the necessity of a homogeneous fluidization, the distributor must provide a pressure drop high enough to guarantee equal resistances through parallel paths inside the bed, thus the number of holes should be low enough from this point of view. Therefore, a compromise between the dead zones and the homogeneous fluidization problems should be reached

to determine the number of holes of the plate.

An analytical model was developed to characterize the total pressure drop along the distributor, i.e. the combination of the grid and the perforated plate effects, as a function of the number of holes. The selected plate was $6\,mm$ in thickness, t_d, to provide a high rigidity. A certain number of $2\,mm$ internal diameter holes, d_h, would be drill in a triangular mesh, as can be seen in Figure 2.12. Therefore, the pitch can be calculated as a function of the number of holes by Equation 2.4.

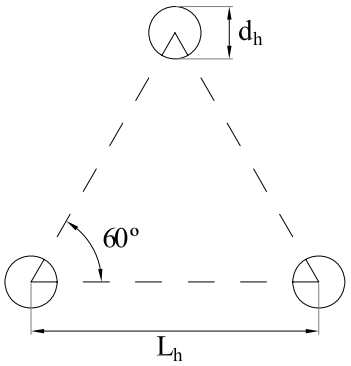

Figure 2.12: Triangular mesh of holes of the perforated plate.

$$L_h = \frac{1}{N_h \cdot \sin(60)} \tag{2.4}$$

As stated in section 2.2.3 the pressure drop along the distributor should be larger than 30 % the pressure drop along the bed, ΔP_{bed} (Equation 2.3), for a proper velocity distribution. The number of holes was selected as the maximum value that fulfilled the pressure drop criterion, in order to reduce the dead zones over the distributor while minimizing the power consumption.

The perforated plate and the grid pressure drops were estimated separately. A discharge coefficient is usually employed to determine the pressure drop produced by a perforated plate, as shown in Equation 2.5.

$$\Delta P_{plate} = \frac{\rho_g}{C_D} \cdot \frac{u_h^2}{2} \tag{2.5}$$

Most authors estimate this coefficient value to be 0.6 (Kunii and Levenspiel, 1991), a typical value for a sharp-edge orifice. Nevertheless, perforated plates are not usually sharp-edged and, therefore, greater values are expected. A better evaluation of the parameter can be found in Karri and Werther (2003). Here the discharge coefficient is calculated depending on the plate thickness, t_d, the holes diameter, d_h, and the pitch, L_h. Using Figure 2.13 a thickness-diameter ratio of 3 gives a value of the parameter τ^* of 0.99, so the discharge coefficient can be calculated from Equation 2.6.

$$C_D = \tau^* \cdot \left(\frac{d_h}{L_h}\right)^{0.1} \tag{2.6}$$

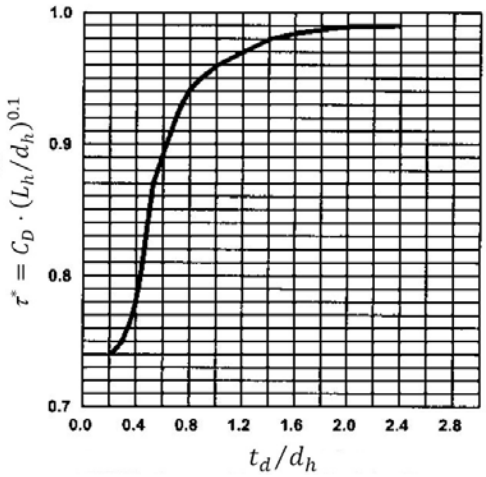

Figure 2.13: Discharge coefficient of the perforated plate (adapted from Karri and Werther (2003)).

The gas pressure drop through the grid was determined according to Fried and Idelchick (1989). Equation 2.7 shows a correlation for the grid pressure drop as a function of the grid open area, f_{grid}, which is valid for a Reynolds number greater than 10^3.

$$\frac{\Delta P_{grid}}{\rho_g \cdot \frac{u_h^2}{2}} = \tau_{grid} = 1.3 \cdot (1 - f_{grid}) + \left(\frac{1}{f_{grid}} - 1\right) \tag{2.7}$$

The analytical estimate of the pressure drop was related to the gas velocity into the holes so far, nevertheless it can be corrected to the gas superficial velocity in the bed by the bed-holes area ratio square, as reported in Equation 2.8

$$\Delta P_{bed} = \Delta P_{plate} + \Delta P_{grid} = \frac{1}{C_D} \cdot \left(\frac{A_{bed}}{N_h \cdot A_h}\right)^2 \cdot \rho_g \cdot \frac{U^2}{2} + \tau_{grid} \cdot \left(\frac{A_{bed}}{N_h \cdot A_h}\right)^2 \cdot \rho_g \cdot \frac{U^2}{2} \tag{2.8}$$

Figure 2.14 illustrates the potential (inverse) dependence of the distributor pressure drop on the perforated plate number of holes, considering a dimensionless gas velocity of 1.5. The 30 % of the bed pressure drop is also plotted in the figure, for a bed aspect ratio, h_b/D, of 0.5.

The analytical model predicts the distributor pressure drop to be lower than the 30 % of the bed pressure drop around 275 holes. Therefore, 275 holes were selected to fulfil the pressure drop criteria with minimum power consumption, giving around 9,500 holes per square meter and a triangular mesh pitch of 11 mm. The open area of the

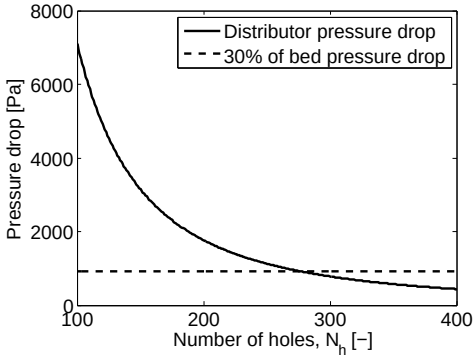

Figure 2.14: Variation of the distributor pressure drop with the number of holes.

distributor is around 3 %. With such a number of holes per square meter, the bubble sizes are virtually the same as those from a porous plate just a few centimeters above the distributor (Geldart and Baeyens, 1985).

Baeyens (1973) studied the influence of bubbles on the particles motion and concluded that for particles to move over the entire perforated plate (reducing dead zones) the condition given at Equation 2.9 must be fulfilled.

$$L_h < \lambda \cdot d_{b0} \tag{2.9}$$

where λ is a function of the particle mobility (for a conservative design λ is fixed to 1 for Geldart B and D solids (Geldart, 1973)), and d_{b0} is the initial bubble size produced at the distributor, which can be calculated from Equation 2.10 (Davidson and Schüller, 1960), resulting in 15.3 mm for the design superficial gas velocity ($1.5U_{mf}$). Therefore, with a pitch of 11 mm the condition of Equation 2.9 is fulfilled and dead zones over the distributor are reduced.

$$d_{b0} = 1.3 \cdot \left(\frac{U^2}{g \cdot N_h^2} \right)^{0.2} \tag{2.10}$$

More recently, Rees et al. (2006) presented a new criteria related to the jet diameter, which they calculate using magnetic resonance. Following their study and correlations, in our case the pitch should be of around 8 mm (with a small variation for the different experimental conditions) to minimize the dead zones. This result is in fair agreement with our selection, which follows the standard procedure. Therefore, the distributor was finally constructed using the results of the first analysis which is well-established.

Perforated plate distributors produce gas jets coming from the holes during its operation. The gas jets influence zone over the distributor must be determined to prevent placing pressure probes in this zone, in order to avoid the effect of jets in the pressure signal. There are several correlations for the jet length in the literature, but

for systems in which there is no secondary gas supply, i.e. all the gas enters the bed through the perforated plate holes, the correlation proposed by Merry (1975) shown in Equation 2.11 is well-established, presenting reasonable agreement with experimental data.

$$\frac{L_J}{d_h} = 5.2 \cdot \left(\frac{\rho_g \cdot d_h}{\rho_p \cdot d_p}\right)^{0.3} \cdot \left[1.3 \cdot \left(\frac{u_h}{g \cdot d_h}\right)^{0.2} - 1\right] \tag{2.11}$$

The jet length predicted by Equation 2.11 is plotted in Figure 2.15 for a wide range of superficial gas velocities, corresponding from 0 to 3 times the minimum fluidization velocity. The jet length increases with the superficial gas velocity, never reaching 15 mm in the velocity range analyzed. Therefore, 30 mm (two times the maximum jet length) over the distributor was considered a proper security zone to avoid the jet influence, and no pressure probes were located there.

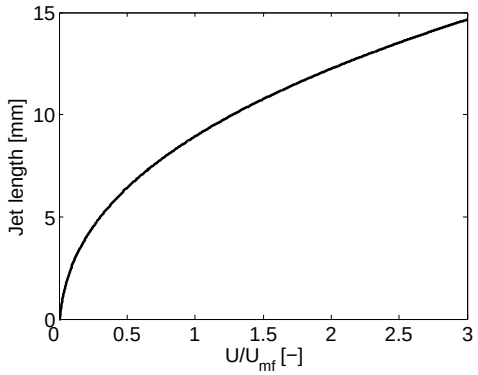

Figure 2.15: Jet length predicted by Equation 2.11.

2.3.2 Measurement system

Two different measurement techniques were applied to the 3-D fluidized bed. Visualization techniques were used to capture the surface of the bed. On the other hand, pressure probes were connected to the plenum chamber and in the bed at 0.2 and 0.3 m above the distributor. Figure 2.16 shows a schematic diagram of the experimental setup with the main components.

The pressure analyzers and the signal postprocessing were those already mentioned for the 2-D facility, section 2.2.2.

During all the tests, the surface of the bed was video recorded with a recording speed of 30 fps. The resolution of the camera was 480×640 pixels. The videos were post-processed using Matlab®. Both the object positions while at the freeboard and the time periods of disappearance from it (the circulation time for the sinking-rising

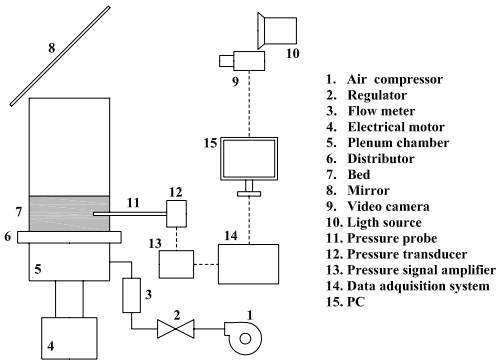

Figure 2.16: Schematic diagram of the measurement system for the 3-D facility.

global cycle) were obtained from the videos.

2.3.3 Bed dynamics

Minimum fluidization velocity

The minimum fluidization velocity was determined from the standard deviation of the pressure signal according to Puncochár et al. (1985) as stated in section 2.2.3.

Figure 2.17 shows the standard deviation of the pressure signal as a function of the air velocity, operating with both the static and the rotating distributor. The linear regression of the standard deviation is also plotted in the graph for both configurations.

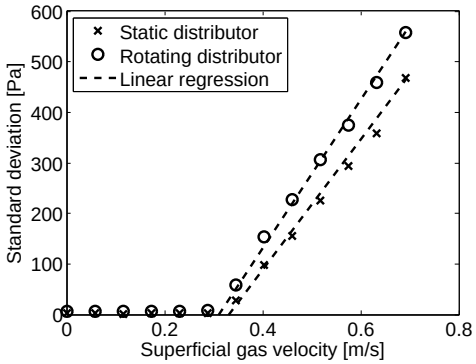

Figure 2.17: Standard deviation of the pressure signal measured at $0.3\,m$ over the distributor (3-D facility).

The minimum fluidization velocity was $0.31\,m/s$ for the rotating distributor bed and $0.33\,m/s$ for the static one, thus the minimum fluidization velocity slightly decreases with the rotation, a result previously stated by Sobrino et al. (2008).

Characteristic frequency of the bed

The characteristic frequency of the 3-D bed was determined by a similar analysis than that employed for the 2-D bed in section 2.2.3. Figure 2.18 shows the power spectra

obtained operating a bed with an aspect ratio, h_b/D, of 0.5 and a dimensionless gas velocity, U/U_{mf}, of 1.44

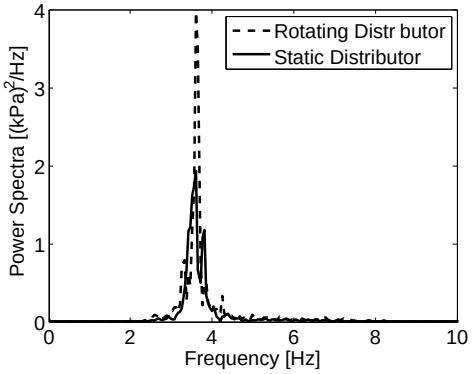

Figure 2.18: Power spectra, operating with the rotating and static distributor. ($U/U_{mf} = 1.44$, $h_b/D = 0.5$).

The power spectra show that the fluidized bed characteristic frequency, $3.61\,Hz$, is not affected by the rotating distributor, but the signal energy is almost doubled when the distributor rotates.

Distributor pressure drop

Once the number of holes of the distributor was selected and the distributor was made, the gas pressure drop through the distributor was experimentally determined by measuring the pressure at the plenum for various superficial gas velocities. Figure 2.19 illustrates the results in comparison with the analytical estimate and with the design criterion level. The analytical estimate was plotted for superficial gas velocities greater than $0.23\,m/s$ to obtain a Reynolds number based on the hole larger than 10^3, which is the necessary condition to apply Equation 2.7. The model prediction adjusts to the experimental data rather accurately for low superficial gas velocities, nevertheless when operating with high superficial gas velocities the experimental pressure drop increases faster than the analytical estimate, thus the pressure drop design criterion is fulfilled for lower gas velocities, producing a more homogeneous fluidization at the cost of higher power consumption. This difference between experimental and analytical data may be due to the fact that gas friction with the holes wall is significant for high gas velocities and was not considered for the estimate.

During the experiments carried out in the 3-D facility the dimensionless gas velocity, U/U_{mf}, were in the range $1.25 - 1.75$.

The pressure drop was also measured when the distributor was rotating. Figure 2.20 reports that the rotation of the distributor has no effect on the gas pressure drop, since the differences between the static and the rotating distributor were always below $4\,\%$.

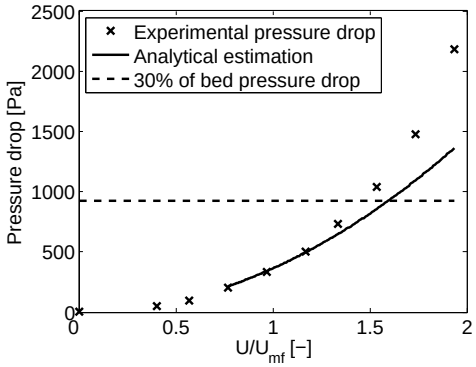

Figure 2.19: Comparison between the analytical estimate of the pressure drop and the experimental data.

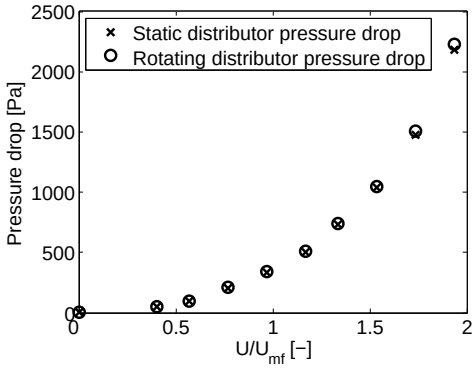

Figure 2.20: Effect of the distributor rotation on the pressure drop.

2.4 Notation

A_{bed} Area of the bed, $[m^2]$

A_h Area of holes of the distributor, $[m^2]$

C_D Discharge coefficient of the perforated plate orifice, $[-]$

D 3-D bed diameter, $[m]$

d_{b0} Initial bubble size, $[m]$

d_h Diameter of the holes of the distributor of the 3-D bed, $[m]$

d_p Dense phase particles diameter, $[m]$

d_0 Diameter of the holes of the distributor of the 2-D bed, $[m]$

d_1 Separation between consecutive holes of the distributor of the 2-D bed, $[m]$

f_{grid} Grid open area, $[-]$

g Gravity, $[m/s^2]$

h_b Fixed bed height, $[m]$

H_{2D} 2-D bed vessel height, $[m]$

H_{3D} 3-D bed vessel height, $[m]$

L_h Pitch of the 3-D bed distributor, $[m]$

L_J Jet length, $[m]$

m Constant, $[kg/(m^2 s)]$

n Constant, $[Pa]$

N_h Number of holes of the distributor of the 3-D bed, $[-]$

s Separation between the two lines of holes of the distributor of the 2-D bed, $[m]$

T 2-D bed thickness, $[m]$

t_d Thickness of the distributor of the 3-D bed, $[m]$

U Superficial gas velocity, $[m/s]$

u_h Gas velocity inside the holes of the distributor, $[m/s]$

U_{mf} Minimum fluidization velocity, $[m/s]$

W 2-D bed width, $[m]$

ΔP_{bed} Bed pressure drop, $[Pa]$

ΔP_{dist} Distributor pressure drop, $[Pa]$

ΔP_{plate} Perforated plate pressure drop, $[Pa]$

ΔP_{grid} Grid pressure drop, $[Pa]$

ε Void fraction of the bed, $[-]$

ε_{packed} Void fraction of the packed bed, $[-]$

λ Constant, $[-]$

ρ_g Gas density, $[kg/m^3]$

ρ_p Density of the dense phase particle, $[kg/m^3]$

σ Standard deviation of the pressure signal, $[Pa]$

τ^* Dimensionless parameter to calculate the discharge coefficient, $[-]$

τ_{grid} Dimensionless pressure drop along the grid, $[-]$

Bibliography

Baeyens J., 1973. Heat transfer in gas fluidized beds. *Phd Thesis*, University of Bradford, United Kingdom.

Bergh H., Tijdeman H., 1965. Theoretical and experimental results for the dynamic response of pressure measuring systems. *Report NLR-TR F.238, National Aero- and Astronautical Research Institute*, Amsterdam, the Netherlands.

Davidson J.F., Schüller B.O.G., 1960. Bubble formation at an orifice in a viscous liquid. *Transactions of the Institution of Chemical Engineers* 38, 145-154.

Fried E., Idelchick I.E., 1989. Flow resistance: a design guide for engineers, 1st ed., Hemisphere publishing corporation, New York, pp. 255-282.

Geldart D., 1973. Types of gas fluidization. *Powder Technology* 7, 285-292.

Geldart D., Baeyens J. 1985. The design of distributors for gas-fluidized Beds. *Powder Technology* 42, 67-78.

Grace J.R., Baeyens J. 1986. In: Geldart D. Gas Fluidization Technology. Wiley, Chichester, p. 415.

Johnsson F., Zijerveldb R.C., Schoutenb J.C., van den Bleek C.M., Leckner B., 2000. Characterization of fluidization regimes by time-series analysis of pressure fluctuations. *International Journal of Multiphase Flow* 26, 663-715.

Karri S.B.R., Werther J., 2003. Gas distributor and plenum design in fluidized beds. In: Yang W. C. Handbook of fluidization and fluid-particle systems, Marcel Dekker Inc., New York, pp. 164-179.

Koornneef J., Junginger M., Faaij A., 2007. Development of fluidized bed combustion - An overview of trends, performance and cost. *Progress in Energy and Combustion Science* 33, 19-55.

Kunii D., Levenspiel O., 1991. Fluidization Engineering, 2nd ed., Butterworth-Heinemann, Boston.

Merry J.M.D., 1975. Penetration of vertical jets into fluidized beds. *AIChE Journal* 21, 507-510.

Pallarès D., Johnsson F., 2006. A novel technique for particle tracking in cold 2-dimensional fluidized beds - Simulating fuel dispersion. *Chemical Engineering Science* 61, 2710-2720.

Puncochár M., Drahos J., Cermák J., Selucký K., 1985. Evaluation of minimum fluidization velocity in gas fluidized beds from pressure fluctuations. *Chemical Engineering Communications* 35, 81-87.

Rees A.C., Davidson J.F., Dennis J.S., Fennell P.S., Gladden L.F., Hayhurst A.N., Mantle M.D., Müller C.R., Sederman A.J., 2006. The nature of the flow just above the perforated plate distributor of a gas-fluidised bed, as imaged using magnetic resonance. *Chemical Engineering Science* 61, 6002-6015.

Sobrino C., Almendros-Ibáñez J.A., Santana D., de Vega M., 2008. Fluidization of Group B particles with a rotating distributor. *Powder Technology* 181, 273-280.

Sveen J.P., 2004. http://www.math.uio.no/∼jks/matpiv. (Last modified in August, 2004. Accesed in 2008).

van Ommen J.R., Schouten J.C., vander Stappen L.M., van den Bleek C.M., 1999. Response characteristics of probe transducer systems for pressure measurements in gas solid fluidized beds how to prevent pitfalls in dynamic pressure measurements. *Powder Technology* 106, 199-218.

Welch P.D., 1967. The use of a fast Fourier transform for the estimation of power spectra. *IEEE Trans. Audio and Electroacoustics* AU-15, 70-73.

Chapter 3

Motion of a neutrally-buoyant object in a 2-D Bubbling Fluidized Bed

Contents

3.1 Abstract **27**

3.2 Introduction **28**

3.3 Experimental Setup **30**

3.4 Results **32**

3.4.1 Dense phase and bubbles 32

3.4.2 Object motion pattern 34

3.4.3 Circulation time 36

3.5 Discussion **41**

3.6 Conclusions **45**

3.7 Notation **46**

Bibliography **48**

3.1 Abstract

The motion of a large object in a bubbling fluidized bed was experimentally studied using Digital Image Analysis (DIA). The experiments were performed in a 2-D bubbling fluidized bed with glass spheres as bed material. The object motion was measured using non-intrusive tracking techniques, while independent measurements of the dense phase

velocity (using Particle Image Velocimetry, PIV) and bubble velocity (using DIA) were carried out. The effect of the dimensionless gas velocity on the object motion was also analyzed.

In this Chapter the circulation patterns of an object with a density similar to that of the bed but much larger in size is characterized. Object size and density remained constant throughout the experiments. A comparison between the motion of sinking objects and the motion of the dense phase provided evidence of the feeble effect of buoyant forces on the motion of sinking objects. In contrast, the motion of rising objects is linked to the motion of bubbles. It was found that objects may be raised to the surface of the bed either by the action of a single bubble (one-jump) or by several passing bubbles (multiple-jumps). Based on these results, the circulation time of the object throughout the bed is a function of two parameters; the maximum depth attained by an object and the number of jumps during its rising path. This relationship is presented along and the multiple-jumps phenomenon is studied in detail. Finally, an estimate of the circulation time of an object based on semi-empirical expressions is presented for different dimensionless gas velocities. The probability density function of the circulation time shows two different modes as the object was less prone to be raised at moderate depths. The estimate of the circulation time was found to be in good agreement with our experimental data.

3.2 Introduction

Bubbling Fluidized Beds (BFB) are widely used in industry, from pharmaceutical to energy conversion systems; they are well-suited for processes involving heat and mass transfer as well as chemical reactions. Examples include drying processes, thermal conversion of solid fuels, and coating of particles. A wide range of these applications involves the motion of large objects within the bed. Examples of objects commonly used in a BFB include fuel particles, catalysts, reactants, and agglomerates; these objects will sink with the dense phase and rise in (or in a trail of) the bubbles. Buoyancy effects may play a significant role in the motion of objects in BFB, depending on the density ratio between the object and the bed. Object motion patterns and their ability to move throughout the bed or stay in a restricted zone has a paramount effect on several factors, including the performance of the reactor, the reaction time, the existence of hot or cold spots, and the behavior of agglomerates.

Several studies have focused on the motion of an object within a BFB, and most of these studies are based on experimental analysis, including experiments in 2-D and 3-D beds and using different measurement techniques. Attending the object characteristics,

the studies can be divided into two categories: those where the object had a similar density and size to the bed material, as well as those where the object was larger. The former were intended to characterize the motion of the dense phase, while the latter provided information of the motion of a fuel, catalyst or agglomerate particle. Several studies have investigated the motion of tracing particles that follow the dense phase using tracking and non-tracking techniques. Tomography-tracking techniques that are employed to characterize the motion of objects in 3-D beds include positron emission (Stein et al., 2000), X-ray (Grassler and Wirth, 2000), and electrical capacitance (Du et al., 2002) methods, while optical techniques (Shen et al., 2004; Bokkers et al., 2004) are used in 2-D beds. The motion of objects in fluidized beds has also been analyzed using non-tracking techniques (collecting data of the motion at a particular position in the bed), such as Laser Doppler Anemometry (Ibsen et al., 2002).

The first studies with regard to the motion of large objects were reviewed by Kunii and Levenspiel (1991). Rios et al. (1986) studied the motion of large objects in 2-D and 3-D beds and discussed the sinking and rising processes. They observed that an object was not always raised to the surface of the bed by a single bubble but was rather lifted small distances by a succession of passing bubbles, rising in a series of small jumps. Pallarès and Johnsson (2006) analyzed the motion of a phosphorescent particle in a 2-D bed for several configurations and observed that a characteristic 2-vortex configuration appears in most cases, with the exception of those where the bed was extremely shallow. In a 2-vortex configuration, an object with a similar density to the dense phase sinks at the side of the bed and rises at the center. Several authors have studied the sinking process. Lim and Agarwal (1994) found that the sinking velocity of a large object in a 2-D bed was in good agreement with the Kunii and Levenspiel (1991) correlation for the velocity of the dense phase for density ratios around 1. However, Tanimoto et al. (1981) and Hoffmann et al. (1993) showed that for large density ratios, a relative motion between an object and the dense phase existed and was linear with density. Nguyen and Grace (1978) and Rees et al. (2005) stated that the net buoyant force on an object in a fluidized bed might differ from what would be expected based on its density due to a de-fluidized hood of bed material that appears on top of the object. The rising velocity is related to the bubble velocity in a complex way. Complicating factors include the multiple jumps effect observed by Rios et al. (1986) and the relative motion between bubble and object, which are far more important than those between object and dense phase in the sinking process. The experimental works of Nienow et al. (1978) , Lim and Agarwal (1994), and more recently Rees et al. (2005) showed different results for the mean rising velocity, which is roughly between 10% and 30% of the mean bubble velocity along the bed.

There is a continued need to investigate the fundamentals of the motion of an object immersed in a fluidized bed, including the study of the limits of proper circulation, the description of the circulation patterns and preferential paths, the evaluation of the circulation time, and the study of the incidence of buoyant forces. This work evaluates the motion of a large object in a $0.5 \times 0.5\, m^2$ 2-D fluidized bed with a similar density to that of the bed. The object size and density remained constant during each experiment. The general patterns are presented and object sinking and rising velocities are determined. The focus of this Chapter is to characterize the cycles described by the object, sinking from the surface of the bed and rising back to this point. The circulation time, which is the time spent by the object in a cycle, was measured, and its dependence on the number of jumps needed and the maximum depth attained was analyzed. The effect of the dimensionless gas velocity on the circulation time of the object was also analyzed. Finally, a simple estimate of the circulation time of the object based on semi-empirical expressions was made.

3.3 Experimental Setup

The experiments were carried out in a 2-D column with a width, W, of $50\, cm$, a height, H_{2D}, of $2\, m$, and a thickness, T, of $1\, cm$. The column was made of aluminum with a glass front wall to allow optical access. The bed material was glass spheres, ballotini particles, with a diameter of $600 - 800\, \mu m$ and a skeletal density of $2,500\, kg/m^3$, type B according to Geldart's classification (Geldart, 1973). The bulk density of the fixed bed was measured to be $1,560\, kg/m^3$. Three piezo-electric pressure transducers (*Kistler type 5015*) were used to measure pressure fluctuations in the bed at the plenum chamber, at 20 and $30\, cm$ above the distributor. The pressure signals were analyzed in the time and in the frequency domains to obtain the minimum fluidization velocity (U_{mf}, $0.32\, m/s$) and the characteristic frequency of the bed (f_B, $1.51\, Hz$), respectively. The fixed bed height, h_b, was $50\, cm$, which is high enough to guarantee the existence of a preferential path of bubbles, operating in a 2-vortex configuration according to Pallarès and Johnsson (2006) nomenclature. The dimensionless gas velocity U/U_{mf} was varied between 1.5 and 3 (2.5 being the nominal case), corresponding to a bubbling fluidization regime and reaching gas velocities similar to that employed in industrial applications (Koornneef et al., 2007). Higher dimensionless gas velocities produced a slugging regime, which is not the focus of this PhD thesis. A schematic diagram of the experimental facility is presented in Figure 3.1.

The air distributor, described in section 2.2.1, produced a pressure drop high enough ($\Delta P_{dist} > 0.3 \cdot \Delta P_{bed}$) to ensure that the bed and the air supply system were independent

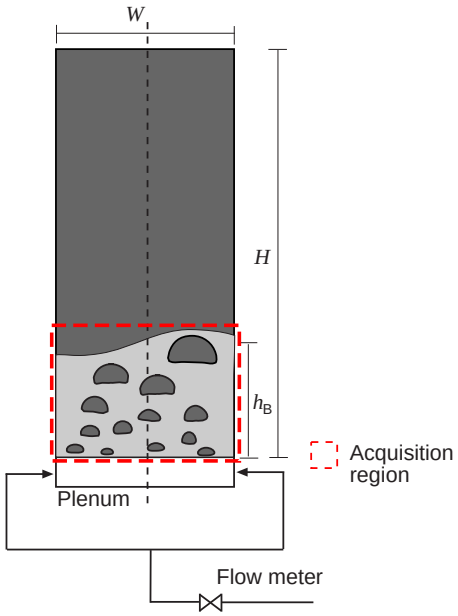

Figure 3.1: Scheme of the experimental facilityEEEE.

(Karri and Werther, 2003; Johnsson et al., 2000). Some industrial devices may operate with a smaller pressure drop in the distributor and this may alter the motion of objects within the bed. A typical drawback in such cases is the incidence of de-fluidized zones. Then the motion of the object should be studied in two cases, depending on whether it reaches a de-fluidized zone or not. In our work, this fact was not considered.

The object was a cylindrical biomass pellet with a density of $1,508\,kg/m^3$, a diameter of $6.4\,mm$, and a length of $19.2\,mm$. Therefore, the object-fixed bed density ratio was 0.97, and the object-bed material characteristic length ratio was approximately 9. The object density was selected in order to reduce the effect of buoyant forces. The effect of buoyant forces will be the focus of Chapter 4. Three different acquisition systems were used during the experiments. A standard camera (*Nikon D80 10.6 Mpx*) was used to obtain the average motion patterns of the object and its velocity. The acquisition frequency was $1.6\,fps$ for position measurements (motion patterns) and $30\,fps$ for velocity measurements. The dense phase and bubble characterizations were obtained using a high speed video camera (*Redlake Motion pro X3 4 Gb*) with an acquisition frequency of $125\,fps$. Average measurements of the object position and velocity and dense phase velocities were obtained. Dense phase and bubbles were discriminated using a threshold of the grayscale map. For the PIV measurements of the dense phase velocity, the MatLab®MatPIV 1.6.1 was used (Sveen, 2004). Digital Image Analysis and averaging techniques were also performed using MatLab®. The measurements of object motion (both position and velocity) were carried out in complete darkness. The object was coated with strontium aluminate to emit green light. Averaged object

position maps were obtained from 16,000 images, representing 10,000 seconds of BFB activity. For object velocity, 21,600 images were recorded, representing 720 seconds. Four spotlights of $650\,W$ were used during the characterization of the bubbles and dense phase to get a uniform illumination on the bed; the rear wall of the bed was covered by a black paper to obtain a high contrast between dense phase (white) and bubbles (black). Bubble and dense phase velocities were determined by averaging 9,810 images, which represent 78 seconds of the BFB activity. This measurement time (78 seconds), although rather small, has proved to give reproducible results.

At the end of the chapter, the object is also tested in the 3-D facility using the same ballotini particles as bed material, giving in this case a minimum fluidization velocity of $0.25\,m/s$. The bed aspect ratio was 1, just the same than for the 2-D bed. The surface of the bed was video recorded for 20 minutes at $30\,fps$, and the images were post-processed using Matlab®, in order to obtain the position of the object on the surface of the bed and the circulation time, defined as the time interval between consecutive appearances of the object at the surface.

3.4 Results

As explained in section 3.2, it is generally accepted that objects with densities similar to that of the bed will describe sinking-rising cycles throughout the whole bed, where the sinking motion is similar to that of the dense phase, and the rising motion is composed of a number of sudden jumps, as a result of the raising effect of passing bubbles. Experimental results in this section include the characterization of the dense phase and bubble motion, the averaged motion patterns of objects, and the study of object average sinking and rising velocities.

3.4.1 Dense phase and bubbles

Two different post-processing techniques, Particle Image Velocimetry (PIV) and Digital Image Analysis (DIA), were applied to characterize the dense phase and bubbles behavior throughout the bed. DIA was applied to establish the boundaries between the dense phase and the bubble phase. The analysis was based on the calculation and application of a threshold level over each image (Otsu, 1979). Using this technique, the two phases (dense phase and bubble phase) were clearly identified. Furthermore, different bubble properties could be calculated, such as the equivalent diameter and the mass center of the bubble. MatPIV 1.6.1 (Sveen, 2004) was employed to calculate PIV in the bed. Several authors have used this application on 2-D fluidized beds to

calculate and analyze dense phase velocities (Müller et al., 2007; Almendros-Ibáñez et al., 2009) and their fluctuations (Sanchez-Delgado et al., 2010). Interrogation windows of 16×16 pixels with a 50% overlap were used in the PIV analyses. The application of the threshold level to the grayscale image converts it into a binary image where the pixels occupied by bubbles have a value of $C = 0$, while the pixels occupied by dense phase have a value $C = 1$. Thus, the relative frequency that a point is occupied by the dense phase, C, can be calculated as follows:

$$C(i,j) = \frac{1}{N_P} \sum_{n=1}^{N_P} C_n(i,j) \tag{3.1}$$

where C_n is the instantaneous concentration once the threshold is applied (1 represents the dense phase and 0 represents the bubble phase), N_P is the total number of images, and i and j represent the pixel x-position and y-position, respectively.

The regions where $C(i,j)$ reaches higher values, close to one, represent a lower relative frequency of bubbles, and the regions with lower values of $C(i,j)$ represent the preferential bubble paths. Figure 3.2(a) shows the relative frequency of the dense phase at each location of the bed, $C(x,y)$. In the lower zone of the bed, close to the distributor, the relative frequency is almost uniform, so bubbles are equally distributed through the width of the bed in this zone. Then, two symmetrical preferential bubble paths are formed and develop from the distributor corners to the center of the bed. Further away from the distributor, the dense phase is more concentrated at the sides of the bed, while bubbles appear at the middle due to coalescence.

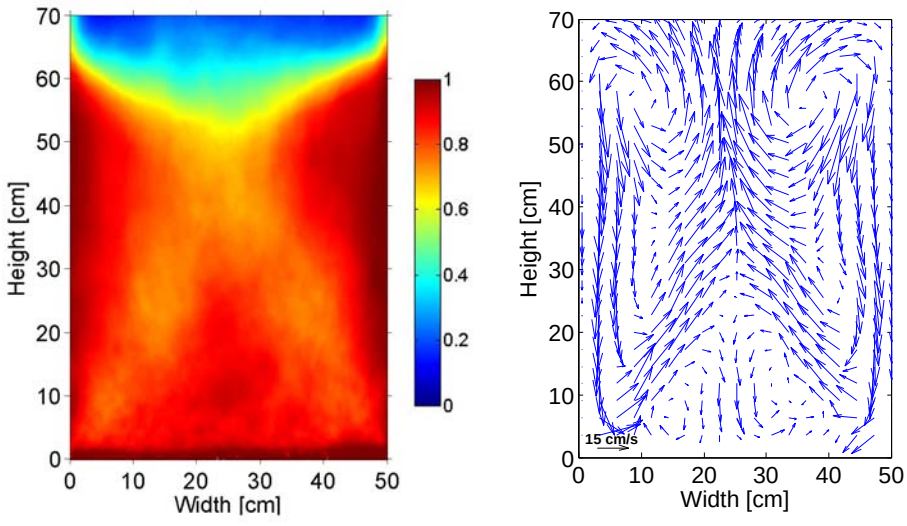

(a) (b)

Figure 3.2: (a) Relative frequency of dense phase and (b) time-averaged dense phase velocity.

The time-averaged dense phase velocity field (Figure 3.2(b)) was calculated by

averaging the instantaneous velocities obtained by PIV, as described in Laverman et al. (2008). The dense phase transport phenomena induced by bubbles during the rising motion (Rowe, 1973; Sanchez-Delgado et al., 2010) is described in Figure 3.2(b). The dense phase was found to descend at the sides of the bed while the ascending motion was located in the middle, corresponding to the bubbles' preferential path. Note that there was a triangular region of low velocities in the bottom zone, where small bubbles with no distinct preferential paths were present.

3.4.2 Object motion pattern

Previous studies (Lim and Agarwal, 1994) showed that objects that differ in size compared to the bed material circulate throughout the whole bed for a wide range of object densities around that of the fluidized bed. In contrast, much denser objects (jetsam) fall straight to the bottom and remain there, while much lighter objects (flotsam) are permanently kept near the surface of the bed. In this sense, a direct measurement of the relative frequency of the object presence at each position is important to characterize the object circulation.

The 16,000 images showing the object emitting a green light were transformed into black and white images applying a threshold. In these images, the center of mass of the object was determined, and the relative frequency of objects at certain positions of the bed was calculated, dividing it in 280 cells of $5 \times 5\, cm^2$. The relative frequency at each cell was calculated as the number of times that the center of mass of the object was present at that cell divided by the total number of images. Therefore, in zones where objects move with a lower velocity, a higher relative frequency will result. Figure 3.3 shows the relative frequency of objects at each position of the bed.

A comparison between Figure 3.2 and Figure 3.3 shows a similar behavior for both the object and the dense phase. An interesting difference is found at the central bottom zone, where objects seldom access. For a clearer understanding of object paths, a distinction between rising and sinking paths can be made in the calculations. Figure 3.4 shows the relative frequency of rising and sinking objects as a function of bed width, considering the entire height of the bed.

The preferential paths for the sinking and rising motions are evident in Figure 3.4. The objects rise at the center of the bed by the action of bubbles and sink at the sides following the dense phase. This is in accordance with bubble patterns and preferential paths in a 2-D BFB shown in Figure 3.2. This behavior is also in agreement with the results of Pallarès and Johnsson (2006).

The relative frequency of objects at each y-position (height above the distributor) is of paramount importance to characterize object circulation since it is an indicator

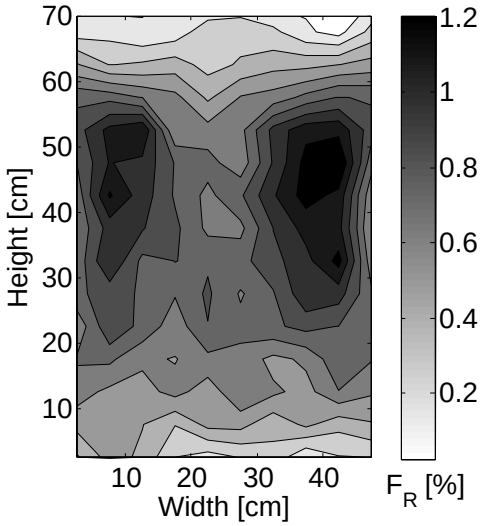

Figure 3.3: Relative frequency of objects at a certain position in the bed. Nominal case ($U/U_{mf} = 2.5$).

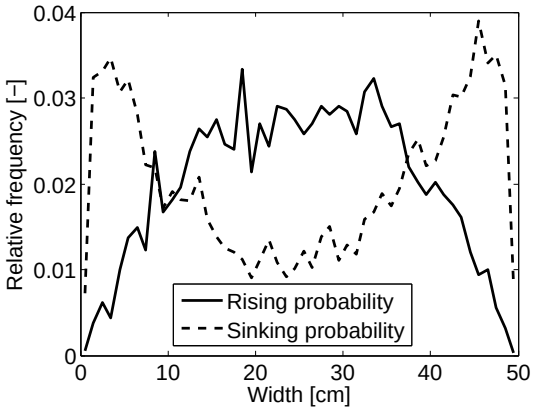

Figure 3.4: Relative frequency of a rising or a sinking object as a function of the x-coordinate of the bed (width). Nominal case ($U/U_{mf} = 2.5$).

of the capability of producing a homogeneous axial mixing. Figure 3.5(a) shows the relative frequency to find the object at each height.

Figure 3.5(a) shows the distribution of the object in the upper 2/3 of the bed was fairly homogeneous, while in the region near the distributor, at heights lower than $20\,cm$, objects were seldom present. This may be related to the inability of objects to reach the central bottom region of the bed described earlier (comparing Figure 3.2(a) and Figure 3.4).

To analyze the effect of the dimensionless gas velocity on object distribution through the entire height of the bed, the relative frequency to find the object in the upper part of the bed (higher than $30\,cm$, considering the fluidized bed average height to be $60\,cm$, 1.2 times the fixed bed height) was calculated. This parameter would be close to 50% for a homogeneous distribution of the object in the bed, close to 100% for flotsam objects that keep near the surface of the bed, and close to 0% for jetsam

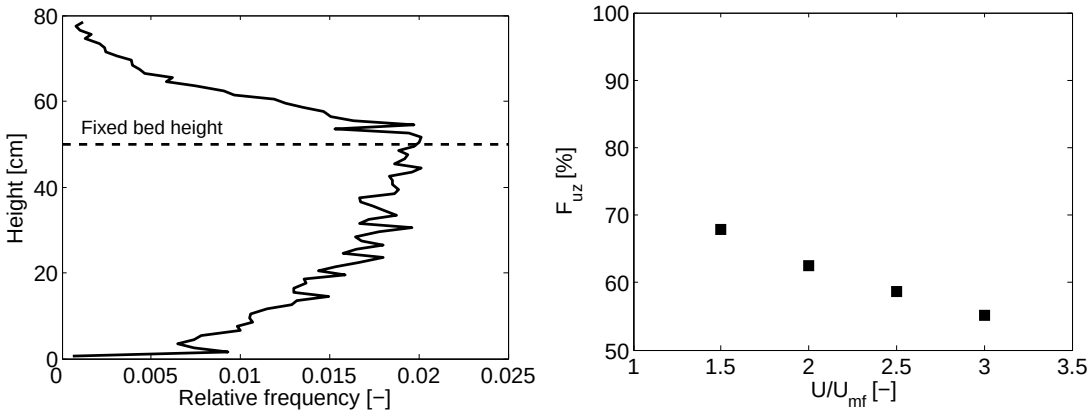

(a) (b)

Figure 3.5: (a) Relative frequency to find the object at a determined position as a function of the y-coordinate (height from the distributor) for the nominal case ($U/U_{mf} = 2.5$), and (b) effect of the dimensionless gas velocity on the distribution of the object through the bed.

objects which are always deep in the bed and seldom appear on the freeboard. The effect of the dimensionless gas velocity on this parameter is analyzed in Figure 3.5(b), where the relative frequency to find the object in the upper half of the bed is plotted. There is a linear relation of this parameter with the dimensionless gas velocity. For a range of dimensionless gas velocities (2, 2.5, and 3), the distribution seems rather homogeneous since the value of F_{uz} is near 50 %. An increase of the dimensionless gas velocity diminishes the relative importance of buoyant forces due to the increase of the fluidization intensity, a result stated previously by Otshitani et al. (2004). However, for very low dimensionless gas velocities ($U/U_{mf} = 1.5$), buoyancy effects become important and the object was more probably found in the upper part of the bed ($F_{uz} \simeq 70\,\%$).

3.4.3 Circulation time

The circulation time of an object is defined as the time interval between the instant when an object sinks into the bed from its surface until it returns to the surface (object cycle). This is one of the main parameters used to describe the motion of an object in a fluidized bed. It can be compared to the characteristic time of a chemical reaction when the object considered is a fuel or a catalyst (Gomez-Barea and Leckner, 2010). Nevertheless, note that during the experiments the object remained consistent in both size and density, and thus the results cannot be directly extended to processes where the object shrinks or changes its density.

The circulation time of an object will depend directly on its velocity during the cycle, so the mean object velocity was characterized during both the sinking and the

rising paths. Object velocity was determined by the difference in its position in two consecutive images divided by the time interval between images. In a first approximation, the mean rising and sinking velocities of an object can be determined averaging the measured positive (upwards) and negative (downwards) velocities, respectively; considering that all the positive velocities are grouped in the rising paths, and all the negative velocities occur during the sinking paths. However, the motion of the object is more complex and this simple procedure can lead to important miscalculations of the mean ascending and descending velocities.

Direct observation showed that the motion of an object could be described as a composition of several processes. There was a succession of jumps interleaved with periods when the object was sinking. During each jump, the object rose in a monotonic ascending manner as it was partially attached to an up-coming bubble (or in its trail). The sinking process was more complex. It followed a step-like descending motion, characterized by large downwards velocities that were maintained a fraction of a second and separated by low velocity periods in which the object vibrated over a given position. The word vibration is used since such a process added up to no net motion in any direction. These three types of motion can be clearly observed in Figure 3.6, where the actual trajectory and velocity of an object in a six seconds lapse is depicted. Figure 3.6(a) shows an image of the bubbling fluidized bed with the object trajectory superimposed. It consists of a sinking path (from A to B) and a rising path (from B to C). The velocities of the object along its trajectory are plotted in Figure 3.6(b). As stated, the object velocity was always positive (upwards) in the rising path, while the sinking path was characterized by small periods (around $0.1\,s$), with a frequency of around $2\,Hz$, in Figure 3.6(b) where the object fell fast, with high negative velocities (downwards), and periods of vibration, in which both negative and positive velocities were present.

Therefore, the rising process can be characterized by the mean ascending velocity inside a jump and the number of jumps, while the sinking process is quite more complex. If we consider it as a whole (for example, from A to B in Figure 3.6(a)) we can calculate a mean descending velocity defined as the distance between A and B divided by the time spent by the object moving from one to the other. This mean velocity will characterize the global sinking motion, even though the object seldom moved at such speed. In contrast, the object moved in the step-like manner previously described, alternating large velocities with periods of vibration in which small ascending and descending velocities occurred.

The mechanisms by which such motion was produced are not evident. It is clear that the source of any net movement is the bubble motion. This is evident enough during

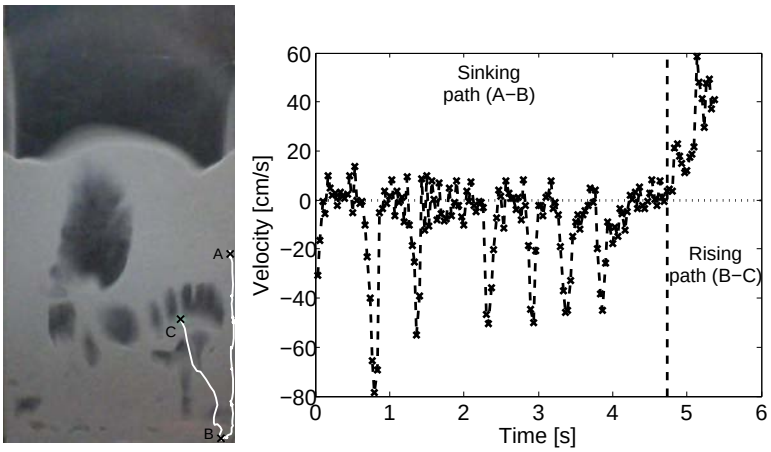

(a) (b)

Figure 3.6: (a) Object path in the bed and (b) Object velocity during the path. Nominal case ($U/U_{mf} = 2.5$).

the object jumps. The large descending velocities in the step-like sinking processes can also be associated with passing bubbles, which were raising dense phase from the bottom and carrying it to the surface of the bed (i.e, carrying particles from below to above the object). Concerning vibration, it can be related with pressure fluctuations in the fluidized bed (also linked with the bubble motion), but further work is needed to clarify this reasoning.

In view of these facts, a time-averaged velocity of an object during the sinking path was calculated as a first step to obtain the circulation time. The position of an object was sampled at different frequencies to determine its velocity. Considering the path described by the object in Figure 3.6(a), we were interested in sampling the position signal at such a frequency that only the object position between instants A and B were considered. Thus, the averaged velocity would be the difference in position at these two instants divided by the time spent by the object moving from A to B. Two complicating factors appeared when doing this automatically: i) to accurately define point B, so no information of the B-C path was used on the mean, and ii) to keep the positive or zero velocities during vibration in the averaging process, since they were part of the sinking process and neglecting them will increase artificially the mean value. The first factor could be minimized by increasing the acquisition frequency, while the second could be minimized by lowering it. Therefore, the sampling frequency had to be defined as a compromise of this two competing factors. Figure 3.7 plots the mean sinking velocity calculated for different sampling frequencies, averaging all of the downward velocities in the bed. The mean sinking velocity greatly diminished when the sampling frequency was reduced from 30 to $2-3\,Hz$ because vibration was being considered. This frequency ($2-3\,Hz$) was almost the measured characteristic frequency of the bed ($1.51\,Hz$). The

sampling of the signal at lower frequencies produced an exponential decay of the mean sinking velocity due to the loss of a well-established point B. An extremely low sampling frequency would produce the same effect as considering the object going directly from A to C describing just a sinking path but for the total time required. As sampling frequency continues diminishing, the mean sinking velocities would tend to zero. A similar effect was observed for different dimensionless gas velocities. Therefore, the mean sinking velocities were calculated in the following using a sampling frequency of $2\,Hz$.

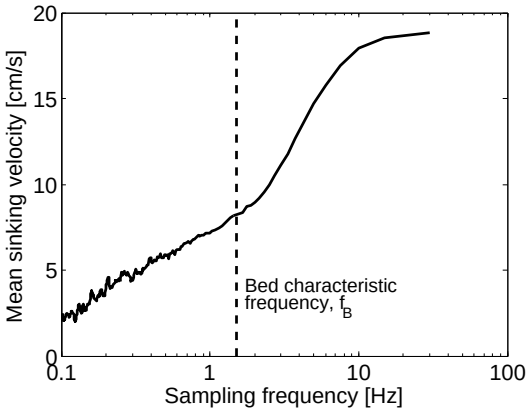

Figure 3.7: Mean sinking velocity in the whole bed, sampling the velocity signal at different frequencies.

Results of the mean sinking and rising velocities of an object for three different dimensionless gas velocities are presented in Figure 3.8. The mean sinking velocity is similar to the Kunii and Levenspiel (1991) correlation for the dense phase downward velocity (Equation 3.2), and it can thus be assumed that the object moves downward with the dense phase, as stated previously in the literature. However, the mean rising velocity represents roughly 20% of the mean velocity of bubbles, calculated with the widely used correlation of Shen et al. (2004) for the bubble diameter (Equation 3.3) and the correlation of Davidson and Harrison (1963) for the bubble velocity (Equation 3.4). This corresponds well with previous experimental evidence presented in section 3.2, although results are widely dispersed in the literature.

$$v_{dp} = \frac{f_w \cdot \delta \cdot U_B}{1 - \delta - f_w \cdot \delta} \tag{3.2}$$

$$D_B = \left[\left(\frac{8 \cdot \left(2^{3/4} - 1\right)}{\lambda} \right) \cdot (U - U_{mf}) \cdot \left(h + \frac{\lambda}{\pi \cdot (2^{3/4} - 1)} \cdot \frac{A_0}{T} \right) \right]^{2/3} \cdot g^{-1/3} \tag{3.3}$$

$$U_B = U - U_{mf} + \phi \sqrt{g \cdot D_B} \tag{3.4}$$

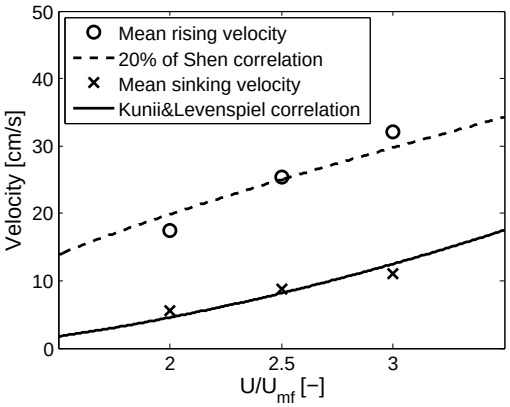

Figure 3.8: Mean sinking and rising velocities of an object compared with models for the dense phase and bubbles velocities.

The experimental circulation times obtained for the object throughout the experiments (more than 1,200 cycles) are shown in Figure 3.9(a) as a function of the maximum depth attained by an object. It can be observed that the greater the depth, the larger the time periods. The minima follow a linear trend that might be attributed to constant sinking and rising velocities throughout the bed. However, there is considerable scatter in the data. This is due to the incidence of multiple jumps during the rising process associated with a series of passing bubbles that do not carry the object directly to the surface of the bed. Figure 3.9(b) shows the same data arranged as a function of the number of jumps needed to raise the object to the surface of the bed in each cycle. Note that the scattered data for a low number of jumps ($< 10\,s$) fits well with the variation of the minima in the time versus depth graph, and thus, the effects of the number of jumps and the attained depth seem to be cumulative. Of course, a high number of jumps in the rising process are more prone to occur when a greater depth is attained or vice versa. The dashed line, which roughly represents a minimum, was determined by a linear regression of the minimum time for the more probable numbers of jumps (from 1 to 5).

The effect of both parameters was studied in more detail. In Figure 3.10(a) the relative frequency of an object attaining a determined depth is plotted (dividing the bed in slices of $5\,cm$). This relative frequency was found to follow a parabolic law, with minimum relative frequency at medium depths. This rather surprising result is in accordance with the dense phase behavior, described in Figure 3.2(b). The object sinks at the sides of the bed (see Figure 3.4), and once in such a zone, it is less prone to move sideward to the preferred bubble path (the middle of the bed) than continuing sinking, so the relative frequency to reach a greater depth is higher. Figure 3.10(b) shows the relative frequency of a determined number of jumps that occurs in each cycle. The graph illustrates an exponential decay of the relative frequency with the

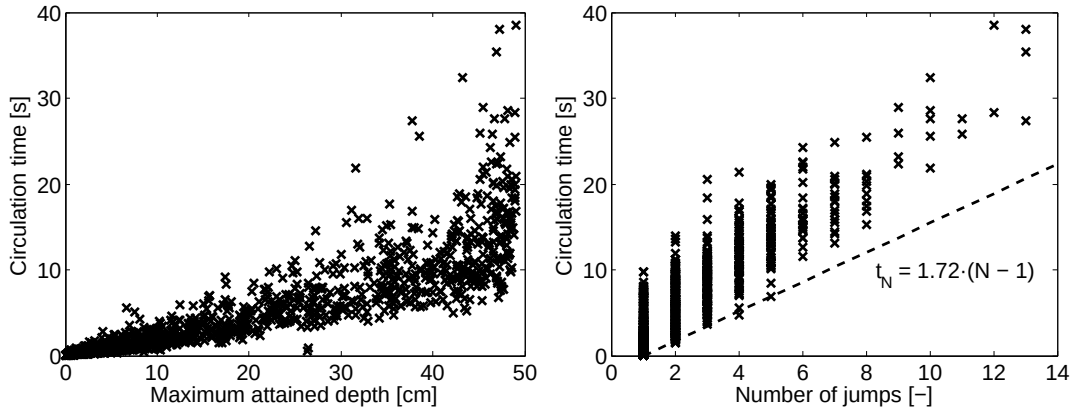

(a) (b)

Figure 3.9: Circulation time of an object for the nominal case ($U/U_{mf} = 2.5$), (a) as a function of the cycle maximum attained depth, and (b) as a function of the number of jumps employed to reach the surface of the bed.

number of jumps. It can be observed that the fitting slightly overestimates the relative frequency to reach high depths and underestimates the relative frequency to find a one-jump cycle.

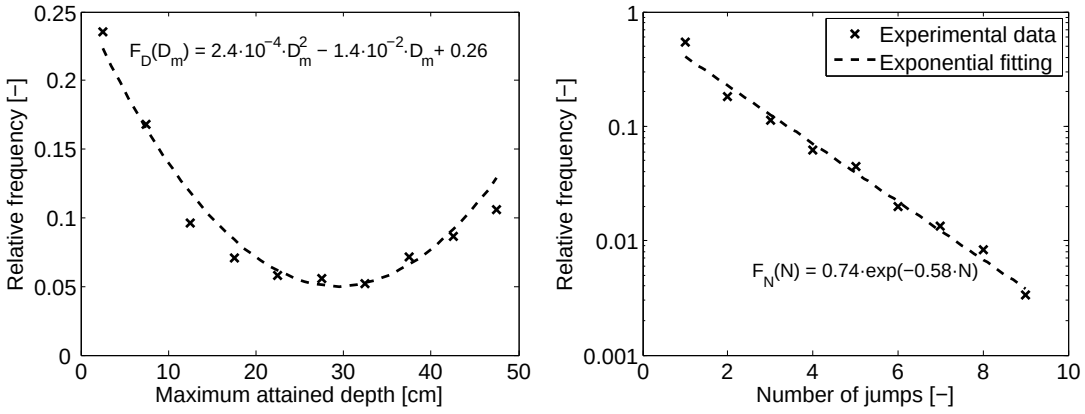

(a) (b)

Figure 3.10: Relative frequency to (a) reach a determined maximum depth, and (b) find cycles with a determined number of jumps. Nominal case ($U/U_{mf} = 2.5$)

The graphs for the other dimensionless gas velocities that produce a proper circulation of the object (U/U_{mf} 2 and 3) showed similar results, and are therefore not included here.

3.5 Discussion

An estimate of the circulation time of an object in a bubbling fluidized bed is important when designing fluidized bed applications such as combustors, gasifiers, dryers, or

coating reactors. During our experiments, the circulation time of an object was found to depend mainly on the number of bubbles needed to raise it to the surface of the bed (number of jumps) and the maximum depth attained by the object. Therefore, an estimate of the circulation time for a determined number of jumps, N, and a maximum attained depth, D_m, was made. The estimation, based on semi-empirical expressions, consists of two different times: i) the time due to the number of jumps, t_N, calculated using the equation in Figure 3.9(b) and ii) the time due to the maximum attained depth, t_D, calculated assuming a constant velocity for the object. The mean velocities are presented in Figure 3.8, both in the sinking, v_s, and the rising, v_r, path.

$$t_N = 1.72 \cdot (N - 1) \tag{3.5a}$$

$$t_D = D_m \cdot \left(\frac{1}{v_s} + \frac{1}{v_r} \right) \tag{3.5b}$$

The total circulation time, t, can then be calculated as the sum of these two times:

$$t = 1.72 \cdot (N - 1) + D_m \cdot \left(\frac{1}{v_s} + \frac{1}{v_r} \right) \tag{3.6}$$

The distribution of relative frequencies of the circulation time can also be estimated using the relative frequencies to find a determined number of jumps, F_N, and to attain a certain depth, F_D, as shown in Figure 3.10. These relative frequencies were transformed into functions of the circulation time using Equation 3.5:

$$F_N(t) = 0.41 \cdot e^{-0.34 \cdot t} \tag{3.7a}$$

$$F_D(t) = 2.4 \cdot 10^{-4} \cdot t^2 \cdot \left(\frac{1}{v_s} + \frac{1}{v_r} \right)^{-2} - 1.4 \cdot 10^{-2} \cdot t \cdot \left(\frac{1}{v_s} + \frac{1}{v_r} \right)^{-1} + 0.26 \tag{3.7b}$$

Finally, the relative frequencies were normalized into probability density functions:

$$P_N(t) = 0.34 \cdot e^{-0.34 \cdot t} \tag{3.8a}$$

$$P_D(t) = 3.8 \cdot 10^{-4} \cdot t^2 \cdot \left(\frac{1}{v_s} + \frac{1}{v_r} \right)^{-2} - 2.2 \cdot 10^{-2} \cdot t \cdot \left(\frac{1}{v_s} + \frac{1}{v_r} \right)^{-1} + 0.41 \tag{3.8b}$$

The functions described in Equation 3.8 are the probability density functions of two independent times. The total time spent by the object in a cycle is the sum of these times, as described in Equation 3.6. The probability density function for such a sum is the convolution of the two functions:

$$P_T(t) = P_N(t) * P_D(t) = \int_0^{+\infty} P_N(x) \cdot P_D(t-x) \cdot dx \tag{3.9}$$

The probability density function of the total circulation time of the object is plotted in Figure 3.11 for the different dimensionless gas velocities. All of the distributions are bi-modal due to the shape of F_D (see Figure 3.10(a)) which presented a minimum probability for the object to reach moderate depths. Nevertheless, the bi-modal shape should not be considered a sound conclusion, since it was sharpened by errors in the exponential fit of Figure 3.10(b). As stated previously, the actual probability for $N = 1$ is larger than that on the fit. Therefore, if a perfect fit had been used, the first peak would have been larger and the second peak smaller. However, the present, simpler procedure was used for clarity purposes. This procedure gives a proper idea of the global distribution.

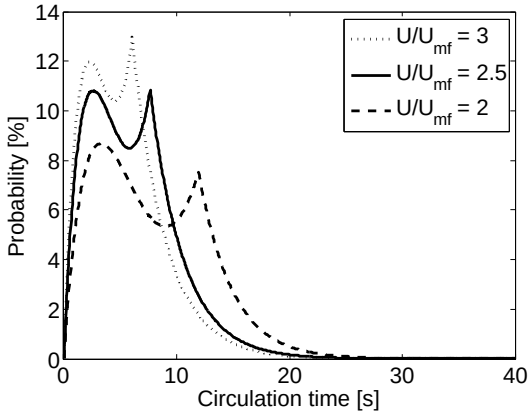

Figure 3.11: Probability density function of the total circulation time of an object.

The reduction of the dimensionless gas velocity produces an increase in the circulation time as a result of the reduction of both rising and sinking velocities of the object. The rest of the parameters were constant. The probability density functions fitted for the dimensionless gas velocity of 2.5 (Equation 3.8) were used to estimate the circulation time of the object for the three different dimensionless gas velocities (2, 2.5, and 3).

Figure 3.12 shows a comparison of our estimate of the circulation time along with the experimental data. The distribution of the experimental circulation times is plotted in a box plot in Figure 3.12(a) for varying dimensionless gas velocities. In a box plot, the distribution of the data is reduced to the median, the lower and upper quartiles (representing 25% and 75% of the population), a confidence interval (defined by the two experimental data that are further away from the quartiles but inside a maximum interval of ± 1.5 times the inter-quartile range), and outliers (that lie out of such a confidence interval). It can be observed that the circulation time decreases with the

dimensionless gas velocity due to the larger sinking and rising velocities of the object. The box plot of the estimated circulation time is also plotted in Figure 3.12(b). The cross in this diagram represents a circulation time with a probability of 0.1%, which is roughly the occurrence probability of an outlier.

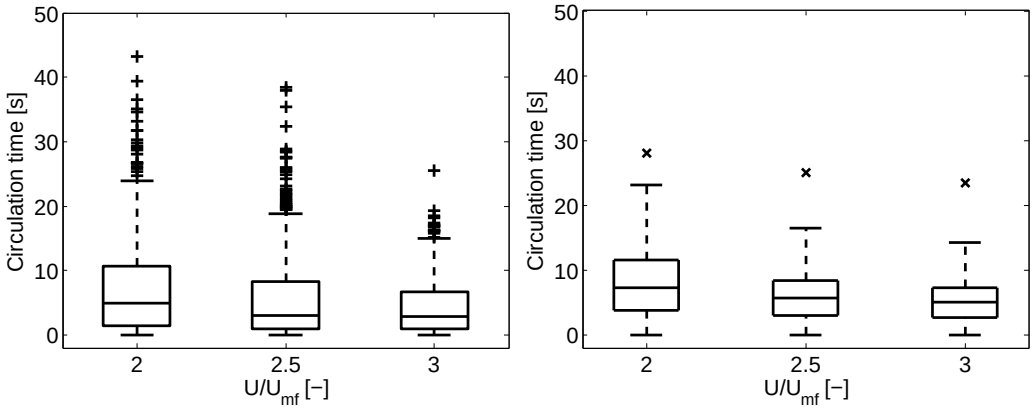

(a) (b)

Figure 3.12: Box plots of (a) the experimental circulation time and (b) the estimated circulation time.

The semi-empirical estimation was found to overestimate the lower times (mainly the lower quartile). This overestimation was due to the underestimation of the probability of a single jump to occur in the fitting, as shown in Figure 3.10(b). The estimation also presents a higher symmetry between the lower and the upper quartiles than the experimental data, due to the overestimation of the probability to attain a high depth (see Figure 3.10(a)). Nevertheless, it seems to predict accurately most of the distribution for the three dimensionless gas velocities. Therefore, the semi-empirical expressions used to estimate the circulation time can be said to be in good agreement with the experimental data.

Finally, the object was tested in a 3-D lab-scale fluidized bed and the circulation time was calculated. The semi-empirical expressions obtained in the 2-D bed was tried to extend to the 3-D bed to estimate the circulation time of the object.

Figure 3.13 shows the experimental circulation time obtained in the 3-D bed for two different gas velocities ($U/U_{mf} = 2$ and 2.5) organized in a box plot. The experimental data can be compared to the box plot of the estimate circulation time based on the 2-D bed semi-empirical expressions. The circulation time decreased with the gas velocity, since both the sinking and rising velocities of the object increases with this parameter. Even though the experimental circulation times are slightly greater, the experimental data and the estimate are in good agreement, since the difference between the most representative values of the distributions, the median, are lower than 10 % for both excess gas velocities.

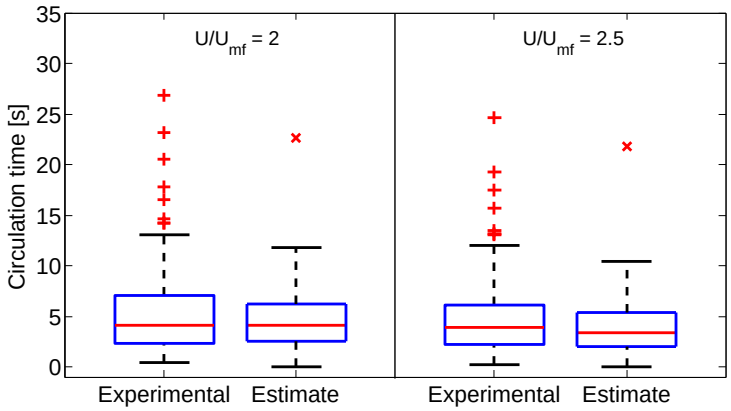

Figure 3.13: Experimental and estimate box plots for the circulation time of the object moving in the 3-D bed.

3.6 Conclusions

The motion of a large object within a 2-D bubbling fluidized bed was studied using imaging techniques and considering the circulation patterns, the object sinking and rising velocities, and the multiple-jumps behavior on the rising path. The effect of the dimensionless gas velocity on the main parameters of the motion was also analyzed.

The object employed was larger than the dense phase with a similar density to the bed, although slightly lower. The object circulated throughout the bed following a typical 2-vortex configuration. Its spatial distribution was quite homogeneous when operating with dimensionless gas velocities from 2 to 3, becoming rather non-homogeneous for low dimensionless gas velocities ($U/U_{mf} = 1.5$), for which buoyancy effects became important.

The sinking and rising paths were identified, differentiated, and independently characterized. The sinking path of the object was characterized by sudden falls with high downwards velocities and vibrations in which both downwards and upwards velocities were present. However, during the rising path (within a single jump), there were only upwards velocities. A mean sinking and rising velocity of an object in the bed was determined considering these facts. The sinking velocity was in accordance with the well-known correlation of Kunii and Levenspiel, and thus the effect of buoyant forces on the sinking motion of the object can be considered negligible. The rising velocity was found to be roughly 20% of the bubbles velocity, a result consistent with previous estimates.

The circulation time of an object depends on the maximum depth attained by the object, and the number of jumps needed for the object to rise back to the surface of the bed. The relation between the circulation time and these two parameters is almost linear. These parameters were considered independent contributions to the circulation

time, and their probability density functions were obtained. The probability of finding cycles with a determined number of jumps has an inverse exponential relation to the number of jumps, while the probability of attaining a determined depth was found to be parabolic, with a minimum at moderate depths due to the tendency of an object to sink deep before moving sideward to the preferential path of bubbles, typical of the 2-vortex configuration.

Semi-empirical expressions were proposed to estimate the circulation time of the object and its probability distribution. The estimate relies on experimental data that are considered independent of the dimensionless gas velocity (provided that the buoyant forces are negligible) and on mean sinking and rising velocities of the object, that were experimentally obtained for each dimensionless gas velocity, but are in good agreement with widely used correlations. Even though our correlation overestimates the lower times, it was found to accurately predict the majority of the experimental distribution.

Finally, the semi-empirical expressions obtained from the analyze of the object motion within the 2-D facility was tried to extend to the motion of the object in a lab-scale 3-D bed. The application of the semi-empirical expressions to the circulation time of the object in the 3-D bed, was found to be in good agreement with the experimental circulation times.

3.7 Notation

A_0 Area of the distributor per number of orifices, $[m^2]$

C Relative frequency to find dense phase at a particular location in the bed, $[-]$

D_m Maximum depth attained by the object, $[m]$

D_B Bubble diameter, $[m]$

f_B Characteristic frequency of the bed, $[Hz]$

f_w Bubble wake fraction, $[-]$

F_D Relative frequency to attain a certain depth, $[-]$

F_N Relative frequency of a certain number of jumps, $[-]$

F_R Relative frequency, $[-]$

F_{uz} Relative frequency to find the object at the upper half of the bed, $[-]$

g Gravity, $[m/s^2]$

h Height measured from the distributor, $[m]$

h_b Fixed bed height, $[m]$

H_{2D} Vessel height, $[m]$

N Number of jumps needed for the object to rise to the surface of the bed, $[-]$

N_P Total number of images employed in the study of dense phase and bubbles, $[-]$

P_D Probability density function to attain a certain depth, $[-]$

P_N Probability density function of the number of jumps, $[-]$

P_T Probability density function of the circulation time, $[-]$

t Circulation time, $[s]$

t_D Minimum circulation time related to the attained depth, $[s]$

t_N Minimum circulation time related to the number of jump, $[s]$

T Bed thickness, $[m]$

U Superficial gas velocity, $[m/s]$

U_B Bubble velocity, $[m/s]$

U_{mf} Minimum fluidization velocity, $[m/s]$

v_{dp} Downward velocity of the dense phase, $[m/s]$

v_r Object mean rising velocity, $[m/s]$

v_s Object mean sinking velocity, $[m/s]$

W Bed width, $[m]$

ΔP_{bed} Bed pressure drop, $[Pa]$

ΔP_{dist} Distributor pressure drop, $[Pa]$

δ Bubble fraction in the bed, [−]

λ Constant determined experimentally, [−]

ϕ Constant determined experimentally, [−]

Bibliography

Almendros-Ibáñez J.A., Sanchez-Delgado S., Sobrino C., Santana D., 2009. Experimental observations on the different mechanisms for solid ejection in gas-fluidized beds. *Chemical Engineering and Processing* 48-3, 734-744.

Bokkers G.A., van Sint Annaland M., Kuipers J.A.M., 2004. Mixing and segregation in a bidisperse gas-solid fluidised bed: a numerical and experimental study. *Powder Technology* 140 (3), 176-186.

Davidson J.F., Harrison D., 1963. Fluidised particles, 1st ed. Cambridge University Press, Cambridge.

Du B., Wei F., Warsito W., 2002. Gas and solids mixing in a turbulent fluidized bed. *AIChE Journal* 48 (9), 1896-1909.

Geldart D., 1973. Types of gas fluidization. *Powder Technology* 7, 285-292.

Gomez-Barea A., Leckner B., 2010. Modelling of biomass gasification in fluidized bed. *Progress in Energy and Combustion Science* 36 (4), 444-509.

Grassler T., Wirth K.-E., 2000. X-ray computer tomography-potential and limitation for the measurement of local solids distribution in circulating fluidized beds. *Chemical Engineering Journal* 77 (1-2), 65-72.

Hoffmann A.C., Janssen L.P., Prins J., 1993. Particle segregation in fluidized binary mixtures. *Chemical Engineering Science* 48(9), 1583-1592.

Ibsen C.H., Solberg T., Hjertager B.H., Johnsson F., 2002. Laser Doppler anemometry measurements in a circulating fluidized bed of metal particles. *Experimental Thermal and Fluid Science* 26 (6-7), 851-859.

Johnsson F., Zijerveldb R.C., Schoutenb J.C., van den Bleek C.M., Leckner B., 2000. Characterization of fluidization regimes by time-series analysis of pressure fluctuations. *International Journal of Multiphase Flow* 26, 663-715.

Karri S.B.R., Werther J., 2003. Gas distributor and plenum design in fluidized beds. In: Yang W. C. Handbook of fluidization and fluid-particle systems, Marcel Dekker Inc., New York, pp. 164-179.

Koornneef J., Junginger M., Faaij A., 2007. Development of fluidized bed combustion - An overview of trends, performance and cost. *Progress in Energy and Combustion Science* 33, 19-55.

Kunii D., Levenspiel O., 1991. Fluidization Engineering, 2nd ed., Butterworth-Heinemann, Boston.

Laverman J.A., Roghair I., Van Sint Annaland M. and Kuipers H., 2008. Investigation into the hydrodynamics of gas-solid fluidized beds using particle image velocimetry coupled with digital image analysis. *The Canadian journal of chemical engineering* 86, 523-535

Lim K.S., Agarwal P.K., 1994. Circulatory motion of a large and lighter sphere in a bubbling fluidized bed of smaller and heavier particles. *Chemical Engineering Science* 49 (3), 421-424.

Müller C.R., Davidson J.F., Dennis J.S. and Hayhurst A.L., 2007. A study of the motion and eruption of a bubble at the surface of a two-dimensional fluidized bed using particle image velocimetry (PIV). *Industrial & Engineering Chemistry Research* 46, 1642-1652.

Nguyen T.H., Grace J.R., 1978. Forces on objects immersed in fluidized beds. *Powder Technology* 19, 255-264.

Nienow A.W., Rowe P.N., Chiba T., 1978. Mixing and segregation of a small portion of large particles in gas fluidized beds of considerably smaller ones. *AIChE Symposium Series* 74, 45-53.

Otshitani J., Keiko O., Makoto I., Zennosuke T., 2004. Effect of particle fluidization intensity on floating and sinking of objects in a gassolid fluidized bed. *Advanced Powder Technology* 15(2), 201-213.

Otsu N., 1979. A threshold selection method from gray-level histograms. *IEEE Transactions on Systems Man and Cybernetics* 9, 62-66.

Pallarès D., Johnsson F., 2006. A novel technique for particle tracking in cold 2-dimensional fluidized beds - Simulating fuel dispersion. *Chemical Engineering Science* 61, 2710-2720.

Rees A.C., Davidson J.F., Hayhurst A.N., 2005. The rise of a buoyant sphere in a gas-fluidized bed. *Chemical Engineering Science* 60, 1143-1153.

Rios G.M., Dang Tran K., Masson H., 1986. Free object motion in a gas fluidized bed. *Chemical Engineering Communications* 47, 247-272.

Rowe P.N., 1973. Estimation of solid circulation rate in bubbling fluidised bed. *Chemical Engineering Science* 28, 979-980.

Sanchez-Delgado S., Marugan-Cruz C., Acosta-Iborra A., Santana D., 2010. Dense phase fluctuation in a 2-D fluidized bed. *Powder Technology* 200, 37-45.

Shen L., Johnsson F., Leckner B., 2004. Digital image analysis of hydrodynamics two-dimensional bubbling fluidized beds. *Chemical Engineering Science* 59, 2607-2617.

Stein, M., Ding, Y.L., Seville, J.P.K., Parker, D.J., 2000. Solids motion in bubbling gas fluidised beds. *Chemical Engineering Science* 55, 5291-5300.

Sveen J.P., 2004. http://www.math.uio.no/∼jks/matpiv. (Last modified in August, 2004. Accesed in 2008).

Tanimoto H., Chiba S., Chiba T., Kobayashi H., 1981. Jetsam descent induced by a single bubble passage in three-dimensional gas-fluidized beds. *Journal of Chemical Engineering of Japan* 14(4), 273-276.

Chapter 4

Buoyancy effects on objects moving in a 2-D Bubbling Fluidized Bed

Contents

4.1 Abstract **51**

4.2 Introduction **52**

4.3 Experimental Setup **54**

4.4 Results **55**

4.5 Conclusions **65**

4.6 Notation **66**

Bibliography **67**

4.1 Abstract

The effect of buoyant forces on the motion of a large object immersed in a bubbling fluidized bed (BFB) was experimentally studied using digital image analysis. The experiments were performed in a 2-D bubbling fluidized bed with glass spheres as bed material and cylindrical objects with different densities and sizes. The object motion was measured using non-intrusive tracking techniques. The effect of gas velocity was also analyzed.

The circulation of an object in a BFB is defined by several parameters. The object might be able to circulate homogeneously throughout the bed or stay in preferred regions, such as the splash zone or the bottom zone. While circulating, the object moves back and forth between the surface of the bed and the inner regions, performing

a series of cycles. Each cycle is composed by sinking and rising paths, which can be one or several, depending on whether a passing bubble is able to lift the object to the surface or the object is detached from it or its drift at an intermediate depth. Therefore, the number of rising paths or number of jumps that the object undergo in a cycle, interleaved with sinking paths, and the maximum attained depth characterize each cycle, together with the mean sinking and rising object velocities. In this chapter, experimental measurements of the probability distributions of the number of jumps and the maximum attained depth, the axial homogeneity of object motion, and rising and sinking object velocities are presented for objects with different sizes and densities. The results show a coherent behavior, independent of density and size, for the probability distributions of the number of jumps. This is also true for the maximum attained depth, but only when a proper circulation throughout the bed is ensured. Such a proper circulation and axial homogeneity is, on the other hand, much affected by object density, size and gas velocity. Rising and sinking velocities are highly dependent on gas velocity, as established in well-known models of bubble and dense phase velocities. Nevertheless, rising velocities are practically unaffected by object density or size, while sinking velocities show a low dependence on density and a steeper one on size. These results suggest that buoyant forces are relevant during the sinking process, and almost neutral during the rising path.

4.2 Introduction

Fluidized beds are employed in industry because of their excellent properties involving heat and mass transfer, and their capability to establish and promote chemical reactions inside them. Several processes can occur inside a fluidized bed, such as drying, thermal conversion of solid fuels, and coating of particles. In parallel to the wide range of applications, there is a wide range of scales concerning fluidized beds, from small dryers to huge fluidized bed reactors. Most of these applications involve the motion of objects inside the bed. Fuel particles, catalysts, and agglomerates are examples of typical objects found inside a fluidized bed. It is necessary to characterize the motion of these objects within the bed to prevent operational problems such as the existence of hot or cold spots and the appearance of de-fluidized zones due to the existence of agglomerates.

Different experimental techniques have been used to describe the motion of tracer particles both in 2-D and 3-D beds. Concerning 3-D beds, tomography-tracking techniques such as positron emission (Stein et al., 2000), X-ray (Grassler and Wirth, 2000), and electrical capacitance (Du et al., 2002) methods are common. Nevertheless non-

tracking techniques have also been employed to collect data of the motion at a particular position in the bed (Ibsen et al., 2002). On the other hand, when analyzing objects motion in a 2-D bed, visualization techniques (Shen et al., 2004; Bokkers et al., 2004) have been employed.

Kunii and Levenspiel (1991) reviewed the first studies intended to characterize the motion of large objects immersed in a fluidized bed. It is generally accepted that objects sink in the bed with the dense phase and rise by the action of ascending bubbles. The motion of large objects in both 2-D and 3-D beds was analyzed by Rios et al. (1986), focusing on the sinking and rising processes. They reported that the mean rising velocity of objects was lower than the velocity of bubbles due to the fact that an object generally needs to be lifted by a number of passing bubbles to rise to the freeboard, conforming a rising path composed of multiple jumps that they called jerks. Pallarès and Johnsson (2006) tracked a phosphorescent particle moving in a 2-D bed for several configurations. In a 2-vortex configuration, a configuration found in most cases with the exception of very shallow beds, they found a general tendency of objects to sink at the sides of the bed and rise at the center, which is generally accepted. Lim and Agarwal (1994) found that a neutrally-buoyant object circulated in a 2-D bed throughout the whole bed, with a sinking velocity which was in good agreement with the Kunii and Levenspiel (1991) correlation for the velocity of the dense phase. The mean rising velocity of the object and its relation with the bubbles velocity is far more complicated, due to the multiple-jump behavior observed by Rios et al. (1986). Nonetheless, the experimental works of Nienow et al. (1978), Lim and Agarwal (1994), and Rees et al. (2005) define a rough estimate that varies between authors and sets the mean rising velocity of objects between 10 % and 30 % of the mean bubble velocity along the bed.

The effect of buoyant forces has been also the focus of several works. Tanimoto et al. (1981) reported a relative motion between an object and the dense phase. The relative velocity was linear with density, for large density ratios. Nevertheless, the buoyant force suffered by an object immersed in a bubbling fluidized bed might differ from what would be expected based on its skeletal density due to a de-fluidized hood of bed material that appears on top of the object, as stated by Nguyen and Grace (1978) and Rees et al. (2005).

In Chapter 3 the motion of a neutrally-buoyant object within a 2-D bed was analyzed. The object was found to describe cycles, moving from the surface of the bed to a certain depth and back to the surface by the action of several passing bubbles, as explained by Rios et al. (1986). The cycles described by the object were characterized in terms of the maximum attained depth and the number of jumps needed for the object

to go back to the surface of the bed. The distribution of the maximum attained depth was found to be parabolic, whereas the distribution of the number of jumps showed an exponential decay.

In this chapter, the experimental procedure described in Chapter 3 has been applied to a variety of objects. The validity of both the parabolic fitting for the maximum depth and the exponential one for the number of jumps has been analyzed for objects with different densities and sizes. The capability of the object to circulate in the bed is discussed. The effect of buoyant forces on the object sinking and rising velocity is also analyzed. Finally, the study has been extended to different fluidized beds, varying the dense phase diameter and the bed height.

4.3 Experimental Setup

The experiments were carried out in the 2-D facility. The bed was set in a column with a width, W, of 0.5 m, a height, H_{2D}, of 2 m, and a thickness, T, of 0.01 m. The fixed bed height, h_b, was 0.5 m, corresponding to a bed aspect ratio of 1. The bed material was glass spheres (ballotini particles) with a skeletal density about $2,500\,kg/m^3$, and a $600 - 800\,\mu m$ of diameter, d_p, type B according to Geldart's classification (Geldart, 1973). The bulk density of the fixed bed, ρ_b, was measured to be $1,560\,kg/m^3$. Minimum fluidization velocity, U_{mf}, was obtained using piezo-electric pressure transducers (*Kistler type 5015*) that measured pressure fluctuations in the bed. It was $0.32\,m/s$. During the experiments, the dimensionless gas velocity (U/U_{mf}) was varied between 1.5 and 3. A standard camera (*Nikon D80 10.6 Mpx*) was used to capture the object motion. The measurements of object motion (to obtain both position and velocity) were carried out in complete darkness. The objects were coated with strontium aluminate to emit green light.

The objects studied were in all cases of cylindrical shape, with a diameter, D_O, of $6.4\,mm$, while their densities and lengths were varied in a broad range. The characteristics of the different objects are given in Table 4.1.

These six objects represented four different density ratios (bed-object density difference over the bulk density of the fixed bed) and three different aspect ratios (length over diameter of the cylinder). Object N represented a neutrally-buoyant object, but it will behave in a slightly flotsam manner due to its density ratio. This object was analyzed in detail in Chapter 3 and it is given here as a quasi-neutral reference in terms of buoyancy effects. Objects F1 and F2 had densities definitely below that of the bed and showed flotsam behavior. Object J had a larger density than the bed density and showed jetsam behavior. Those four objects had the same aspect ratio. The last two

Object	Density ratio $((\rho_b - \rho_o)/\rho_b)$	Shape ratio (L_O/D_O)
F1	0.66	3
F2	0.21	3
N	0.03	3
J	-0.09	3
LN	0.03	5
SN	0.03	1

Table 4.1: Characteristics of the objects used in the experiments.

objects, objects LN and SN, were respectively larger and smaller than object N, and with the same density and diameter. The dimensionless gas velocity was varied during the experiments between 1.5 and 3. For small velocities, some objects, particularly Objects J and F1, did not circulate.

Finally, some experiments were performed to study the effect of bed height and bed material. In the first case, a shallower bed was used, with 0.75 bed aspect ratio (nominal case was 1). In the second case, the bed material was ballotini particles with a diameter in the range $400 - 600\,\mu m$ (smaller than the nominal case), and with the same skeletal density. Those particles still correspond to Geldart's group B (Geldart, 1973).

4.4 Results

The circulation time of an object immersed in a bubbling fluidized bed varies for each object cycle as a function of its mean sinking and rising velocities and of two varying parameters: the maximum depth attained by the object and the number of jumps needed to get back to the surface of the bed. The distribution of these two parameters will, therefore, define the circulation time distribution of an object in a BFB. In Chapter 3, the distributions were obtained for the neutrally-buoyant object, N. In this chapter, the effect of the object characteristics or the bed parameters on such distributions is analyzed.

Figure 4.1 shows the results obtained in the previous chapter for the neutrally-buoyant object, N, and compares them with those for a flotsam object (Object F1). Graph (a) shows the relative frequency to find cycles with a determined number of jumps and graph (b) the relative frequency to find cycles that reach a determined maximum depth. The results were obtained for a dimensionless gas velocity of $U/U_{mf} = 3$. The fitting curves for the results of the neutrally-buoyant object are also depicted in the graphs, taken from Chapter 3. The distribution of the number of jumps follows a

negative exponential distribution, and the distribution of the maximum attained depth is parabolic. The experimental results are quite similar for both objects and the fittings seem to represent accurately both distributions, independently of the object density.

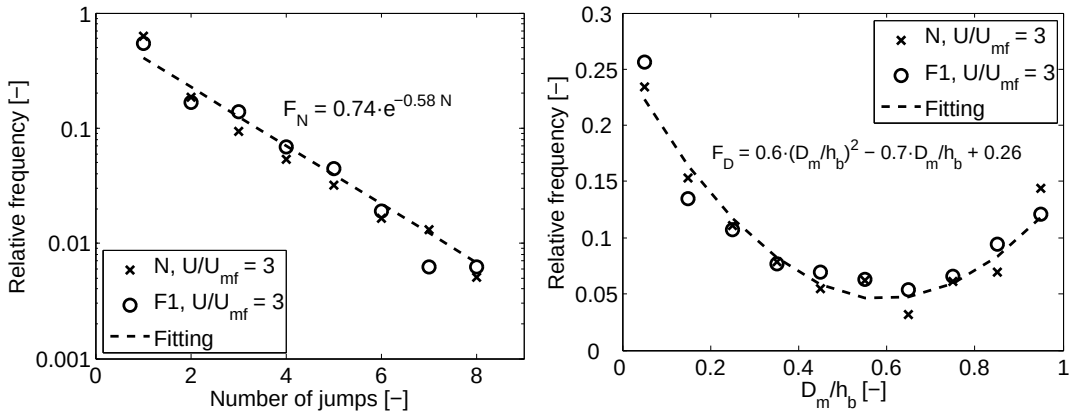

(a) (b)

Figure 4.1: Relative frequency (a) to find cycles with a determined number of jumps, and (b) to find cycles that reach a determined maximum depth.

The motion of the rest of objects was analyzed at different air velocities, showing in most cases similar results to the ones already shown in Figure 4.1. An adjustment coefficient to the fittings obtained for the neutrally-buoyant object was calculated to characterize the suitability of the fittings for the different cases. The coefficient, R^2, is calculated by the least-squares method. In the number of jumps curve, the coefficient is calculated over the logarithmic data.

Figure 4.2 shows the R^2 coefficients for the exponential fitting of the number of jumps for objects with different densities (a) and sizes (b), and for a range of air velocities.

In all cases, the R^2 coefficient of the exponential fitting for the number of jumps was higher than 0.85, a value that can still be considered adequate. Therefore, the global behavior can be said to be independent of the object density and size, and of the air velocity, for the ranges studied. So the incidence of cycles with an increasing number of jumps is found to decay exponentially in all cases. The experimental data corresponding to all the tests are plotted in Figure 4.3 with the exponential fitting. A small scatter of the data can be observed in the figure, but a similar behavior is evident, independent of the varying parameters: object density, object aspect ratio and excess gas velocity.

The probability that an object has, when it begins to rise, to be lifted directly to the bed surface may depend on its initial position and other factors, but it seems independent of its previous history of jumps. Therefore, the process of having to perform

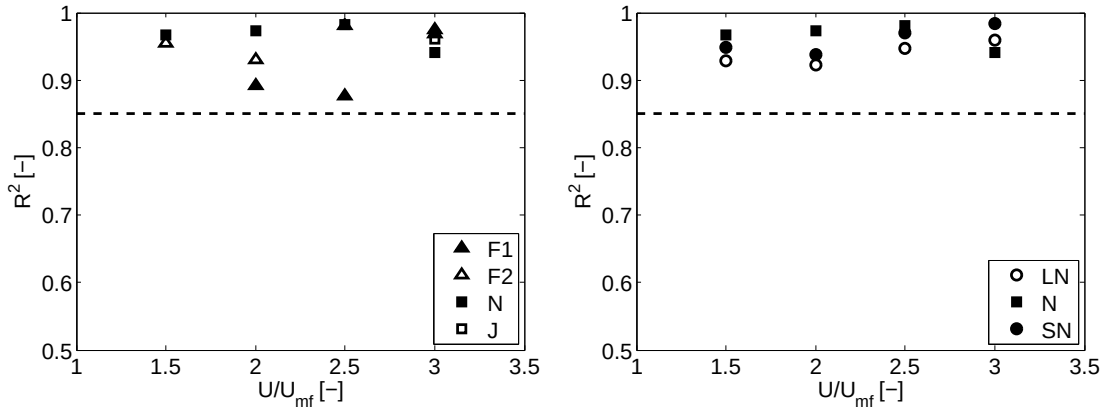

(a) (b)

Figure 4.2: R^2 coefficient of the exponential fitting of the number of jumps for objects of different densities (a) and sizes (b).

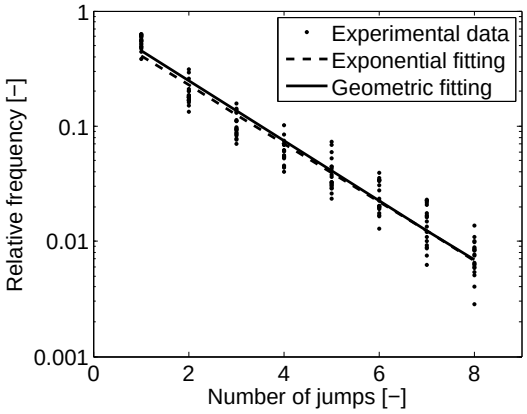

Figure 4.3: Relative frequency to find cycles with a determined number of jumps for all the tests.

a new jump might be considered a memoryless process. The exponential distribution may well represent this type of processes, but it is a continuous distribution while the number of jumps is a discrete variable ($N = 1, 2, 3$). Therefore, the exponential fitting should be transformed into a discrete distribution. The discrete analog of the exponential distribution is the geometric distribution. Its probability density function is given by Equation 4.1:

$$P_N = p \cdot (1 - p)^{N-1} \tag{4.1}$$

The geometric distribution fitting for the data of Figure 4.3 is also plotted in that figure, showing minor differences with the exponential fitting and a proper adjustment to the experimental data. The value of p in the fitting ($p = 0.45$) describes the average probability of an object to, once started to rise, be lifted directly to the bed surface. The value $1 - p$, $(1 - p = 0.55)$, describes de average probability of an object to, once

started to rise, detach from the bubble or its drift and begin a new sinking process.

The main result in Figure 4.3 is that those average probabilities for the object rising path, a 45 % probability to arrive to the surface and a 55 % probability to detach and start a new sinking process, are independent of object parameters such as density and size. In a first guess, it would seem reasonable that such parameters, specially a dramatic change of the density, from jetsam to flotsam objects, would affect those probabilities. The excess gas velocity, a parameter that controls the average diameter and velocity of the bubbles in the bed, would have seemed even more relevant. On the other hand, this is an average probability. The experiments showed that, when the averaging was performed separating the different depths at which the object begins to rise, the average probabilities varied. Evidently enough, probabilities to reach the bed surface were higher for lower depths. This distribution for varying depths may change. Also, the probability of the object to begin its rise at a certain depth varies with depth and may vary for the different experimental conditions. But the global average remains constant as established in Figure 4.3.

At the end of this section, the effect of bed height and bed material on these average probabilities will be also discussed.

The distribution of probability of the attained depth was also studied in detail. The R^2 coefficient was calculated for the parabolic fitting shown in Figure 4.1 (b) for the maximum attained depth. The results for all the tests are reported in Figure 4.4. As done previously, the validity of the fitting was accepted for R^2 coefficients larger than 0.85. All objects showed a proper adjustment to the fitting for the highest dimensionless air velocity tested ($U/U_{mf} = 3$). For lower gas velocities, density and size effects became important and the distribution changes, first for lower densities and larger objects and finally ($U/U_{mf} = 1.5$) for all objects. The distribution obtained for the jetsam object (only tested for $U/U_{mf} = 3$, as it did not circulate for lower air velocities) was symmetrical to those of the flotsam objects. Compared to the symmetrical of F_D, it showed a proper adjustment ($R^2 = 0.87$).

The results in Figure 4.4 should be associated to the incidence of buoyant forces during the sinking path of the object. Reducing the object density would produce a higher buoyant force and therefore smaller sinking velocities. This prevented the object from sinking deep in the bed, so the object moved just in the upper zone of the bed. Therefore, the probability to attain large depths diminished and the parabolic behavior was not fulfilled. The effect of the size seems to act in a quite similar way, larger objects experimented higher buoyant forces. The strong air velocity effect can be considered to be due to the increase of the fluidization intensity (Otshitani et al., 2004). The fluidization intensity when operating at high air velocities reduced the

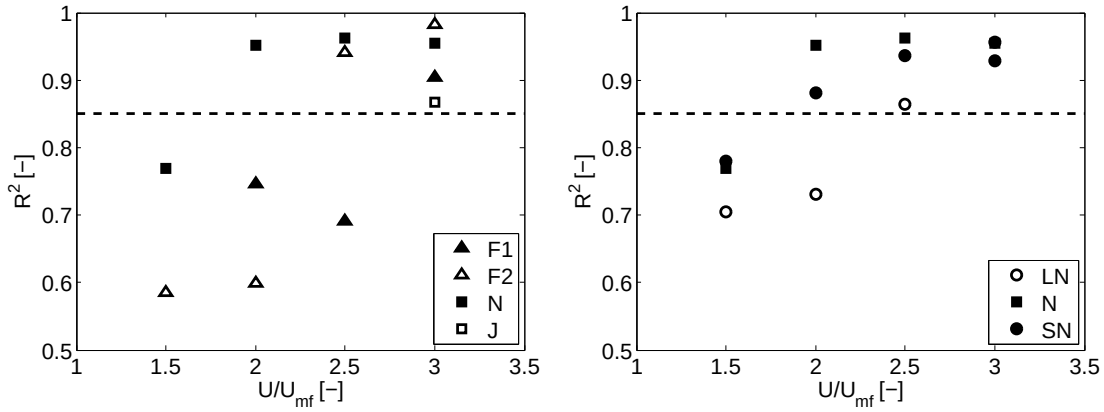

(a) (b)

Figure 4.4: Determination coefficient of the parabolic fitting of the maximum attained depth for objects of different densities (a) and sizes (b).

effect of buoyant forces, allowing the object to move throughout the whole bed.

Therefore, the parabolic fitting can be considered to represent the motion of all objects when their ability to move throughout the bed is ascertained. All the tests where the results differ considerably ($R^2 < 0.85$ in Figure 4.4) from the initial fitting obtained for the neutrally-buoyant object showed a similar tendency. The object moved in a restricted zone at the top of the bed. Although the results for medium or small depths still followed the fitting curve, this was not the case for positions near the bed surface and for large depths. This can be explained by the inadequate circulation. Most of the time the objects were retained in the surroundings of the bed surface and they seldom descended to high depths. Therefore, there is a transfer of relative frequencies from higher to lower depths. This is shown in Figure 4.5, where the results for the flotsam object F2, operating at $U/U_{mf} = 1.5$, are presented. All other tests where the fitting was invalid showed similar results.

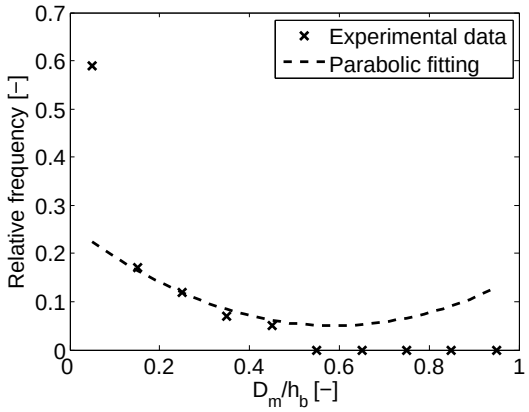

Figure 4.5: Relative frequency to reach a determined depth. Flotsam object F2, operating at $U/U_{mf} = 1.5$.

The probability density function for the maximum attained depth can be obtained from the parabolic fitting. The attained depth is a continuous variable in contrast to the number of jumps. Therefore, its probability density function is obtained by normalizing it, giving Equation 4.2:

$$P_D = 5.45 \cdot \left(\frac{D_m}{h_b}\right)^2 - 6.36 \cdot \left(\frac{D_m}{h_b}\right) + 2.36 \tag{4.2}$$

The bed capability of maintaining the object circulating throughout the whole bed, as a function of object and bed parameters, is a key point. For a proper understanding, it has been analyzed using a different approach. The object position was recorded during all the experiments and a parameter, F_{uz}, was defined and calculated as the probability to find the object in the upper half of the bed. This parameter would be close to 50 % for an object that circulates evenly throughout the bed, and can be indistinctly found at the higher or at the lower part of the bed. This would be the case for an adequate bed dynamics and for neutrally-buoyant objects. On the other hand, its value would approach 100 % for highly flotsam objects and poor dynamics, which maintain the objects in the surrounding of the bed surface. In such cases, the object seldom appears at the bottom zone. Finally, its value would be close to 0 % for highly jetsam objects and poor bed dynamics, in which case the object sinks and remains over the distributor and rarely rises to the surface.

The results of the parameter F_{uz} for the different objects and excess gas velocities are shown in Figure 4.6. These results can be compared with those shown in Figure 4.4, since a low R^2 coefficient in those graphs was linked to poor circulation. The two dashed lines in the graphs of Figure 4.6 are obtained from this comparison. They represent a ± 15 % interval around $F_{uz} = 50$ %. The data outside such an interval showed low R^2 coefficients as a result of poor circulation, while the data inside the interval correspond to R^2 coefficients higher than 0.85. The results are, therefore, consistent between the two different approaches.

All the objects tested had a proper circulation throughout the bed for the highest gas velocity tested ($U/U_{mf} = 3$). The neutrally-buoyant object, N, had a proper circulation for a range of dimensionless gas velocities, but it drifts from the 50 % zone for decreasing gas velocities and reaches the limit for $U/U_{mf} = 1.5$. Reducing the density ratio, the case of objects F2 and F1, produced a steeper effect of the gas velocity. The object F2 circulated properly throughout the bed for dimensionless gas velocities higher than 2.5, but for lower values (1.5 and 2) buoyancy effects became important and the probability to find the object in the upper half of the bed was higher. Operating with less dense objects, such as F1, buoyant forces precluded the

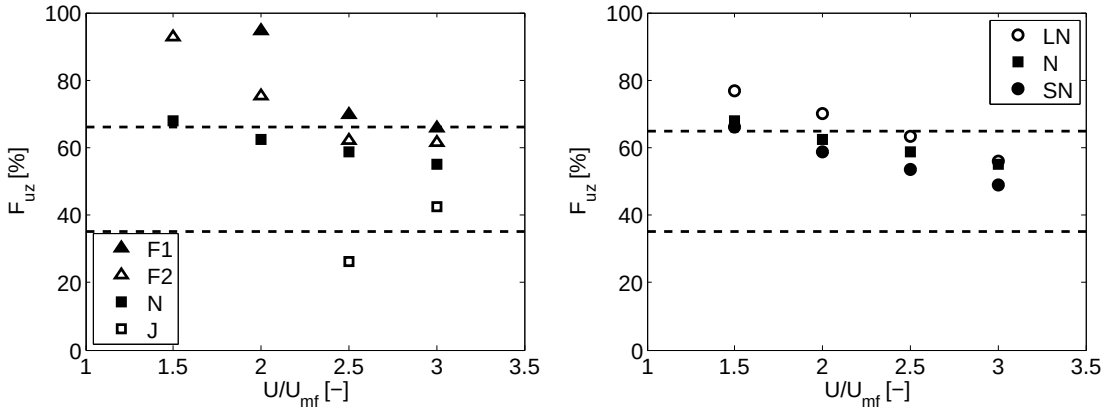

(a) (b)

Figure 4.6: Probability to find the object in the upper half of the bed for (a) different object densities and (b) sizes.

proper circulation of the object for dimensionless gas velocities as high as 2.5, but the object circulated throughout the whole bed for $U/U_{mf} = 3$. The jetsam object, J, was capable of circulate within the bed for the highest dimensionless air velocity tested ($U/U_{mf} = 3$), but when reducing the air velocity it sank deep in the bed due to buoyant forces. In this second case, the object seldom reached the bed surface, so a small number of cycles were achieved and for such a reason it is absent in Figure 4.4. In all cases, an increase of the air velocity and the linked increase of the fluidization intensity improved the circulation of objects throughout the bed, reducing the effect of buoyant forces.

A higher effect of density differences between object and bed is apparent for the jetsam object (density ratio -0.09) in comparison with the flotsam objects (density ratios 0.21 and 0.66). This effect seems to be a consequence of the opposite or identical directions between buoyant forces and dense phase motion. The neutrally-buoyant object has shown a rather flotsam behavior in all the results presented, but this difference is small and can be neglected in comparison with the density differences for flotsam and jetsam objects.

The effect of object size, shown in Figure 4.6 (b), is smaller, but some coherent evolution can also be seen. Larger objects were more prone to be found in the upper part of the bed.

Finally, the object velocity inside the bed was measured and compared to well-established correlations for bubbles and dense phase motion. The mean rising velocity of the object can be observed in Figure 4.7 for all experimental conditions and objects. The results show similar mean rising velocities for all the objects, and a quasi-linear behavior with gas velocity. Objects were unable to circulate properly throughout the

bed for $U/U_{mf} = 1.5$ so those results are missing. The results are compared with the mean velocity of bubbles, calculated using the correlation of Shen et al. (2004) for the bubble diameter, D_B, and the correlation of Davidson and Harrison (1963) for the bubble velocity, U_B. These correlations are:

$$D_B = \left[\left(\frac{8\cdot\left(2^{3/4}-1\right)}{\lambda}\right)\cdot(U-U_{mf})\cdot\left(h+\frac{\lambda}{\pi\cdot(2^{3/4}-1)}\cdot\frac{A_0}{T}\right)\right]^{2/3}\cdot g^{-1/3} \tag{4.3}$$

$$U_B = U - U_{mf} + \phi\sqrt{g\cdot D_B} \tag{4.4}$$

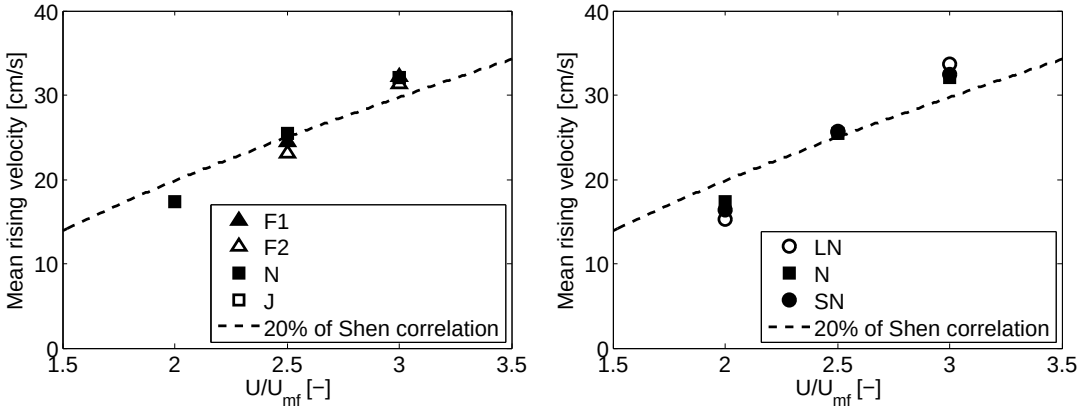

(a) (b)

Figure 4.7: Mean rising velocity of objects with different densities (a) and sizes (b).

Several authors (Rios et al., 1986; Nienow et al., 1978; Lim and Agarwal, 1994; Rees et al., 2005) have studied the mean rising velocity of objects in fluidized beds, but their results present a wide dispersion. The ratio of the mean rising velocity of the object and the mean bubble velocity along the bed ranged between 10 % and 30 % depending on the study. Our results show a reasonable agreement for a 20 % ratio.

The low variability of the object rising velocity with the density and size suggests that the bubbles capability of raising them is not influenced by these parameters.

The mean sinking velocities for all objects and excess gas velocities are shown in Figure 4.8. A certain effect of buoyant forces can be established. The sinking velocities of heavier objects are larger. A similar thing happens for smaller objects. This suggests the existence of a super-imposed buoyant velocity that is a function of these two parameters: the density difference between the object and the surrounding bed, and the object length. A comparison with the dense phase velocity is also given, using the correlation of Kunii and Levenspiel (1991). It shows a reasonable agreement with the data for Object N. The correlation is given in Equation 4.5.

$$v_{dp} = \frac{f_w \cdot \delta \cdot U_B}{1 - \delta - f_w \cdot \delta} \tag{4.5}$$

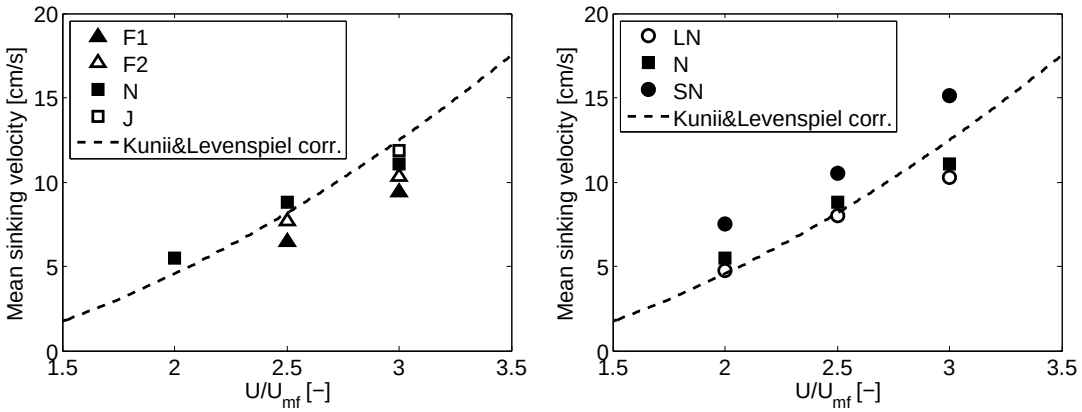

(a) (b)

Figure 4.8: Mean sinking velocity of objects with different densities (a) and sizes (b).

The experimental results of Figure 4.1 to 4.8 gave a coherent characterization of the effect of buoyant forces in the motion of objects immersed in a bed, for the range of parameters presented. The rising process is connected to the bubble motion and the rising velocity dependence on gas velocity follows well-established correlations for bubble velocity. On the other hand, buoyant effects seem inexistent concerning the rising path: the number of jumps and the rising velocity are not much affected by object density or size. Nevertheless, the sinking process and parameters related show a clear buoyant effect. This is evident when looking at Figures 4.6 and 4.8, and for the cases in Figures 4.4 and 4.5 that do not follow the otherwise general parabolic fit. Increasing the gas velocity produces a more vigorous fluidization and enables the object to circulate throughout the bed, diminishing the effect of buoyant forces. Figure 4.8 suggests that buoyant velocities remains constant with gas velocity, but their ratio with the sinking velocity of the dense phase decreases, and thus they become less significant.

The results previously shown for the probability distributions of the number of jumps and the attained depth indicate that the distributions remain similar for different objects and gas velocities. In order to test the validity and range of those expressions, the effects of bed height and bed material were also tested.

Previous experiments were carried out in a bed with a bed aspect ratio (height over width) of 1. Figure 4.9 shows the results for a lower bed height ($h_b/W = 0.75$). Note that the abscissas in Figure 4.9 (b) denote different depths for different bed heights.

Finally, the effect of the bed material was tested. Previous experiments were carried out in a bed conformed by ballotini particles with $600 - 800\,\mu m$ diameter range. In

the experiments shown in Figure 4.10, the motion of the neutrally-buoyant object, N, was studied in a bed of ballotini particles with $400 - 600\,\mu m$ diameter range. The skeletal density of the particles remained constant, and in all cases they correspond to Geldart's group B (Geldart, 1973).

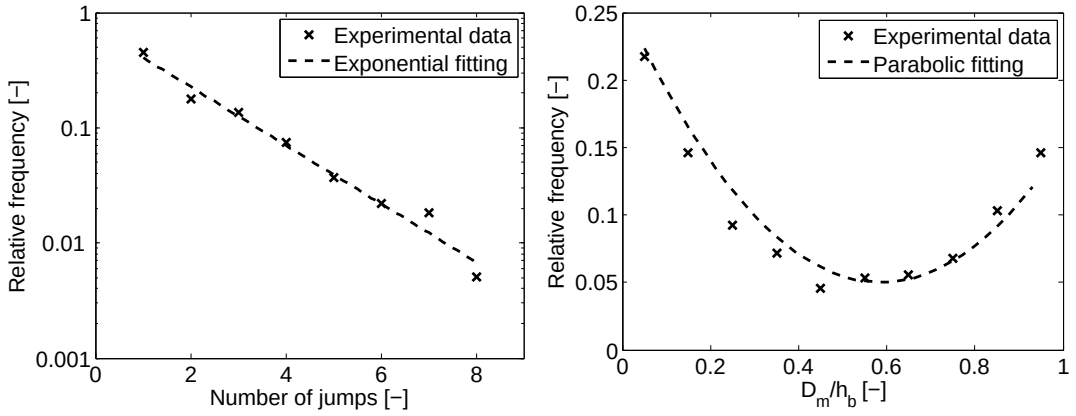

(a) (b)

Figure 4.9: Relative frequency to (a) find cycles with a determined number of jumps, and (b) reach a determined maximum depth, for the neutrally-buoyant object moving in a bed with a bed aspect ratio $h_b/W = 0.75$ operating at $U/U_{mf} = 3$.

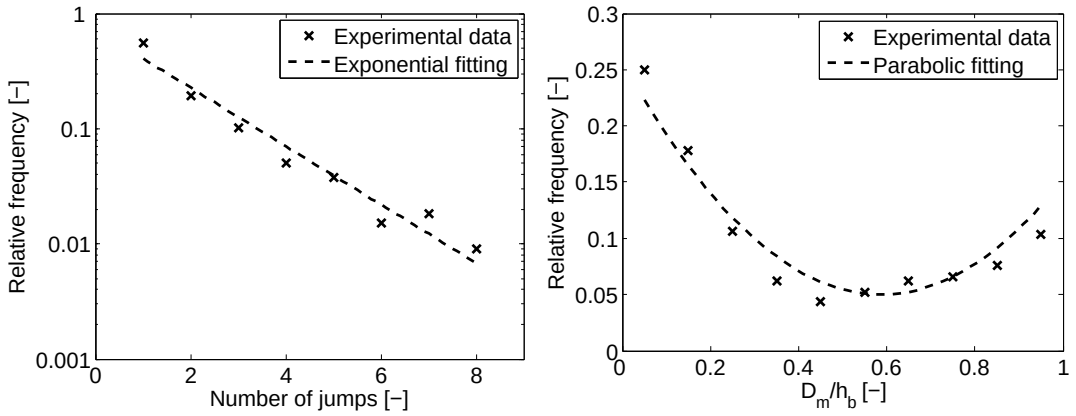

(a) (b)

Figure 4.10: Relative frequency to (a) find cycles with a determined number of jumps, and (b) reach a determined maximum depth, for the neutrally-buoyant object moving in a bed with dense material of a diameter $400 - 600\,\mu m$ operating at $U/U_{mf} = 3$.

No important differences can be observed between the experimental data in Figures 4.9 and 4.10 and the correlations obtained for the previous experiments. Therefore, the probability distributions given in Equations 4.1 and 4.2 remain also independent of the bed height and the bed material diameter. Those expressions could be used to estimate the circulation time of the different objects, as described in Chapter 3.

4.5 Conclusions

The effect of buoyant forces on the motion of a large cylindrical object immersed in a 2-D bubbling fluidized bed was experimentally studied using digital image analysis. The object density and size were varied and their effect on relevant parameters that characterize the object motion within the bed was analyzed. The parameters include the circulation homogeneity throughout the bed, the mean rising and sinking velocities, and other characteristic cycle parameters such as the number of jumps that the object undergo in his evolution from the bed surface and back to it, and the maximum attained depth. The effect of the dimensionless gas velocity was also analyzed.

Depending on its buoyant characteristics, an object might be able to circulate homogeneously throughout the bed or stay in preferred regions, such as the splash zone or the bottom zone. A parameter that measure the axial homogeneity of object motion is presented in the form of a coefficient between the time the object is in the upper half of the bed and the total time. The results show that a proper circulation and axial homogeneity is much affected by object density, size and gas velocity. Jetsam objects seldom appear on the bed surface while flotsam objects hardly ever reach high depths. Increasing the object size has a similar but less intense effect than decreasing object density.

While circulating, the object moves back and forth between the surface of the bed and the inner regions, performing a series of cycles. Each cycle is composed by sinking and rising paths, which can be one or several, depending on whether a passing bubble is able to lift the object to the surface of the bed or the object is detached from it or its drift at an intermediate depth. This defines a number of jumps for each cycle. The results show that the probability distribution of the number of jumps is independent of density and size of the object and gas velocity, and also of other bed parameters such as the bed height and the particle size distribution of the bed material. In all cases, the probabilities followed a geometric distribution for the number of jumps of the form $P_N = 0.45 \cdot (0.55)^{N-1}$. The value 0.45 describes the average probability of an object to, once started to rise, be lifted directly to the bed surface and is found to remain constant for all experimental conditions, including gas velocity changes and varying object density and size.

A similar result is found for the probability distribution of the maximum attained depth, which is found to follow the same parabolic law in all cases. Nevertheless, this is only valid when a proper circulation throughout the bed is ensured. When this is not the case, not all depths can be attained and the continuous distribution cannot be fulfilled.

Rising and sinking velocities are highly dependent on gas velocity, as established in well known models of bubble and dense phase velocities. Nevertheless, rising velocities are practically unaffected by object density or size, while sinking velocities show a low dependence on density and a steeper one on size.

As a main conclusion, buoyant forces are found to be relevant during the sinking process, but no effect is observed during the rising path. Rising motion is unaffected for the ranges of variation studied in this chapter, and the bubbles capability of rising objects and their mean rising velocity is unaffected by object density and size. On the other hand, the sinking motion varies with the incidence of buoyant forces, showing axial circulation non-homogeneity, mean sinking velocity variations and restrictions of flotsam or jetsam objects to remain in the upper or bottom region respectively. Nevertheless, the effect of buoyant forces on the object motion can be reduced by increasing the gas velocity.

4.6 Notation

A_0 Area of the distributor per number of orifices, $[m^2]$

d_p Dense phase particles diameter, $[m]$

D_O Object diameter, $[m]$

D_B Bubble diameter, $[m]$

D_m Maximum attained depth, $[m]$

f_w Bubble wake fraction, $[-]$

F_D Relative frequency to attain a certain depth, $[-]$

F_N Relative frequency of a certain number of jumps, $[-]$

F_{uz} Relative frequency to find the object at the upper half of the bed, $[-]$

g Gravity, $[m/s^2]$

h Height over the distributor, $[m]$

h_b Fixed bed height, $[m]$

H_{2D} Vessel height, $[m]$

L_O Object length, $[m]$

N Number of jumps needed for the object to rise to the surface of the bed, $[-]$

p Average probability of a rising object to be lifted directly to the bed surface, $[-]$

P_D Probability density function to attain a certain depth, $[-]$

P_N Probability density function of the number of jumps, $[-]$

R^2 Determination coefficient, $[-]$

T Bed thickness, $[m]$

U Superficial gas velocity, $[m/s]$

U_B Bubble velocity, $[m/s]$

U_{mf} Minimum fluidization velocity, $[m/s]$

v_{dp} Downward velocity of the dense phase, $[m/s]$

W Bed width, $[m]$

δ Bubble fraction in the bed, $[-]$

λ Constant determined experimentally, $[-]$

ϕ Constant determined experimentally, $[-]$

ρ_b Packed bed density, $[kg/m^3]$

ρ_o Object density, $[kg/m^3]$

Bibliography

Bokkers G.A., van Sint Annaland M., Kuipers J.A.M., 2004. Mixing and segregation in a bidisperse gas-solid fluidised bed: a numerical and experimental study. *Powder Technology* 140 (3), 176-186.

Davidson J.F., Harrison D., 1963. Fluidised particles, 1st ed. Cambridge University Press, Cambridge.

Du B., Wei F., Warsito W., 2002. Gas and solids mixing in a turbulent fluidized bed. *AIChE Journal* 48 (9), 1896-1909.

Geldart D., 1973. Types of gas fluidization. *Powder Technology* 7, 285-292.

Grassler T., Wirth K.-E., 2000. X-ray computer tomography-potential and limitation for the measurement of local solids distribution in circulating fluidized beds. *Chemical Engineering Journal* 77 (1-2), 65-72.

Ibsen C.H., Solberg T., Hjertager B.H., Johnsson F., 2002. Laser Doppler anemometry measurements in a circulating fluidized bed of metal particles. *Experimental Thermal and Fluid Science* 26 (6-7), 851-859.

Kunii D., Levenspiel O., 1991. Fluidization Engineering, 2nd ed., Butterworth-Heinemann, Boston.

Lim K.S., Agarwal P.K., 1994. Circulatory motion of a large and lighter sphere in a bubbling fluidized bed of smaller and heavier particles. *Chemical Engineering Science* 49 (3), 421-424.

Nguyen T.H., Grace J.R., 1978. Forces on objects immersed in fluidized beds. *Powder Technology* 19, 255-264.

Nienow A.W., Rowe P.N., Chiba T., 1978. Mixing and segregation of a small portion of large particles in gas fluidized beds of considerably smaller ones. *AIChE Symposium Series* 74, 45-53.

Otshitani J., Keiko O., Makoto I., Zennosuke T., 2004. Effect of particle fluidization intensity on floating and sinking of objects in a gassolid fluidized bed. *Advanced Powder Technology* 15(2), 201-213.

Pallarès D., Johnsson F., 2006. A novel technique for particle tracking in cold 2-dimensional fluidized beds - Simulating fuel dispersion. *Chemical Engineering Science* 61, 2710-2720.

Rees A.C., Davidson J.F., Hayhurst A.N., 2005. The rise of a buoyant sphere in a gas-fluidized bed. *Chemical Engineering Science* 60, 1143-1153.

Rios G.M., Dang Tran K., Masson H., 1986. Free object motion in a gas fluidized bed. *Chemical Engineering Communications* 47, 247-272.

Shen L., Johnsson F., Leckner B., 2004. Digital image analysis of hydrodynamics two-dimensional bubbling fluidized beds. *Chemical Engineering Science* 59, 2607-2617.

Stein, M., Ding, Y.L., Seville, J.P.K., Parker, D.J., 2000. Solids motion in bubbling gas fluidised beds. *Chemical Engineering Science* 55, 5291-5300.

Tanimoto H., Chiba S., Chiba T., Kobayashi H., 1981. Jetsam descent induced by a single bubble passage in three-dimensional gas-fluidized beds. *Journal of Chemical Engineering of Japan* 14(4), 273-276.

Chapter 5

Motion of objects in a 3-D Bubbling Fluidized Bed with a rotating distributor

Contents

5.1 Abstract 71

5.2 Introduction 72

5.3 Experimental Setup 74

5.4 Results 76

5.4.1 Object loss 76

5.4.2 Circulation time distribution 80

5.5 Conclusions 84

5.6 Notation 86

Bibliography 87

5.1 Abstract

In this chapter the effect of a low-frequency rotating distributor on the motion of a large object immersed in a lab-scale 3-D bubbling fluidized bed is studied. The object size and density differ from those of the inert solids that conform the bed. It might represent a passive particle, a catalyst, or a reactant. The rotation modifies the bed dynamics in the surroundings of the distributor and affects the motion of the object within the bed.

A set of experiments was carried out on a lab-scale cylindrical bed, equipped with a perforated plate distributor that can rotate at around 1Hz, for different bed aspect ratios, gas velocities, and object characteristics. Sizes were far larger than that of the solids of the dense phase and densities ranged from half the bed density to values around it. The experiments were video recorded, capturing the surface of the bed from above.

As have often been noted, objects might remain in stagnant regions near the distributor and be "lost" or precluded to circulate. This can be avoided in most practical cases forcing the distributor to rotate. Also, the effect of the distributor rotation on the circulation times of the objects is presented, showing a general reduction of large circulation times.

5.2 Introduction

Different measurement techniques have been used both in 2-D and 3-D beds to analyze the motion of objects immersed in the bed. In some of these studies (Stein et al., 2000; Grassler and Wirth, 2000; Du et al., 2002; Shen et al., 2004; Bokkers et al., 2004; Ibsen et al., 2002) the object had a similar density and size to the bed material. These works were intended to characterize the motion of the dense phase and are beyond the aim of this PhD thesis. Kunii and Levenspiel (1991) reviewed the first studies focussed on the motion of large objects in a bed. Rios et al. (1986) studied the motion of large objects in 2-D and 3-D beds and discussed the sinking and rising processes. Concerning the rising process, Rios et al. (1986) found that the rising motion of objects was not a monotonic ascending motion, but the object was lifted small distances by a succession of passing bubbles, rising in a series of small jumps. The relation between the rising velocity of the object and the bubble velocity is complex due to the multiple jumps effect observed by Rios et al. (1986) and the relative motion between bubble and object, which are far more important than those between object and dense phase in the sinking process. Nevertheless, the object rising velocity is roughly between 10 % and 30 % of the mean bubble velocity along the bed, according to the experimental works of Nienow et al. (1978), Lim and Agarwal (1994), and Rees et al. (2005). Several authors have studied the sinking process. Lim and Agarwal (1994) found that the sinking velocity of a large object in a 2-D bed was in good agreement with the Kunii and Levenspiel (1991) correlation for the velocity of the dense phase for density ratios around 1. The net buoyant force on an object immersed in a fluidized bed might differ from what would be expected based on its density due to a de-fluidized hood of bed material that appears on top of the object, as stated by Nguyen and Grace (1978) and Rees et al.

(2005). For large density ratios, Tanimoto et al. (1981) and Hoffmann et al. (1993) studied the relative motion of sinking objects and dense phase and obtained a linear relation with the density and a potential relation (exponent 1/3) with the diameter, but their results cannot be accurately extrapolated to our study.

Finally, most of the authors (Rios et al., 1986; Nguyen and Grace, 1978; Sanderson and Rhodes, 2003; Nienow et al., 1978; Keillor and Bergougnou, 1975) noticed that the object, quite regardless of its density, may stop circulating within the bed and be captured in stagnant zones over the distributor, a typical fact for very dense objects. Sanderson and Rhodes (2003) showed that the reappearance of a lost object was possible increasing the dimensionless gas velocity over $3U_{mf}$. Also, by analyzing experimental data for various 3-D bed sizes, they showed that the motion of objects inside the bed was a scalable phenomenon, following hydrodynamic similarity criteria for bubbling beds.

In this chapter a comparison of results obtained for a standard bubbling fluidized bed and a "forced" BFB is presented. Several works have proposed the use of actuators, imposed on a BFB to modify its dynamics. Passive or active control tools are motivated by general drawbacks of BFB, such as poor radial mixing, large bubbles and gas by-pass, or agglomerates and the incidence of heterogeneous fluidization. Proposed solutions include pulsed gas flow (Moussa et al., 1982; van Ommen et al., 2007), vibrating beds (Noda et al., 1998; Mawatari et al., 2003), and the use of advanced distributor designs, including spiral (Ouyang and Levenspiel, 1986; Sreenivasan and Ragahavan, 2002), swirl (Chyang and Lin, 2002) and rotating distributors (Sobrino et al., 2008, 2009).

Sobrino et al. (2008), using a similar experimental setup to the one used in our experiments, showed that a rotating distributor may affect global bed parameters. For instance, they showed that, as a consequence of rotation, bubble diameter is affected, and become more homogeneous along the bed and minimum fluidization velocity decreases.

The effect on the bed dynamics of allowing the bed distributor to rotate, by means of studying its effect on the motion of an object submerged in the bed is studied in this chapter. The experimental work was performed on a lab-scale cylindrical BFB, equipped with a perforated plate distributor that can either remain static or rotate, at a low frequency around $1\,Hz$. Also, the influence of gas velocity, bed height, and the density and shape of the object was analyzed throughout the experiments for both the static and the rotating distributor configurations.

5.3 Experimental Setup

The experimental setup consists on a lab-scale cylindrical BFB, an electrical motor that allows the distributor to rotate and an image acquisition system to capture the bed surface. The bed performance was characterized by means of pressure measurements. Figure 5.1 shows a schematic diagram of the experimental setup with the main components.

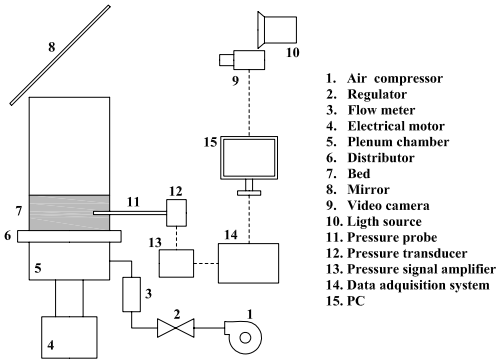

Figure 5.1: Scheme of the experimental facility.

The cylindrical vessel of the bed is a transparent tube with an inner diameter, D, of $0.192\,m$ and $1\,m$ in height, H_{3D}. The fixed bed height, h_b, was varied throughout the experiments between $0.25D$ and $0.75D$. The minimum fluidization velocity was measured to be $0.31\,m/s$ for the rotating distributor bed and $0.33\,m/s$ for the static one, thus the minimum fluidization velocity slightly decreases with the rotation, in agreement with Sobrino et al. (2008).

Sand with a measured density of $2,632.5\,kg/m^3$ was used as bed material. The bulk density of the fixed bed was measured to be $1,630\,kg/m^3$, which gave the void fraction of the packed bed, $\varepsilon_{packed} = 0.38$. The diameter of the cylindrical object, D_O, was $6.4\,mm$ while the density and length was varied throughout the experiments, as shown in Table 5.1.

	Density, ρ_o $[kg/m^3]$	Length, L_O $[mm]$
a	1,380	6.4
b		19.2
c		32.0
d	840	19.2
e	1,010	
f	1,750	

Table 5.1: Density, ρ_o, and length, L_O, of the cylindrical objects used in the experiments. Diameter, D_O, was always $6.4\,mm$.

Therefore, objects a to e are flotsam particles (buoyant) within the fluidized bed, while object f is a jetsam particle.

The distributor is a $6\,mm$ width perforated plate with 275 holes of $2\,mm$ diameter, distributed in a triangular mess of $11\,mm$ pitch. According to Karri and Werther (2003) and Kunii and Levenspiel (1991) the pressure drop along the distributor should be larger than $30\,\%$ the pressure drop along the bed for an homogeneous fluidization. The distributor was designed according to this criterion and trying to reduce the dead zones over the distributor, as explained in section 2.3.1. The distributor might be forced to rotate at a constant velocity of $100\,rpm$ by an electrical motor.

Pressure fluctuations inside the bed were measured through a $4\,mm$ internal diameter and $50\,mm$ long steel tube connected to a piezo-electric pressure transducer (*Kistler type 5015*). The signal from the piezo-electric sensor was amplified by a Kistler amplifier. The response of this kind of probe and transducer is in good agreement with the model of Bergh and Tijdeman (1965), as stated by van Ommen et al. (1999). This model predicts the first resonance frequency to occur at $670\,Hz$, which is far away from typical characteristic frequencies in fluidized beds (in the $1-5\,Hz$ range). The sampling frequency was $200\,Hz$ and $12,032$ samples per test were recorded. The amplifier acts as a high-pass filter with a frequency of $0.16\,Hz$, in order to obtain the pressure fluctuations relative to the local average pressure. The signal was also low-pass filtered at the Nyquist frequency by the amplifier.

The characteristic frequency of the fluidized bed (f_B, $3.61\,Hz$) was determined by a frequency domain analysis for the nominal case ($U/U_{mf} = 1.44$, $h_b/D = 0.5$).

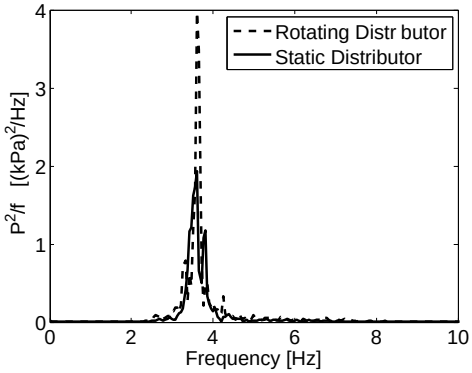

Figure 5.2: Power spectra for the rotating and static distributor configurations. Nominal case ($U/U_{mf} = 1.44$, $h_b/D = 0.5$).

During all the tests, the fluidized bed freeboard was video recorded during 10 minutes with a recording speed of $30\,fps$. The resolution of the camera was 480×640 pixels. The videos were post-processed using Matlab®. Both the object positions while on the bed surface and the time periods of disappearance from it (the circulation time of the sinking-rising global cycle) were obtained from the videos. The experimen-

tal results of the next section are based on the circulation time measurements, since the object location while at the freeboard showed no relevant pattern.

Experiments were run for a range of gas velocities, bed heights and object characteristics and for both the static and the rotating distributor configurations of the BFB. Test parameters are shown in Table 5.2, where h_b is the total bed height and D is the bed diameter, U and U_{mf} are the superficial air velocity and the minimum fluidization velocity, L_O and D_O are the object length and diameter, ρ_b and ρ_o are the packed bed density and the object density and n is the rotating angular velocity. A nominal case was selected for comparison and is highlighted in bold format in the table. Whereas one parameter was varied in the experiments, the rest of them were kept as in the nominal case.

Bed aspect ratio $h_b/D\,[-]$	(0.25; **0.5**; 0.75)
Dimensionless gas velocity $U/U_{mf}\,[-]$	(1.26; **1.44**; 1.63)
Object aspect ratio $L_O/D_O\,[-]$	(1; **3**; 5)
Bed-object density ratio $\rho_b - \rho_o)/\rho_b\,[-]$	(-0.07; **0.15**; 0.38, 0.48)
Rotating angular velocity $n\,[rpm]$	(0; 100)

Table 5.2: Experimental parameters. Nominal case is in bold format.

5.4 Results

The experimental results are grouped in two sections. In the first one, the probability of loosing the object (i.e. it did not spring up on the freeboard) is studied. In the second section, a general study of the circulation time distribution is presented.

5.4.1 Object loss

The first key point observed was that the object was lost after a determined time when operating with the static distributor. As stated in section 5.2, these losses have often been reported in the literature as a typical drawback of non-porous (non-homogeneous) distributors. Although during the design of the distributor special care was taken in this aspect, losses happened for almost all the tests with the static distributor. Only for very light objects and large bed aspect ratios the probability of losing the object

could be considered negligible. Every time the object disappeared, the bed material was extracted in order to find its position. Evidently, it was always found to be settled out at the bottom of the bed, placed on the small dead zones between the holes of the distributor (a triangular mess of $11\,mm$ pitch, with object diameter $6.4\,mm$ and lengths ranging from 6.4 to $32\,mm$).

Nevertheless, when operating with the rotating distributor, those losses were completely inexistent. Moreover, if the distributor was forced to rotate after the object was lost in a static configuration; it reappeared almost immediately, in a $3-5$ seconds lapse. This time lapse should not be considered as the time needed for the object to arrive to the top, because also a certain starting time is needed for the electrical motor to acquire the operating frequency. The fact that the rotating distributor is even capable of maintaining in circulation an object denser than the bed (object f) is significant. Far denser objects (around the dense phase density) did not circulate independent of the distributor, and were immediately lost. If the incidence of object losses should be avoided, the distributor rotation may prove a better methodology to "activate" the circulation of lost objects with intermediate densities than increasing the gas velocity, as suggested by Sanderson and Rhodes (2003), since the loss of fines will be avoided. Obviously, the feasibility of a rotating distributor will strongly depend on the bed geometry and dimensions.

Object loss is of course a bottom zone mechanism. That zone is characterized by the distributor geometry, and will show both air jets and de-fluidized zones (minimized by the pitch selection), as shown by Geldart and Baeyens (1985) and Rees et al. (2006). The rotation of the distributor: i) varies the jet location, and ii) is able to move the bottom bed material, producing a $3\,cm$ shear layer (rough estimation, observed by visual inspection) in the de-fluidized particles. These two superposed effects completely avoid the formation of stagnant regions and are able to immediately restore the object into circulation.

This effect of preventing object losses is the main result of these experiments. Some results of the incidence of object losses in static distributor beds follows. The main interest of these results is to state in which cases the preventing effect of the rotating distributor is more relevant. With such a purpose, ten tests of 10 minutes were video recorded and post-processed for each experimental condition in order to determine the loss probability and time needed for the object to be lost in each configuration with the static distributor. Ten is not a statistically relevant number, but the aim is only qualitative. The loss probability, defined as one over the number of times the object left the bed surface along the experiment, is presented. It is a more reliable factor than the time till the object sinks for the last time. It seems reasonable to consider each cycle

of the object independent of the previous history, and the time till the object sinks for the last time will of course be influenced by the circulation times of the previous cycles of the object.

Results for the loss probability in a static distributor configuration are shown in Figure 5.3. The mean value and the maximum and minimum values (± interval) of the loss probability are plotted as a function of the experiments varying parameters. The nominal case (highlighted) is plotted in all the graphs. According to the definition of loss probability, we have presented the results with a log scale in the probability axis. The four graphs of Figure 5.3 present the separated effects of bed aspect ratio and gas velocity, object density and object aspect ratio on the object loss probability.

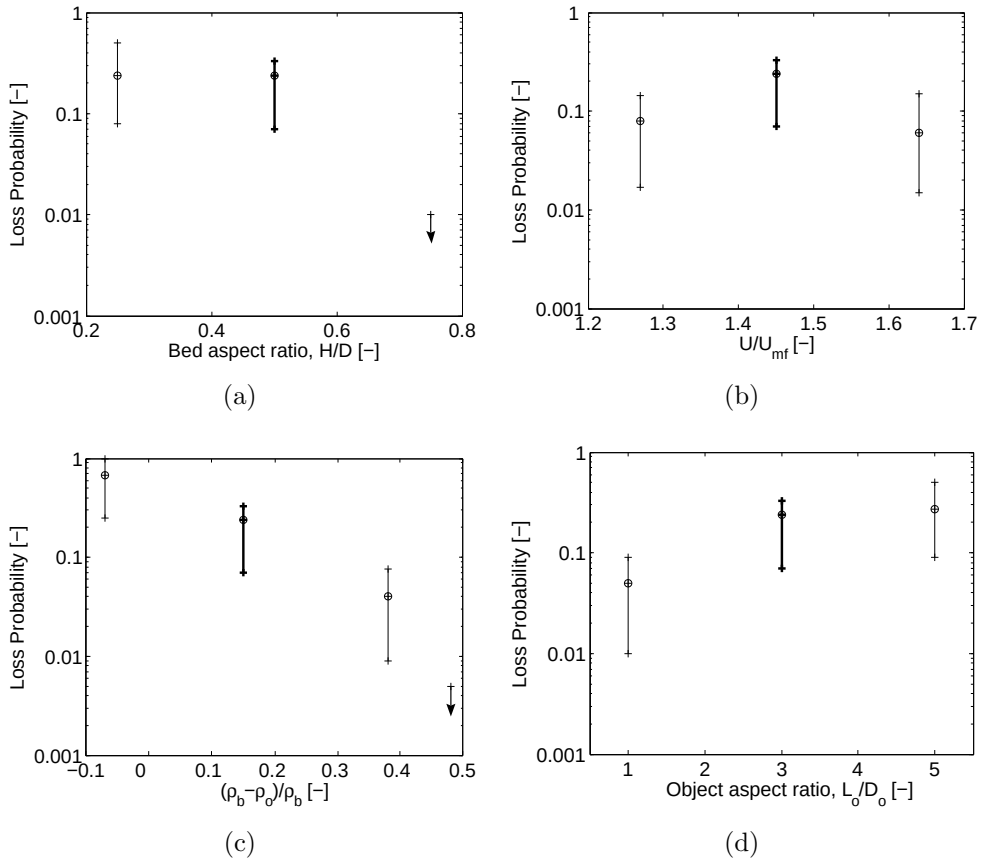

Figure 5.3: Object loss probability with the static distributor. Variation with: (a) bed aspect ratio, (b) dimensionless gas velocity, (c) bed-object density ratio, and (d) object aspect ratio.

Figure 5.3 (a) and (b) present the influence of the BFB dynamics, and Figure 5.3 (c) and (d) that of the object characteristics. As explained above, the results can only be considered as qualitative information, so minor changes will not be discussed. With such a consideration, three different behaviors can be disregarded. First, those configurations in which the object rapidly stopped circulating, corresponding to values of the loss probability between 1 and 0.1, meaning 0 to 9 times that the object sprang back

to the bed surface before being lost. Such cases include the nominal case and those for a shallow bed, a denser object or a larger one. Here the effect of the rotating distributor is extremely remarkable. Next, we can consider those configurations in which the object stopped circulating after a rather large number of cycles, corresponding to values of the loss probability between 0.1 and 0.01, meaning 10 to 100 object cycles before being lost. Such cases correspond to smaller or larger gas velocities, a lighter object or a smaller one. Here the effect of the rotating distributor is still important.

Last, there are those configurations in which the object did not stop circulating during the 10 minutes tests. In such cases, the experimental value of the loss probability is zero or, more precisely, it is at least smaller than one over the number of cycles that the object has performed during those 10 minutes. Those cases are for a large bed ($h_b/D = 0.75$) and for a low density object ($840\,kg/m^3$, which gives a bed-object density ratio of 0.48). In the graphs they are represented with a dot and an arrow, meaning that their probability is at least smaller than the given value. Here the rotation of the distributor is of no use. In both cases, it is clear that the ability of the object to reach the bottom zone is reduced. First by a larger depth and thus a need of a larger residence time in the dense phase, and also because of the existence of larger bubbles near the freeboard, with increasing probability to interact with the object. And second by a lower density, and thus buoyant forces becoming more important and precluding the object to sink deep. This last case is not really relevant, as the object merely stayed in the bed surface and did not circulate homogeneously throughout the bed. On the contrary, the restriction for shallow beds is important, and the conclusions of this work are not valid for deep beds, where object losses seldom appear.

The effect of bed aspect ratio and object density on the loss probability seems quite straightforward. Above a certain height, the probability for an object to reach the bottom zone rapidly diminishes for the reasons suggested in the previous paragraph. Decreasing the object density and thus increasing the related buoyant forces also decrease the probability of the object traveling to the bottom. Therefore, in both cases, losses are prevented. The influence of air velocity and object aspect ratio on the loss probability was not so straightforward. The results in Figure 5.3 (b) suggest the existence of competing mechanisms when the gas velocity changes. Decreasing loss probabilities for increasing gas velocity was the expected result, as the intensity of the fluidization is improved (Otshitani et al., 2004), and both the rising and sinking velocities are increased. The low probability datum for the lower gas velocity might be related to a change in the bed structure. For example, the gas velocity might be too low for establishing the typical 2-vortex configuration, as shown by Pallarès and Johnsson (2006), but this fact cannot be established with our data. Finally, Figure 5.3

(d) shows that the incidence of object losses decreases for smaller objects, while no difference is observed between the two larger objects (aspect ratio 3 and 5). It seems reasonable that objects with larger aspect ratios (which means larger objects, as the diameter of the cylindrical objects is constant) could not be easily risen by bubbles due to their larger inertia. In contrast, smaller objects could be easily risen. Nevertheless, this is in fact beyond the purpose of this work, which is focused in establishing the effects of the rotating distributor.

Industrial applications often rely on the very good vertical mixing associated with fluidized beds, so that the ability of large objects to move through all zones within the bed (including the bottom zone) is envisaged. Therefore, object loss may occur and might cause minor or severe problems, depending on the application, including reactant loss, hot spots, agglomeration, corrosion, etc. A method of re-releasing the objects is therefore necessary, and an actuator applied to the distributor, such as a low frequency rotation, may be a more efficient tool than increasing the gas velocity for small scale applications.

5.4.2 Circulation time distribution

The distribution of circulation times for the object was also considered in this study to characterize the effect of the rotating distributor. The circulation time datasets were obtained performing 10 minutes tests for all the experimental configurations. The number of data in the datasets was always beyond 100, which can be considered an adequate number for statistical analysis. Figure 5.4 shows the histograms of the circulation times for both the rotating and the static distributor configurations. In both cases, the experiments were run for the nominal experimental conditions ($U/U_{mf} = 1.44$, $h_b/D = 0.5$ and nominal object parameters). Time intervals in the histograms were chosen to give a sufficient number of appearances in each bar (> 5), for all the experimental conditions. For the static distributor, the object losses are taken into account in the $t > 8,5\,s$ interval.

Chi-square tests of population homogeneity were performed, as a first step to establish that different datasets correspond to different dynamics, and thus the effect of the rotation on the circulation times is beyond statistical uncertainty. The Chi-square test of population homogeneity between the histograms of the two datasets gives a p-value, and values smaller than 0.05 mean that there is sufficient statistical evidence to guarantee that the two datasets are different. Chi-square tests of population homogeneity were performed between static and rotating distributor measurements maintaining all other conditions identical. The result for the nominal case showed a p-value of 0.012, so the two sets can be considered different, and a certain effect due to the rotation did

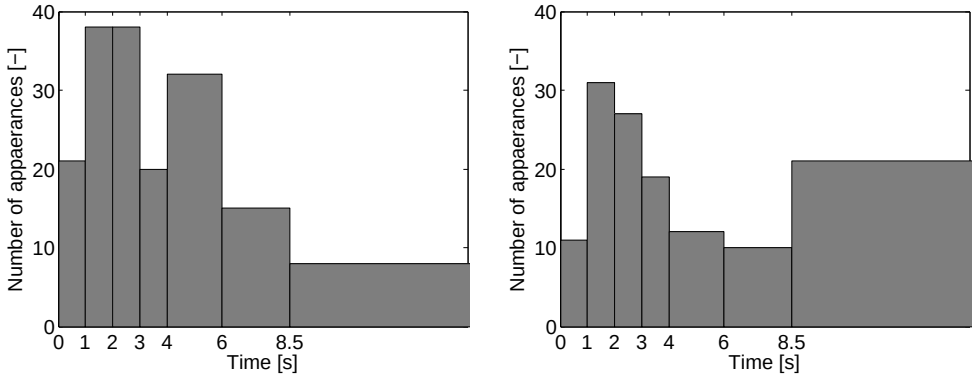

Figure 5.4: Histograms of the circulation time for the object to return to the bed surface: (a) rotating distributor, (b) static distributor. Nominal case ($U/U_{mf} = 1.44$, $h_b/D = 0.5$).

exists. But, of course, the mechanisms related to object losses has already been shown to be extremely different with and without rotation. This mechanism affected the data for large times, although it is not the only cause for large circulation times. Repeating the Chi-square test disregarding the $t > 8.5\,s$ data for both the static and the rotating distributor cases gives a new p-value of 0.27, so there is no statistical evidence to guarantee that these two datasets correspond to different dynamics. Therefore, the effect of the rotating distributor is only evident for cycles of large circulation time. This means that the rotation only affects the bottom of the bed, and not the regions above that zone. Chi-square tests were performed for all the experimental conditions defined in Table 5.2, giving similar evidence in all the cases.

The circulation time was calculated for all the experimental conditions as the time lapse between consecutive appearances of the object at the bed surface. The medians of all the circulation time distributions are shown in the graphs of Figure 5.5 for comparison with the rest of conditions, varying object and bed parameters, and with and without rotation.

There is an absence of data in three experimental conditions corresponding to the static distributor configuration. In those cases the object was lost in the different experiments without even reaching the bed surface once, or after 2 or 3 cycles, so there was not enough data for a proper estimation. Those cases are for a shallow bed ($h_b/D = 0.25$), for a high density object ($1,750\,kg/m^3$, higher than the bed density, which gives a negative bed-object density ratio of -0.07), and for an object of high aspect ratio ($L_O = 32\,mm$, which gives an object aspect ratio of 5). In all these cases, the object seldom appeared back in the freeboard throughout the experiments. This was also the case for the nominal conditions, but in that case a far larger number of experiments were performed in order to obtain a sufficiently large dataset.

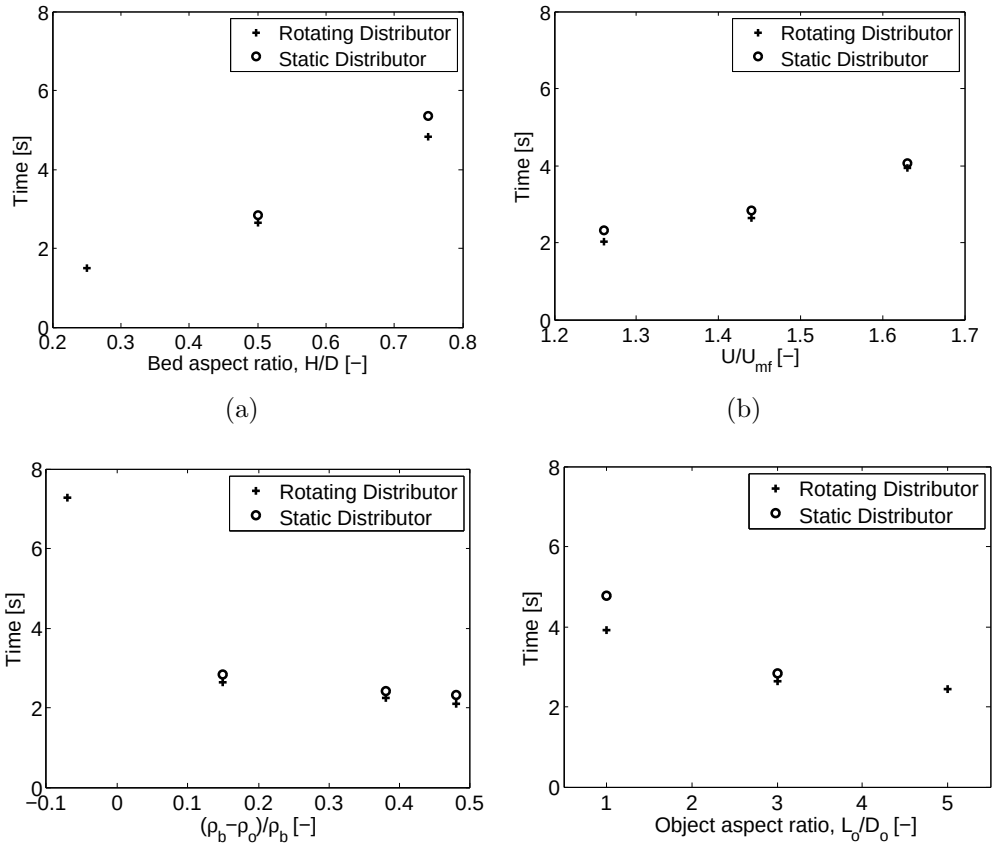

Figure 5.5: Median of the object circulation time distributions, variation with (a) bed aspect ratio, (b) dimensionless gas velocity, (c) bed-object density ratio, and (d) object aspect ratio.

The results for the medians show just a slight reduction when using the rotating distributor. Therefore, there is no relevant effect of the distributor rotation, apart from the cases where the absence of data for the static distributor shows the ability of the rotating distributor to maintain the object in circulation. This was rather expected, as it has been shown that only large circulation times were modified and the median is a parameter that remains quite unaffected with such variations.

On the other hand, the results in Figure 5.5 show the effect of the varying parameters on the circulation times. As has been done previously, a first step is to establish that the different datasets shown in each graph correspond to different dynamics, and thus that the differences are beyond statistical uncertainty. For such a purpose we have used the Chi-square tests. Therefore, tests of population homogeneity were carried out between the datasets for each experimental condition and the nominal cases. Chi-square tests showed p-values always smaller than 0.05 for all the combinations. Thus, the influence of the different parameters (bed aspect ratio, dimensionless gas velocity, object density and size, and rotation) on the circulation of the objects can be

considered as well established.

The results showed an increase of the median value for increasing bed aspect ratios and a slight increase for increasing gas velocities. The first effect could be attributed to the average depth attained in a cycle, a parameter that will reasonably increase for larger bed depths. The effect of the gas velocity is not so straightforward. It would seem reasonable to expect a reduction of the circulation times for increasing gas velocities. Such an increase will produce higher sinking and rising velocities, according to the well established correlations for the bubble and dense phase velocities (Darton et al., 1977; Kunii and Levenspiel, 1991). No definitive explanation is given, as the effect is not very pronounced and it is less evident for the whole dataset, as will be seen in Figure 5.7.

When varying object parameters, the median value decreased for increasing object aspect ratios and bed-object density ratios, although in this last case, the large difference between the flotsam objects and the jetsam object was the main feature. This might be explained by the fact that the jetsam object reached the bottom zone in practically every cycle. Thus, its dynamics were associated with the rotation and the related mechanisms that released the object from such a zone. This is in accordance with the results presented in the object losses section. On the other hand, most of the flotsam objects cycles will be restricted to the upper layer, and the median represents these cycles. The effect of the object aspect ratio might be attributed to the higher buoyant forces suffered by a larger object.

For a deeper analysis of the distributor effect, the information of the median is not sufficient. To give information of the larger circulation times, box plots were used rather than histograms, as they give the information in a more compact form. Box plots are commonly used for a brief understanding of a statistical dataset. In a box plot, the information is reduced to the median, the lower and upper quartiles (representing 25 % and 75 % of the population), a confidence interval (defined by the two experimental data that are further away from the median but inside a maximum interval of ± 1.5 times the inter-quartile range from the quartiles), and outliers (that lie out of such a confidence interval). Figure 5.6 shows the box plots of the data given in Figure 5.4. There is a significant difference concerning outliers. The lost object data for the static distributor were included in the calculation of median and intervals, although they were not shown as outliers. Removing them would lead to a non-representative dataset. Note that for the median and intervals calculation the only important fact is that they represent large times, but it is unimportant to know how large (as is the case for mean or standard deviation). They were not pointed as outliers because the time required to rise to the freeboard is unknown, although at least larger than the

experiment runtime.

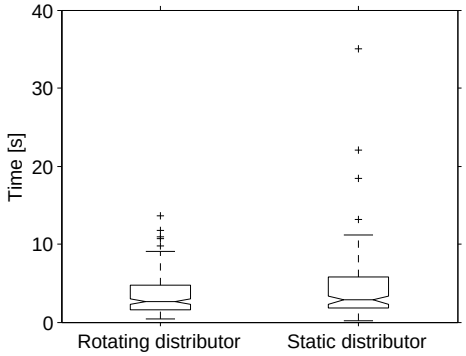

Figure 5.6: Box plots of the circulation time distributions in Figure 5.4. Nominal case ($U/U_{mf} = 1.44$, $h_b/D = 0.5$).

The eight graphs of Figure 5.7 present the box plots of the circulation time datasets as a function of bed aspect ratio and dimensionless gas velocity (note the change of scale for this plot), object density and object shape, considering both the static and the rotating distributor configurations. The nominal case shown in Figure 5.6 is highlighted in the eight graphs.

Once again, the effect of maintaining the object in circulation when a rotation is applied to the distributor is observed in those graphs where the data for the static configuration is missing. Apart from that, the effect of the distributor in the incidence of large circulation times can be observed in most cases, the distributor rotation being a mechanism to shorten those times. This is probably due to its effect in releasing the object from the quasi-stagnant regions near the distributor plate. Such an effect is evident, and probably enhanced, for varying object size or density.

5.5 Conclusions

The motion of a large object within a lab-scale BFB was analyzed, operating with a rotating distributor or in a static distributor conventional bed. Several tests were carried out for a range of bed characteristics (bed height and gas velocity) and object parameters (density and size).

During the operation with the static distributor, after a number of cycles out and back to the surface of the bed, the object ended motionless in the small dead zones between holes over the distributor, for almost all test configurations. This effect has often been referred in the literature but was not the case for the rotating configuration, where no object losses were reported. In some cases, for large and dense objects, or operating in a shallow bed, and even for the nominal conditions of our experiments, the rotation of the distributor permitted the continuous motion within the bed of objects

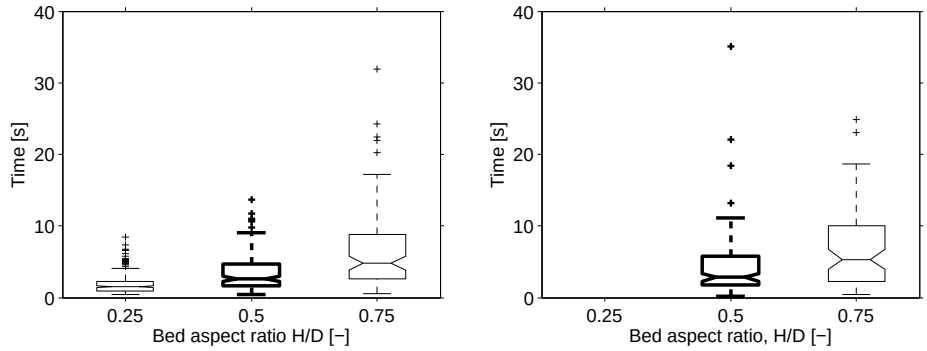

(a) Bed aspect ratio (rd)

(b) Bed aspect ratio (sd)

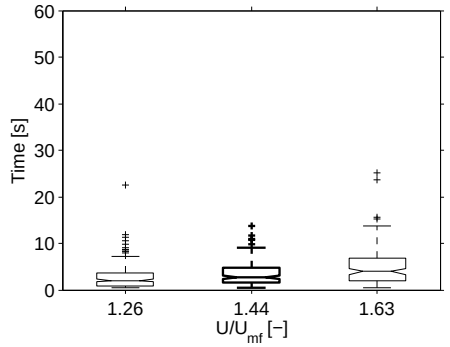

(c) Dimensionless gas velocity (rd)

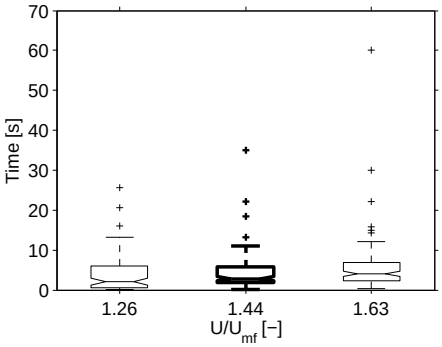

(d) Dimensionless gas velocity (sd)

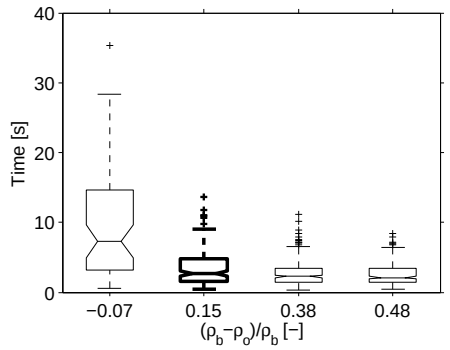

(e) Bed-object density ratio (rd)

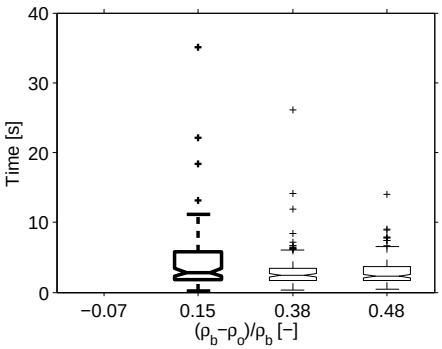

(f) Bed-object density ratio (sd)

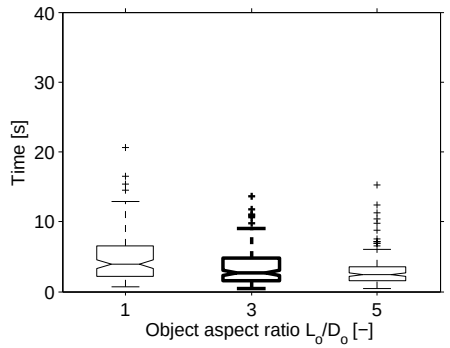

(g) Object aspect ratio (rd)

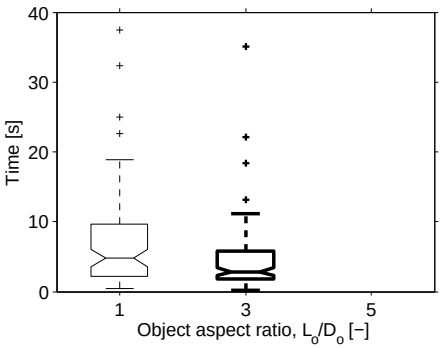

(h) Object aspect ratio (sd)

Figure 5.7: Box plots of the circulation time distributions for varying conditions, (rd) Rotating Distributor, (sd) Static Distributor.

that were immediately lost and did not circulate at all with the static configuration. Moreover, when an object was lost in a static configuration it could be recovered almost immediately, by forcing the distributor to rotate. The rotation breaks the layout of gas jets and stagnant zones just above the distributor, improving the radial and axial mixing at the bottom of the bed.

The circulation time distribution was presented for the different configurations and varying parameters. A statistical analysis of the data was performed, showing a slight effect of rotation in large circulation times. The distribution shows that most of the results are confined in a small interval (around $0 - 5\,s$ for most configurations), and then there is a series of outliers (going up to $40\,s$) that describe the physics of multiple-jump rising and bottom bed phenomena. The rotation was found to strongly affect the dynamics of such cycles.

Therefore, rotation of the distributor (either continuous or applied at given intervals) might prove useful (mostly in small scale applications due to the inherent complications of imposing rotation on a large distributor) when the circulation of the objects throughout the bed is envisaged and object losses or large circulation times should be prevented.

5.6 Notation

D Bed diameter, $[m]$

D_O Object diameter, $[m]$

f_b Characteristic frequency of the bed, $[Hz]$

h_b Fixed bed height, $[m]$

H_{3D} Vessel height, $[m]$

L_O Object length, $[m]$

n Rotating angular velocity, $[rpm]$

U Gas velocity, $[m/s]$

U_{mf} Minimum fluidization velocity, $[m/s]$

ε_{packed} Void fraction of the packed bed, $[-]$

ρ_b Packed bed density, $[kg/m^3]$

ρ_o Object density, $[kg/m^3]$

Bibliography

Bergh H., Tijdeman H., 1965. Theoretical and experimental results for the dynamic response of pressure measuring systems. *Report NLR-TR F.238, National Aero- and Astronautical Research Institute*, Amsterdam, the Netherlands.

Bokkers G.A., van Sint Annaland M., Kuipers J.A.M., 2004. Mixing and segregation in a bidisperse gas-solid fluidised bed: a numerical and experimental study. *Powder Technology* 140 (3), 176-186.

Chyang C.S., Lin Y.C., 2002. A study in the swirling fluidizing pattern. *Journal of Chemical Engineering of Japan* 35, 503-512.

Darton R.C., LaNauze R.D., Davidson J.F., Harrison D., 1977. Bubble growth due to coalescence in fluidized beds. *Transactions of the Institute of Chemical Engineering* 55, 274-280.

Du B., Wei F., Warsito W., 2002. Gas and solids mixing in a turbulent fluidized bed. *AIChE Journal* 48 (9), 1896-1909.

Geldart D., Baeyens J., 1985. The design of distributors for gas-fluidized beds. *Powder Technology* 45, 67-78.

Grassler T., Wirth K.-E., 2000. X-ray computer tomography-potential and limitation for the measurement of local solids distribution in circulating fluidized beds. *Chemical Engineering Journal* 77 (1-2), 65-72.

Hoffmann A.C., Janssen L.P., Prins J., 1993. Particle segregation in fluidized binary mixtures. *Chemical Engineering Science* 48(9), 1583-1592.

Ibsen C.H., Solberg T., Hjertager B.H., Johnsson F., 2002. Laser Doppler anemometry measurements in a circulating fluidized bed of metal particles. *Experimental Thermal and Fluid Science* 26 (6-7), 851-859.

Karri S.B.R., Werther J., 2003. Gas distributor and plenum design in fluidized beds. In: Yang W. C. Handbook of fluidization and fluid-particle systems, Marcel Dekker Inc., New York, pp. 164-179.

Keillor S.A., Bergougnou M.A., 1975. A study of the action of floating bubble breakers in fluidized beds by interactive computer graphics. *Fluidization Technology* 2, 95-109.

Kunii D., Levenspiel O., 1991. Fluidization Engineering, 2nd ed., Butterworth-Heinemann, Boston.

Lim K.S., Agarwal P.K., 1994. Circulatory motion of a large and lighter sphere in a bubbling fluidized bed of smaller and heavier particles. *Chemical Engineering Science* 49 (3), 421-424.

Mawatari Y., Tatemoto Y., Noda K., 2003. Prediction of minimum fluidization velocity for vibrated fluidized beds. *Powder Technology* 131, 66-70.

Moussa N.A., Fowle A.A., Delichatsios M.M., Caron R.N., Wilson R., 1982. Advanced design for pulsed atmospheric fluidized bed combustion. *Final Report to DOE/METC, Morgantown Energy Technology Center.*

Nguyen T.H., Grace J.R., 1978. Forces on objects immersed in fluidized beds. *Powder Technology* 19, 255-264.

Nienow A.W., Rowe P.N., Chiba T., 1978. Mixing and segregation of a small portion of large particles in gas fluidized beds of considerably smaller ones. *AIChE Symposium Series* 74, 45-53.

Noda K., Mawatari Y., Uchida S., 1998. Flow patterns of fine particles in a vibrated fluidized bed under atmospheric or reduced pressure. *Powder Technology* 99, 11-14.

Otshitani J., Keiko O., Makoto I., Zennosuke T., 2004. Effect of particle fluidization intensity on floating and sinking of objects in a gassolid fluidized bed. *Advanced Powder Technology* 15(2), 201-213.

Ouyang F., Levenspiel O., 1986. Spiral distributor for fluidized beds. *Industrial & Engineering Chemistry Process Design and Development* 25, 504-507.

Pallarès D., Johnsson F., 2006. A novel technique for particle tracking in cold 2-dimensional fluidized beds - Simulating fuel dispersion. *Chemical Engineering Science* 61, 2710-2720.

Rees A.C., Davidson J.F., Hayhurst A.N., 2005. The rise of a buoyant sphere in a gas-fluidized bed. *Chemical Engineering Science* 60, 1143-1153.

Rees A.C., Davidson J.F., Dennis J.S., Fennell P.S., Gladden L.F., Hayhurst A.N., Mantle M.D., Müller C.R., Sederman A.J., 2006. The nature of the flow just above

the perforated plate distributor of a gas-fluidised bed, as imaged using magnetic resonance. *Chemical Engineering Science* 61, 6002-6015.

Rios G.M., Dang Tran K., Masson H., 1986. Free object motion in a gas fluidized bed. *Chemical Engineering Communications* 47, 247-272.

Sanderson, J., Rhodes, M. 2003. Hydrodynamic similarity of solids motion and mixing in bubbling fluidized beds. *AIChE Journal* 49(9), 2317-2327.

Shen L., Johnsson F., Leckner B., 2004. Digital image analysis of hydrodynamics two-dimensional bubbling fluidized beds. *Chemical Engineering Science* 59, 2607-2617.

Sobrino C., Almendros-Ibáñez J.A., Santana D., de Vega M., 2008. Fluidization of Group B particles with a rotating distributor. *Powder Technology* 181, 273-280.

Sobrino C., Acosta-Iborra A., Santana D., de Vega M., 2009. Bubble characteristics in a bubbling fluidized bed with a rotating distributor. *International Journal of Multiphase Flow* 35(10), 970-976.

Sreenivasan B., Ragahavan V.R., 2002. Hydrodynamics of a swirling fluidised bed. *Chemical Engineering Science* 41, 99-106.

Stein M., Ding Y.L., Seville J.P.K., Parker D.J., 2000. Solids motion in bubbling gas fluidised beds. *Chemical Engineering Science* 55, 5291-5300.

Tanimoto H., Chiba S., Chiba T., Kobayashi H., 1981. Jetsam descent induced by a single bubble passage in three-dimensional gas-fluidized beds. *Journal of Chemical Engineering of Japan* 14(4), 273-276.

van Ommen J.R., Schouten J.C., vander Stappen L.M., van den Bleek C.M., 1999. Response characteristics of probe transducer systems for pressure measurements in gas solid fluidized beds how to prevent pitfalls in dynamic pressure measurements. *Powder Technology* 106, 199-218.

van Ommen J.R., Nijenhuis J, van den Bleek C.M., Coppens M.O., 2007. Four ways to introduce structure in fluidized bed reactors. *Industrial & Engineering Chemistry Research* 46, 4236-4244.

Chapter 6

Conclusions

This PhD thesis presents experimental studies on the motion of objects immersed in bubbling fluidized beds. The experiments were carried out in two different experimental setups, a 2-D facility and a lab-scale 3-D fluidized bed. Measurement techniques included visualization techniques for tracking the object and characterizing the bubbles, particle image velocimetry for determining the dense phase velocity, and pressure measurements for analyzing the bed dynamics.

The 2-D studies were aimed to establish the main characteristics of the object motion within the bed. The object was tracked throughout its path and its sinking and rising behavior was determined. The incidence of buoyancy effects was also established varying the object density and size, ranging from flotsam to jetsam objects. Different gas velocities were tested and in some particular cases, the bed height and the bed material size distribution were also varied.

The first tests established the object preferential regions and paths. The ranges of object size and density and of gas velocity were selected to ensure at least a minimum object circulation throughout the bed, so no strongly flotsam or jetsam objects (that remain in the surface of the bed or sink to rest at the distributor) were tested. The preferential object paths showed them sinking at the sides of the bed following the dense phase and rising at the center following the preferential bubble paths. The object moved throughout the whole bed, describing cycles going from the surface of the bed to a certain depth and back to the surface. In some cases, the circulation was not homogeneous due to the appearance of buoyant forces. In such cases (large density differences or larger objects) the circulation could be improved increasing the gas velocity, a procedure that reduces the relative importance of buoyant forces.

The object trajectory was composed of interleaved sinking and rising paths. The object did sometimes rise to the freeboard by the action of a single bubble, but usually it was detached before reaching the surface of the bed. Then, its trajectory showed how

several bubbles raised the object small distances, a process established in the literature and called multiple-jerk or multiple-jump behavior. This phenomenon was studied and the rising and sinking paths were discriminated to calculate average sinking and rising velocities. This discrimination might be a source of errors. Moreover, while there were only upward velocities during the rising path within a single jump, the sinking path of the object was characterized by sudden falls with high downwards velocities interleaved with larger lapses of vibration, in which both upwards and downwards velocities were present. These vibration velocities should also be discriminated for a proper average velocity calculation since they do not produce a net displacement. A procedure to average the object velocity has been presented in this work.

The obtained average sinking velocity of the object was then compared with widely used correlations found in the literature for the dense phase. It showed a good agreement for object-bed density ratios close to unity, when buoyant forces could be considered negligible. For other object densities and sizes, some differences were obtained. Decreasing the object density produced a reduction of the sinking velocity. The effect of the object size is inverse, when the object size was decreased, its mean sinking velocity was increased. Increasing the gas velocity diminished these effects. These results quantified the effect of buoyant forces within the bed. On the other hand, the average rising velocity was compared with widely used correlations found in the literature for the bubble velocity. It correlated with the 20 % of the average bubble velocity. Previous results reported in the literature show a large scatter, giving results from a 10 % to a 30 % ratio. Variations of the object density and size showed no distinct effect on this velocity, while variations of the gas velocity were coherent with the above given ratio, taking into account the relation between gas velocity and bubble velocity.

The multiple-jump behavior was studied in detail and an empirical expression for the distribution of the number of jumps was obtained. It followed an inverse exponential distribution, a result that suggests that each jump is an independent phenomenon. The number of jumps being a discrete variable, the exponential distribution was transformed into a (discrete) geometric distribution. The experimental results provided a ratio p for the geometric distribution of 0.45, meaning that there is an average probability of 45 % for a bubble to raise an object directly to the freeboard. This geometric distribution was found to be applicable to all the objects tested in all the configurations, that is, no changes were reported for varying gas velocity, object size and object density, and even for a bed of finer particles, or a shallower bed. Therefore, the average probability for a bubble to lift an object directly to the bed surface is independent of the object size and density, the bubble size and velocity, and the bed characteristics in the ranges described. It seems to be just a function of the contact area between bubble and object,

but further work is needed to confirm this hypothesis.

Another main parameter to characterize object motion is de maximum depth attained in each cycle out and back to the freeboard. The probability distribution to reach a determined maximum depth was obtained. It followed a parabolic distribution, with a minimum at moderate depths. This can be explained with a look at the preferential bubble and object paths, obtained in a preliminary study. It showed the existence of a minimum of the probability to find a bubble at moderate heights at the sides of the bed where the object sinking process usually occurred. Buoyant forces related with object density and size did not seem to alter these distributions, either qualitatively or quantitatively, although a symmetric distribution should be used when changing from flotsam to jetsam objects. Nevertheless, for large density differences or large sizes, the distribution was changed as a result of poor object circulation. In such cases, large depths were precluded and the probability was transferred to minima depths. This was coherent with the non homogeneous circulation of the object obtained in the first tests. Nevertheless, all the objects tested in this PhD thesis had a proper circulation throughout the bed provided that the air velocity was sufficiently high. Thus the fluidization intensity inside the bed reduces the effect of buoyant forces.

The circulation time of the object moving in a 2-D bed, defined as the time spent by an object to describe a cycle, diving from the surface of the bed and rising back to it, was analyzed. This time was modeled to depend on the four main factors described above, the average sinking and rising velocities of the object, the maximum depth attained in the cycle, and the number of jumps needed for the object to rise back to the freeboard. Semi-empirical expression were determined, based on the distributions of the number of jumps and the maximum depth attained, in order to estimate the distribution of the circulation time of the object inside the 2-D bed. This expression described reasonably the distribution of circulation times obtained experimentally. The empirical constants in the expression have been shown to remain for changing object and bed parameters, except in the case of the sinking velocity, where some correction should be made, and in the case of poor circulation, where the distribution of attained depths might change. The semi-empirical expressions were finally extended to estimate the circulation time of the object moving in a 3-D bed, obtaining a good agreement with the experimental data.

Finally, a 3-D application is presented. The circulation characteristics of an object were studied and a method to modify such characteristics and intensified certain processes was presented. The method consists on applying a rotating distributor. Its effect on the motion of objects inside a 3-D bubbling fluidized bed was analyzed. When operating the bed with a static distributor, almost all the objects ended settled out over

the distributor after a short period of time. This is a typical drawback of perforated plate distributors and such a behavior was prevented when operating with the rotating distributor. Then, the dynamics at the bottom of the bed were totally changed, the layout of air jets and the stagnant zones just above the distributor being altered. Moreover, the rotation of the distributor served to recover objects that were lost preciously when operating with the static distributor. Circulation times were also measured for all the objects operating with both the static and the rotating distributor. The rotating distributor reduced the large circulation times, which correspond to objects that sunk deep, reaching the bottom of the bed. Therefore, the rotation of the distributor was proved to be useful for those applications in which the circulation of objects through the bed is envisaged, and large circulation times or object losses must be prevented.

Bibliography

Almendros-Ibáñez J.A., Sanchez-Delgado S., Sobrino C., Santana D., 2009. Experimental observations on the different mechanisms for solid ejection in gas-fluidized beds. *Chemical Engineering and Processing* 48-3, 734-744.

Baeyens J., 1973. Heat transfer in gas fluidized beds. *Phd Thesis*, University of Bradford, United Kingdom.

Bergh H., Tijdeman H., 1965. Theoretical and experimental results for the dynamic response of pressure measuring systems. *Report NLR-TR F.238, National Aero- and Astronautical Research Institute*, Amsterdam, the Netherlands.

Bokkers G.A., van Sint Annaland M., Kuipers J.A.M., 2004. Mixing and segregation in a bidisperse gas-solid fluidised bed: a numerical and experimental study. *Powder Technology* 140 (3), 176-186.

Chyang C.S., Lin Y.C., 2002. A study in the swirling fluidizing pattern. *Journal of Chemical Engineering of Japan* 35, 503-512.

Darton R.C., LaNauze R.D., Davidson J.F., Harrison D., 1977. Bubble growth due to coalescence in fluidized beds. *Transactions of the Institute of Chemical Engineering* 55, 274-280.

Davidson J.F., Harrison D., 1963. Fluidised particles, 1st ed. Cambridge University Press, Cambridge.

Davidson J.F., Schüller B.O.G., 1960. Bubble formation at an orifice in a viscous liquid. *Transactions of the Institution of Chemical Engineers* 38, 145-154.

Du B., Wei F., Warsito W., 2002. Gas and solids mixing in a turbulent fluidized bed. *AIChE Journal* 48 (9), 1896-1909.

Fried E., Idelchick I.E., 1989. Flow resistance: a design guide for engineers, 1st ed., Hemisphere publishing corporation, New York, pp. 255-282.

Geldart D., 1973. Types of gas fluidization. *Powder Technology* 7, 285-292.

Geldart D., Baeyens J. 1985. The design of distributors for gas-fluidized Beds. *Powder Technology* 42, 67-78.

Gomez-Barea A., Leckner B., 2010. Modelling of biomass gasification in fluidized bed. *Progress in Energy and Combustion Science* 36 (4), 444-509.

Grace J.R., Baeyens J. 1986. In: Geldart D. Gas Fluidization Technology. Wiley, Chichester, p. 415.

Grassler T., Wirth K.-E., 2000. X-ray computer tomography-potential and limitation for the measurement of local solids distribution in circulating fluidized beds. *Chemical Engineering Journal* 77 (1-2), 65-72.

Hoffmann A.C., Janssen L.P., Prins J., 1993. Particle segregation in fluidized binary mixtures. *Chemical Engineering Science* 48(9), 1583-1592.

Ibsen C.H., Solberg T., Hjertager B.H., Johnsson F., 2002. Laser Doppler anemometry measurements in a circulating fluidized bed of metal particles. *Experimental Thermal and Fluid Science* 26 (6-7), 851-859.

Johnsson F., Zijerveldb R.C., Schoutenb J.C., van den Bleek C.M., Leckner B., 2000. Characterization of fluidization regimes by time-series analysis of pressure fluctuations. *International Journal of Multiphase Flow* 26, 663-715.

Karri S.B.R., Werther J., 2003. Gas distributor and plenum design in fluidized beds. In: Yang W. C. Handbook of fluidization and fluid-particle systems, Marcel Dekker Inc., New York, pp. 164-179.

Keillor S.A., Bergougnou M.A., 1975. A study of the action of floating bubble breakers in fluidized beds by interactive computer graphics. *Fluidization Technology* 2, 95-109.

Koornneef J., Junginger M., Faaij A., 2007. Development of fluidized bed combustion - An overview of trends, performance and cost. *Progress in Energy and Combustion Science* 33, 19-55.

Kunii D., Levenspiel O., 1991. Fluidization Engineering, 2nd ed., Butterworth-Heinemann, Boston.

Laverman J.A., Roghair I., Van Sint Annaland M. and Kuipers H., 2008. Investigation into the hydrodynamics of gas-solid fluidized beds using particle image velocimetry coupled with digital image analysis. *The Canadian journal of chemical engineering* 86, 523-535

Lim K.S., Agarwal P.K., 1994. Circulatory motion of a large and lighter sphere in a bubbling fluidized bed of smaller and heavier particles. *Chemical Engineering Science* 49 (3), 421-424.

Mawatari Y., Tatemoto Y., Noda K., 2003. Prediction of minimum fluidization velocity for vibrated fluidized beds. *Powder Technology* 131, 66-70.

Merry J.M.D., 1975. Penetration of vertical jets into fluidized beds. *AIChE Journal* 21, 507-510.

Molerus O., 1982. Interpretation of Geldart's type A, B, C, and D powders by taking into account interparticle cohesion forces. *Powder Technology* 33, 81-87.

Moussa N.A., Fowle A.A., Delichatsios M.M., Caron R.N., Wilson R., 1982. Advanced design for pulsed atmospheric fluidized bed combustion. *Final Report to DOE/METC, Morgantown Energy Technology Center.*

Müller C.R., Davidson J.F., Dennis J.S. and Hayhurst A.L., 2007. A study of the motion and eruption of a bubble at the surface of a two-dimensional fluidized bed using particle image velocimetry (PIV). *Industrial & Engineering Chemistry Research* 46, 1642-1652.

Nguyen T.H., Grace J.R., 1978. Forces on objects immersed in fluidized beds. *Powder Technology* 19, 255-264.

Nienow A.W., Rowe P.N., Chiba T., 1978. Mixing and segregation of a small portion of large particles in gas fluidized beds of considerably smaller ones. *AIChE Symposium Series* 74, 45-53.

Noda K., Mawatari Y., Uchida S., 1998. Flow patterns of fine particles in a vibrated fluidized bed under atmospheric or reduced pressure. *Powder Technology* 99, 11-14.

Otshitani J., Keiko O., Makoto I., Zennosuke T., 2004. Effect of particle fluidization intensity on floating and sinking of objects in a gassolid fluidized bed. *Advanced Powder Technology* 15(2), 201-213.

Otsu N., 1979. A threshold selection method from gray-level histograms. *IEEE Transactions on Systems Man and Cybernetics* 9, 62-66.

Ouyang F., Levenspiel O., 1986. Spiral distributor for fluidized beds. *Industrial & Engineering Chemistry Process Design and Development* 25, 504-507.

Pallarès D., Johnsson F., 2006. A novel technique for particle tracking in cold 2-dimensional fluidized beds - Simulating fuel dispersion. *Chemical Engineering Science* 61, 2710-2720.

Puncochár M., Drahos J., Cermák J., Selucký K., 1985. Evaluation of minimum fluidization velocity in gas fluidized beds from pressure fluctuations. *Chemical Engineering Communications* 35, 81-87.

Rees A.C., Davidson J.F., Hayhurst A.N., 2005. The rise of a buoyant sphere in a gas-fluidized bed. *Chemical Engineering Science* 60, 1143-1153.

Rees A.C., Davidson J.F., Dennis J.S., Fennell P.S., Gladden L.F., Hayhurst A.N., Mantle M.D., Müller C.R., Sederman A.J., 2006. The nature of the flow just above the perforated plate distributor of a gas-fluidised bed, as imaged using magnetic resonance. *Chemical Engineering Science* 61, 6002-6015.

Rios G.M., Dang Tran K., Masson H., 1986. Free object motion in a gas fluidized bed. *Chemical Engineering Communications* 47, 247-272.

Rowe P.N., 1973. Estimation of solid circulation rate in bubbling fluidised bed. *Chemical Engineering Science* 28, 979-980.

Sanchez-Delgado S., Marugan-Cruz C., Acosta-Iborra A., Santana D., 2010. Dense phase fluctuation in a 2-D fluidized bed. *Powder Technology* 200, 37-45.

Sanderson, J., Rhodes, M. 2003. Hydrodynamic similarity of solids motion and mixing in bubbling fluidized beds. *AIChE Journal* 49(9), 2317-2327.

Shen L., Johnsson F., Leckner B., 2004. Digital image analysis of hydrodynamics two-dimensional bubbling fluidized beds. *Chemical Engineering Science* 59, 2607-2617.

Sobrino C., Almendros-Ibáñez J.A., Santana D., de Vega M., 2008. Fluidization of Group B particles with a rotating distributor. *Powder Technology* 181, 273-280.

Sobrino C., Acosta-Iborra A., Santana D., de Vega M., 2009. Bubble characteristics in a bubbling fluidized bed with a rotating distributor. *International Journal of Multiphase Flow* 35(10), 970-976.

Sreenivasan B., Ragahavan V.R., 2002. Hydrodynamics of a swirling fluidised bed. *Chemical Engineering Science* 41, 99-106.

Stein, M., Ding, Y.L., Seville, J.P.K., Parker, D.J., 2000. Solids motion in bubbling gas fluidised beds. *Chemical Engineering Science* 55, 5291-5300.

Sveen J.P., 2004. http://www.math.uio.no/∼jks/matpiv. (Last modified in August, 2004. Accesed in 2008).

Tanimoto H., Chiba S., Chiba T., Kobayashi H., 1981. Jetsam descent induced by a single bubble passage in three-dimensional gas-fluidized beds. *Journal of Chemical Engineering of Japan* 14(4), 273-276.

van Ommen J.R., Schouten J.C., vander Stappen L.M., van den Bleek C.M., 1999. Response characteristics of probe transducer systems for pressure measurements in gas solid fluidized beds how to prevent pitfalls in dynamic pressure measurements. *Powder Technology* 106, 199-218.

van Ommen J.R., Nijenhuis J, van den Bleek C.M., Coppens M.O., 2007. Four ways to introduce structure in fluidized bed reactors. *Industrial & Engineering Chemistry Research* 46, 4236-4244.

Welch P.D., 1967. The use of a fast Fourier transform for the estimation of power spectra. *IEEE Trans. Audio and Electroacoustics* AU-15, 70-73.